

Figure 2. Relocated epicenters for 700+ earthquakes in the Loma Prieta area, including background (pre October 1989) seismicity and 1989 aftershocks. The coordinate system is that defined for the inversion grid in Figure 1. Major faults in the area are shown: SAF=San Andreas, SF=Sargent, BeF=Berrocal, BuF=Butano, ZF=Zayante, VF=Vergeles.

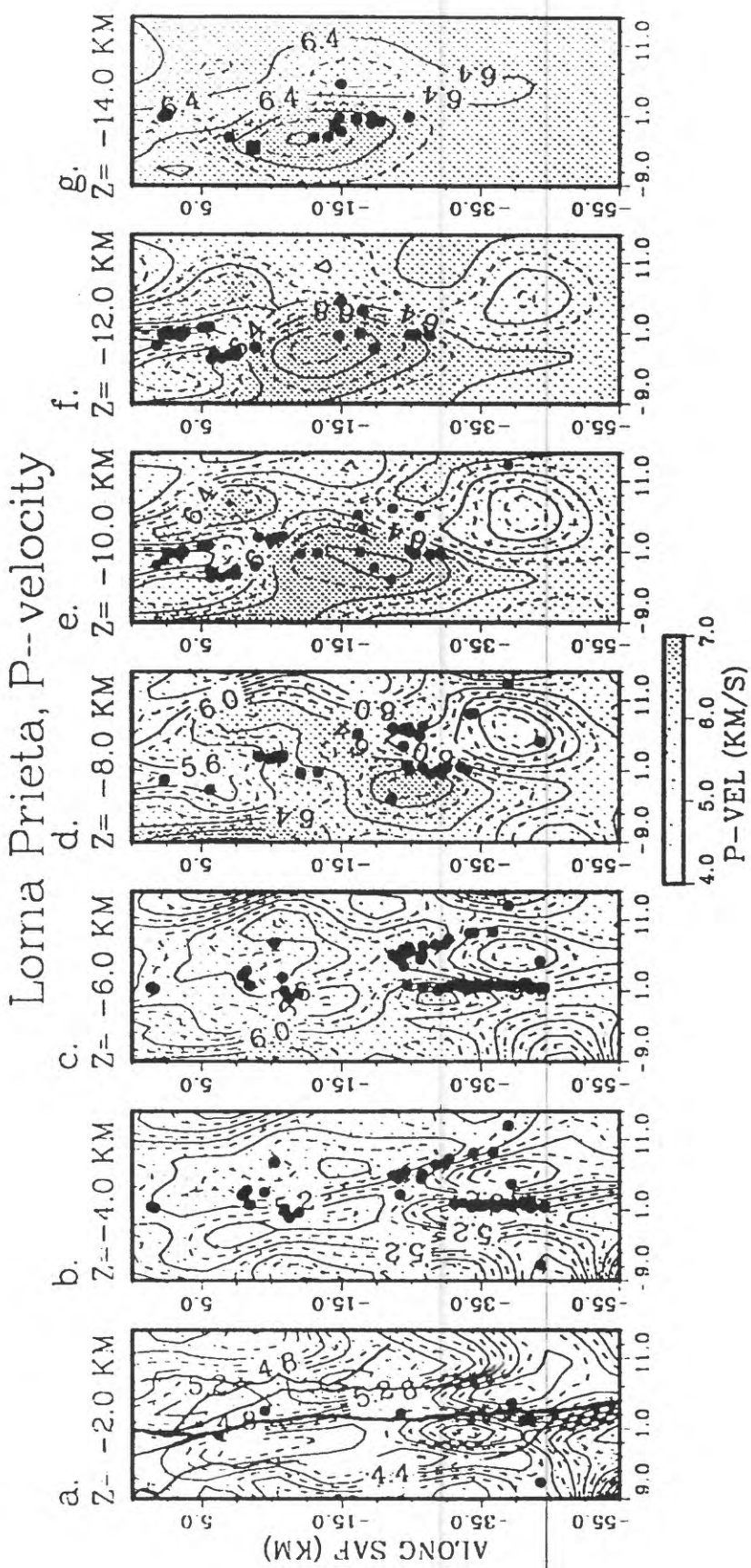


Figure 3. Final P-velocity model for Loma Prieta region, displayed in horizontal plan-view sections from 2-km depth to 14-km depth and extending horizontally over the grid in Figure 1, from $x,y=-9,-55$ to $x,y=15,15$. Velocity values are contoured and shaded, with higher values more darkly shaded. Hypocenters determined in the joint inversion are plotted on their appropriate levels.

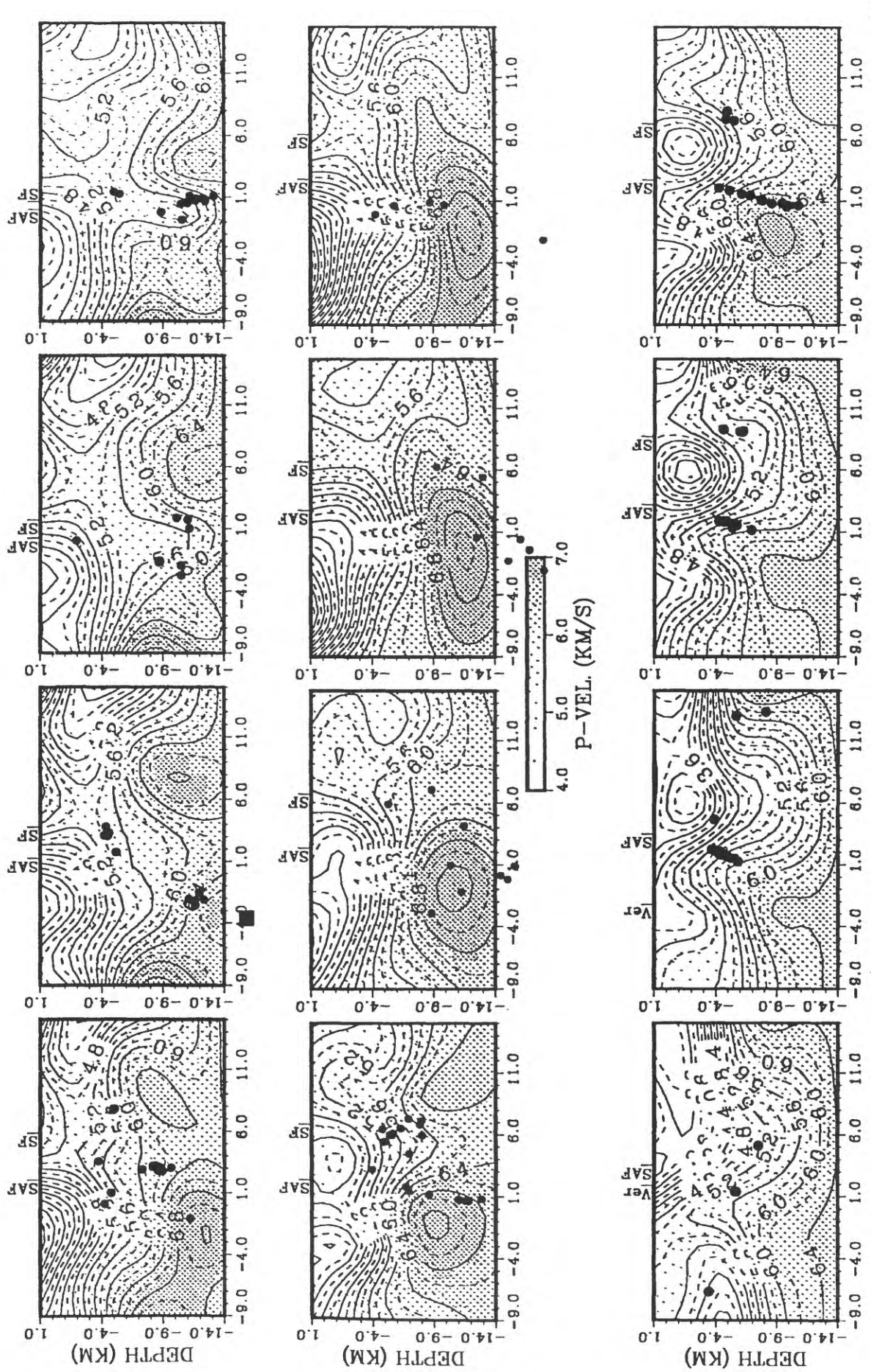


Figure 4. Final P-velocity model for Loma Prieta region, displayed in twelve fault-normal sections from $y=-45$ km (southeast, lower left frame) to $y=+10$ km (northwest, upper right frame) at 5 km intervals along the fault. Velocity values are contoured and shaded, with higher values more darkly shaded. Hypocenters determined in the joint inversion are plotted on their appropriate sections.

Loma Prieta, P-velocity

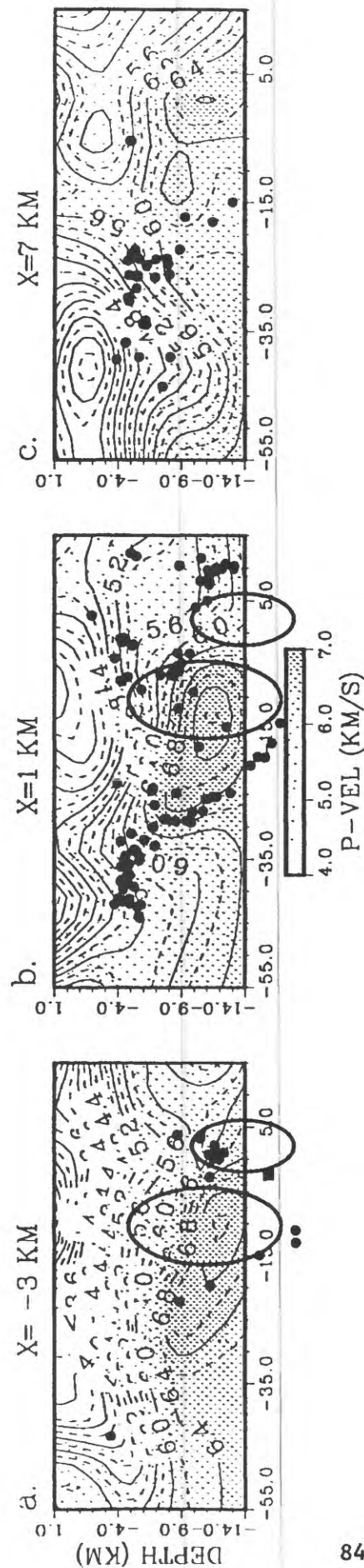


Figure 5. Final P-velocity model for Loma Prieta region, displayed in three fault-parallel sections at $x=-3$, $+1$, $+7$ km. View is from the northeast (northwest is to the right). Velocity values are contoured and shaded, with higher values more darkly shaded. Hypocenters determined in the joint inversion are plotted on their appropriate sections. Ellipses are the inferred fault zone asperities from the Loma Prieta mainshock source study of Choy and Boatwright (1990).

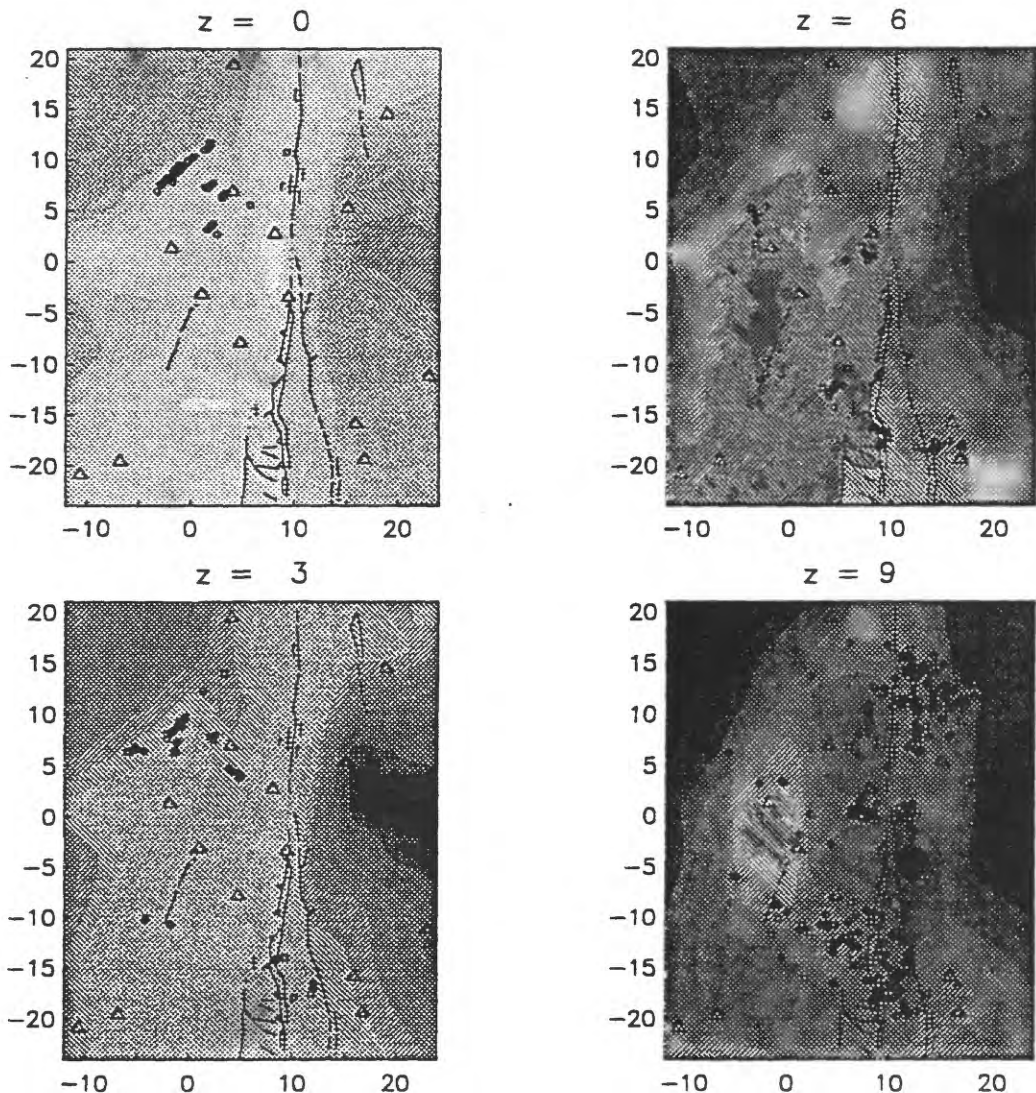


Figure 4. Horizontal cross-sections through the 3D P-wave velocity structure with the surface traces of the branches of the San Jacinto Fault superimposed. The scale is in kilometers and the map is rotated 50 degrees east of north and depths are referenced to sea level. Events are plotted at the level closest to their depth. Features at 0 km depth are very poorly determined, as well as features near the edges of the grid in the crossections at 3,6, and 9 km depth.

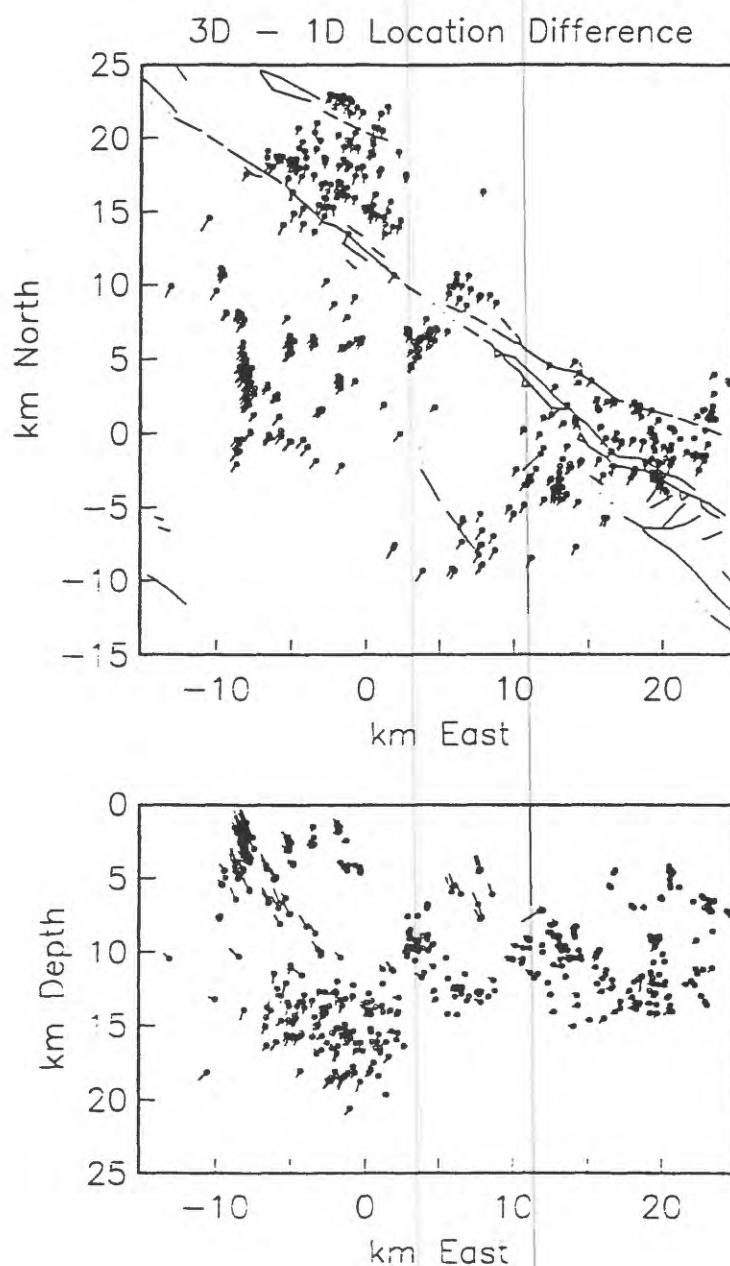


Figure 5. Difference in locations calculated for events in the 3D model vs those calculated in the 1D model. 3D location is at the circle and the length of the line is plotted to the same scale as the axes.

Index Map for Northern California Primary Arc Reoccupation

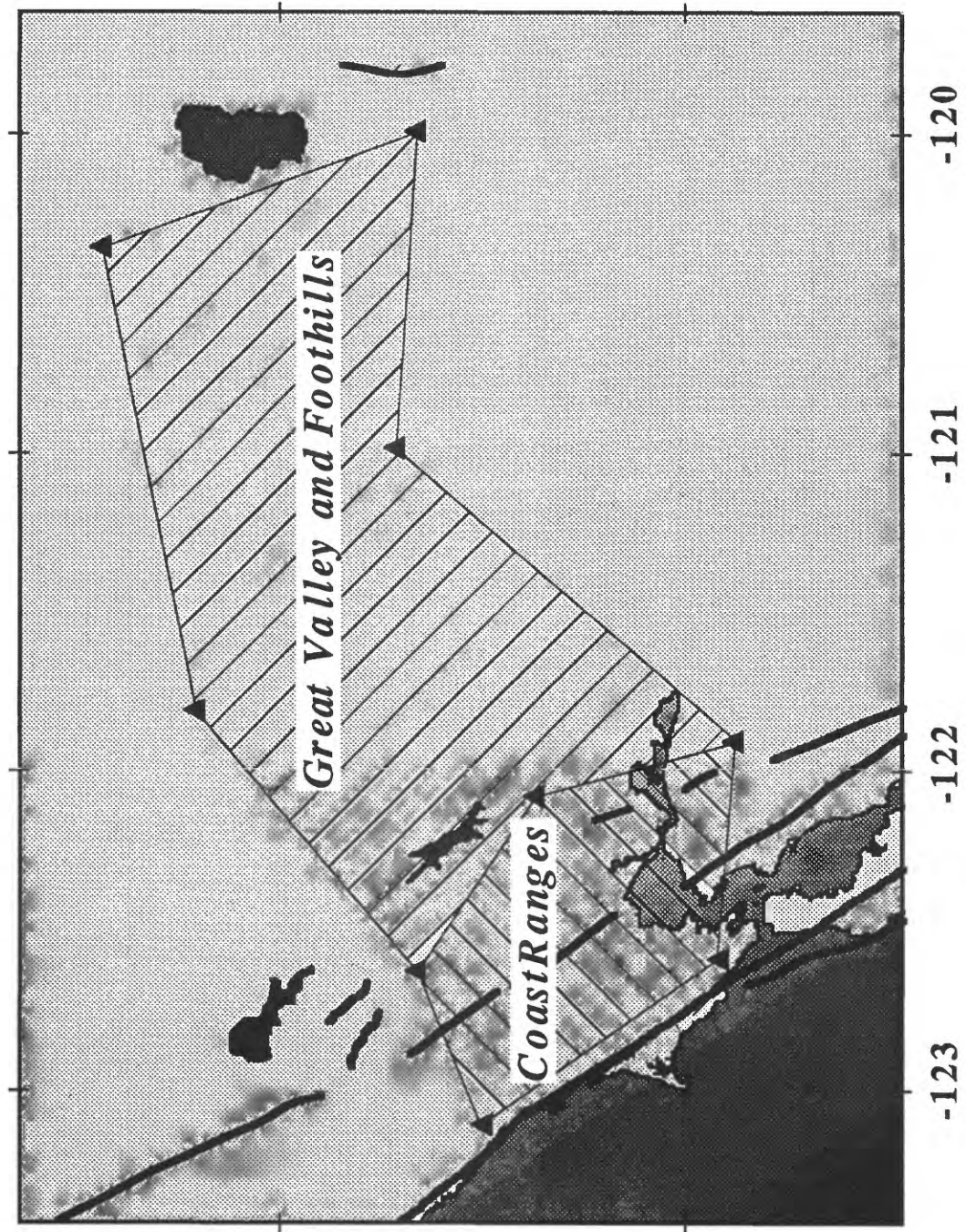


Figure 1

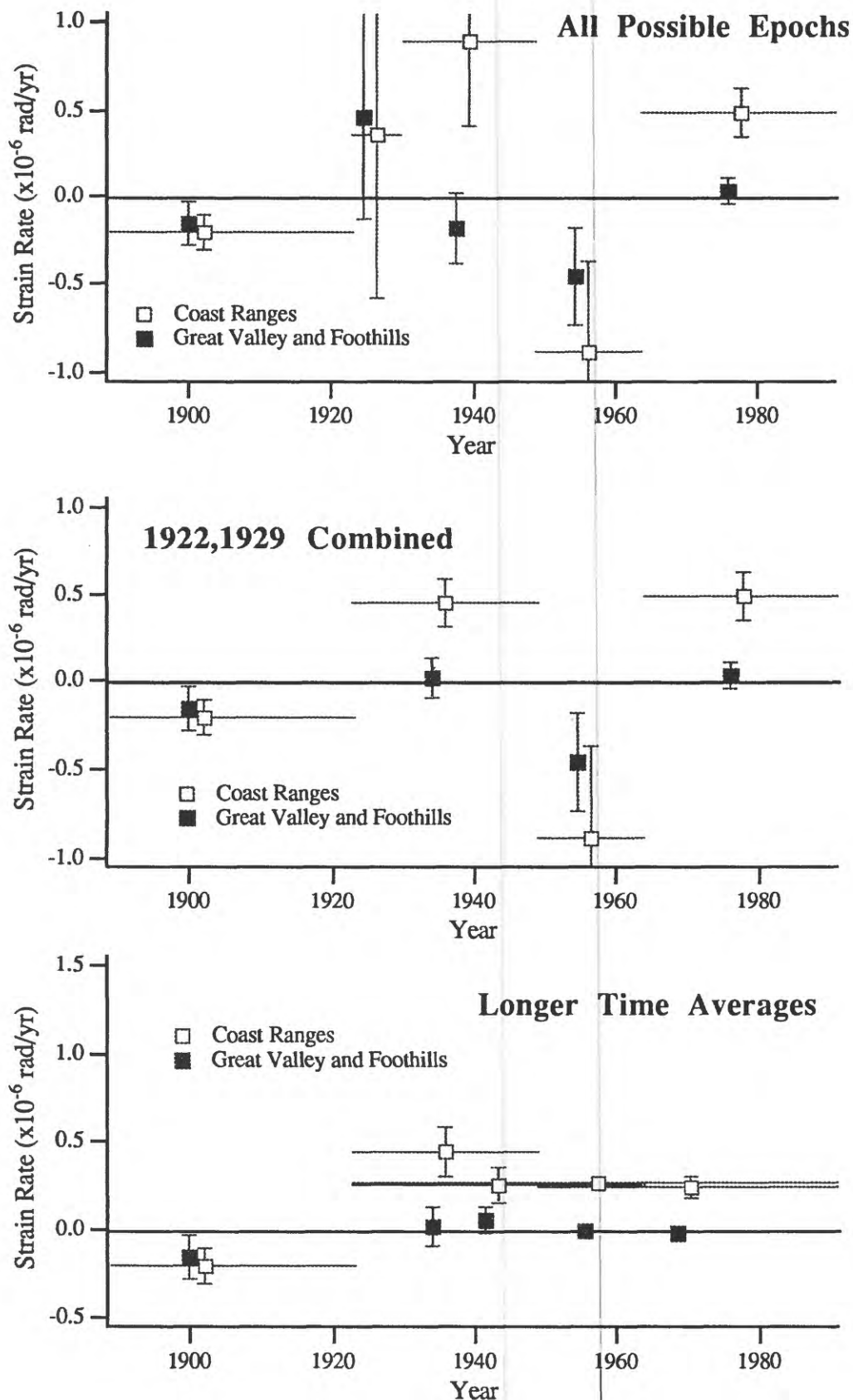
γ_1 ;*Coast Ranges / Great Valley and Foothills*

Figure 2

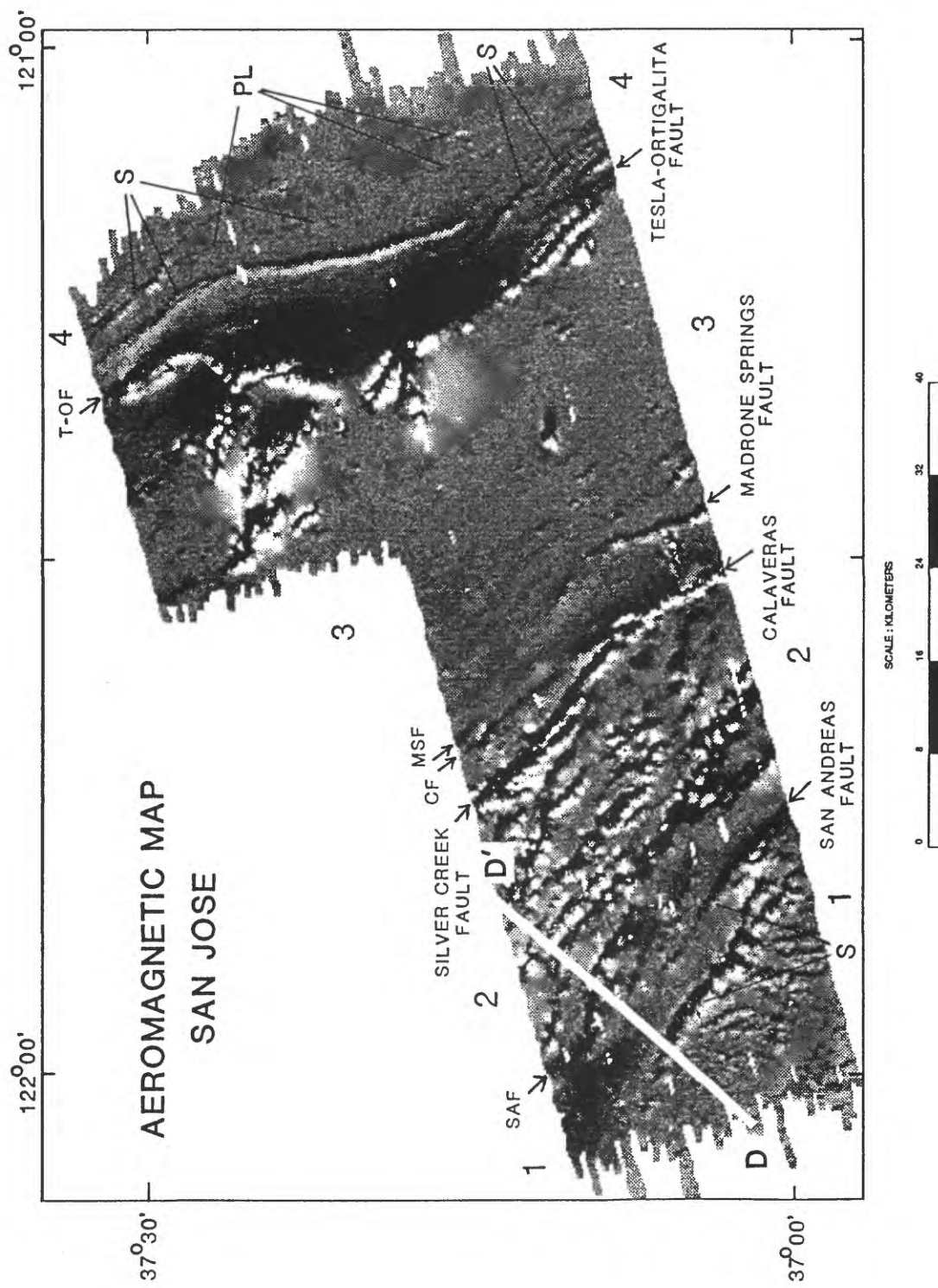


Figure 2. Shaded-relief map of the residual magnetic field along a transect of the California Coast Ranges south of San Jose, California. This presentation emphasizes short-wavelength anomalies. "Sun" azimuth--255°, height--20°. Symbols: "S" magnetic anomalies caused by sedimentary rocks; "PL" magnetic anomalies probably caused by cultural features such as powerlines and pipelines. Most of the unlabeled anomalies are caused by magnetic ophiolitic rocks and associated serpentinites. D-D' is location of modeled profile shown in figure 3.

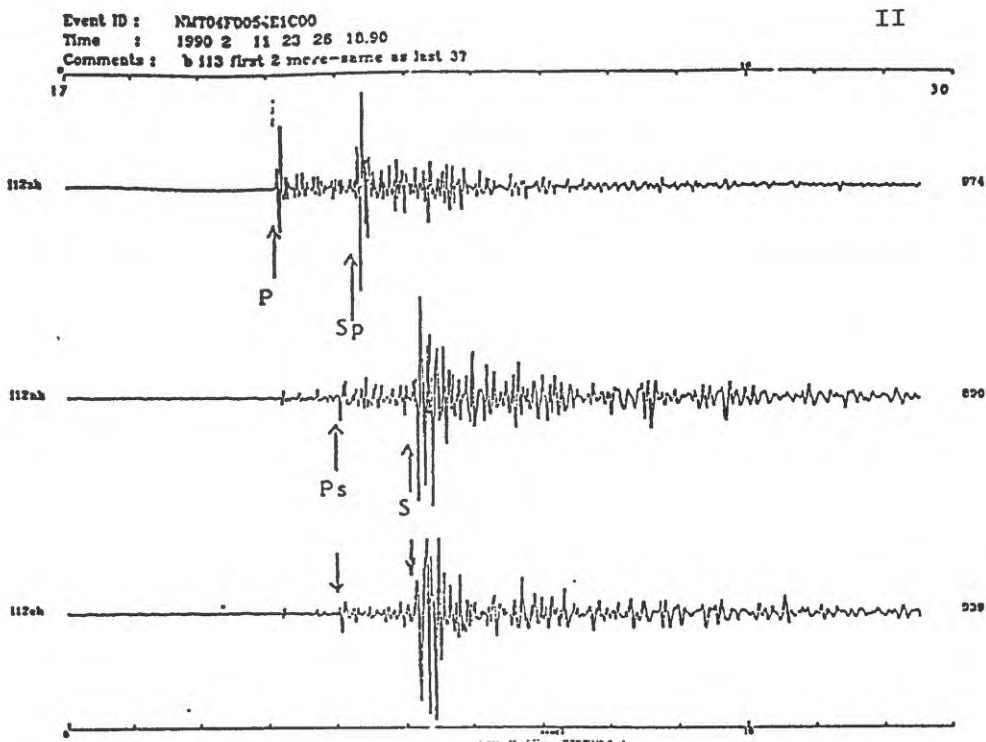


Figure 1. Typical three-component digital seismograms recorded by the PANDA station in the New Madrid seismic zone.

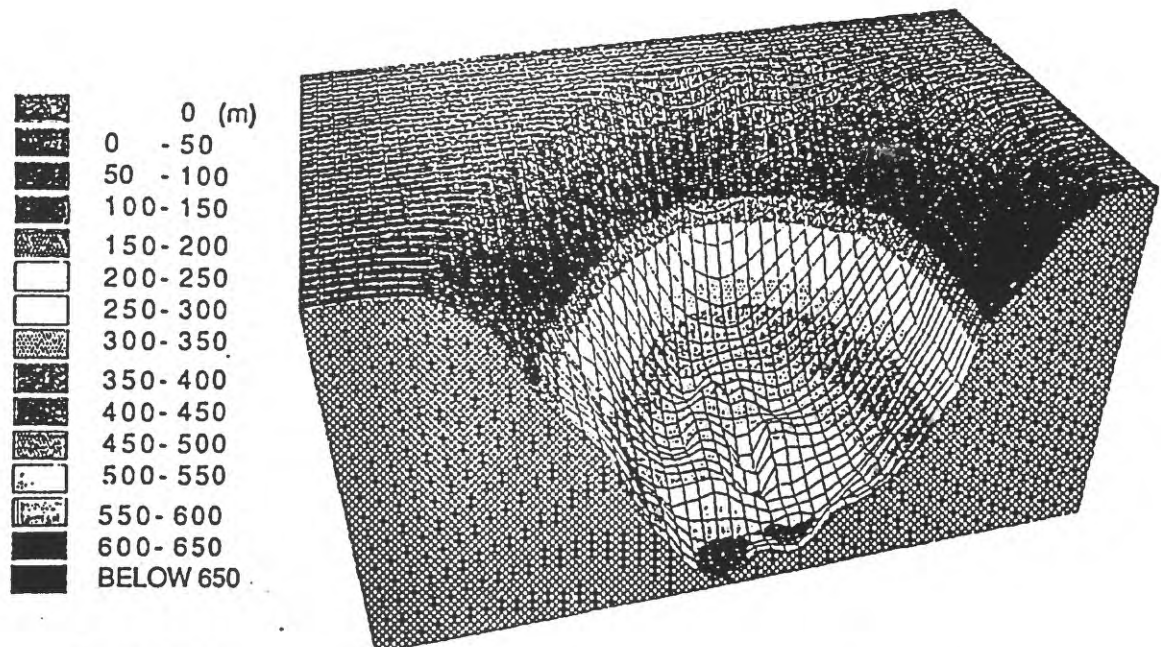
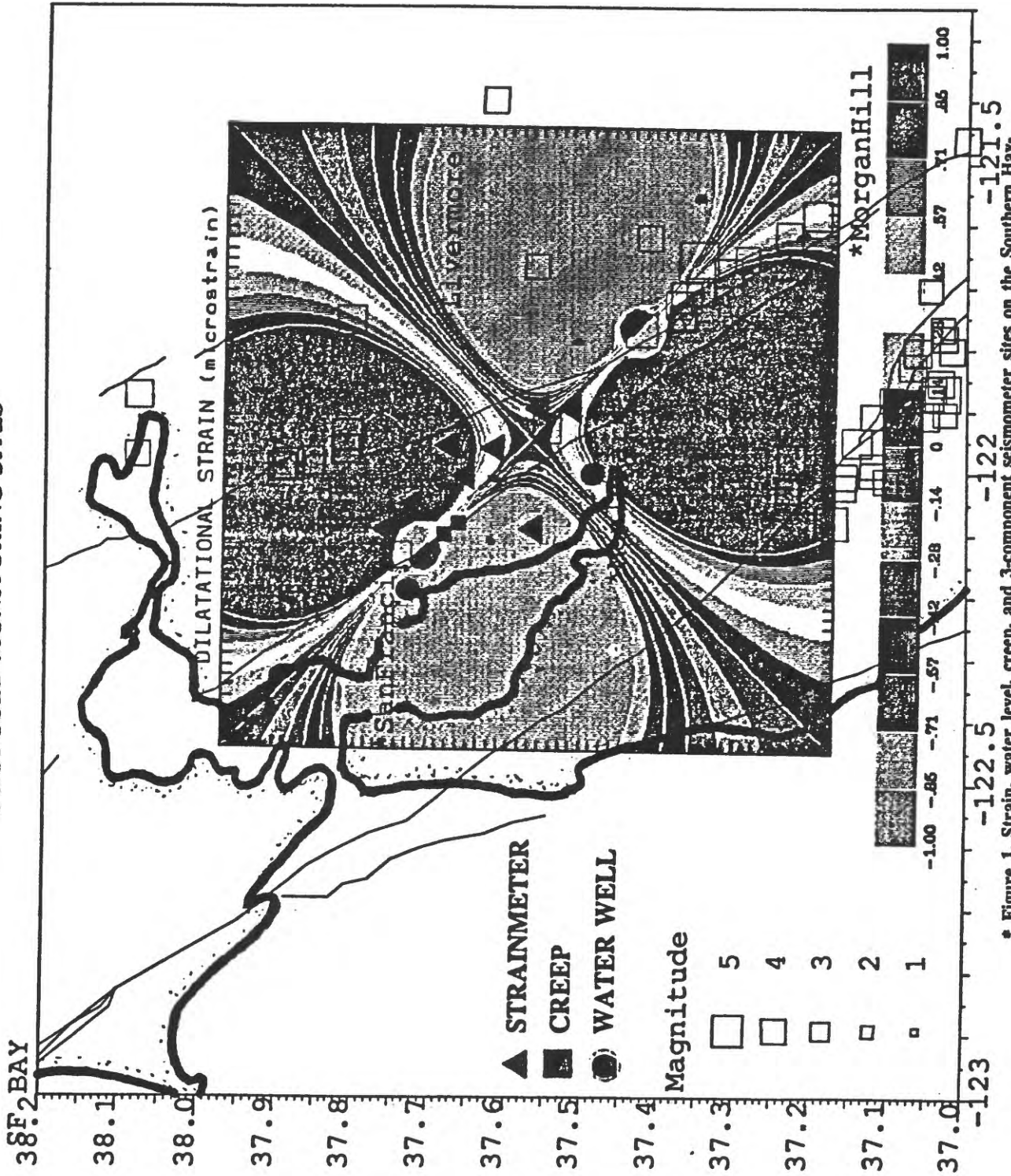


Figure 2. Three-dimensional representation of the geometry of the sedimentary basin in the upper Mississippi embayment determined from the delay time between the direct waves and the converted waves from the bottom of the sedimentary basin.

PROPOSED MONITORING SITES



* Figure 1. Strain, water level, creep, and 3-component seismometer sites on the Southern Hayward fault. The contour plot shows expected strain resulting from a "worst case" scenario for rupture between San Leandro and Calaveras Reservoir as expected for a magnitude 7+ earthquake.

[2] SLOW EARTHQUAKES WITHIN THE SAN ANDREAS FAULT SYSTEM

Slow earthquakes (ie fault slip episodes without seismic radiation in the normal seismic frequency bands) are of three main types: 1) s_p - Slow earthquakes that precede, and evolve, into "normal" earthquakes, 2) s_f - Slow earthquakes that follow "normal" earthquakes, and 3) s_{NS} - Slow earthquakes with no associated seismicity. Evidence for these events has generally been indirect (eg enhanced tsunami generation, anomalous normal modes, earthquake code, etc) with a few exceptions. Quantification of these events is now possible with networks of high-resolution borehole strainmeters recently installed in western U.S., Japan, and Iceland. For the 16 earthquakes with $M_L > 5.5$ that have occurred in California during the past eight years with recording borehole strainmeters less than 10 rupture lengths away, no indication of s_p events has yet been found. s_f followed the April 24, 1984 M_L 6.1 Morgan Hill earthquake and the October 18, 1989 M_L 7.1 Loma Prieta earthquake. More than 30 s_{NS} events have occurred. These events are mostly associated with fault creep episodes or occur within the Long Valley volcanic caldera. For the San Andreas fault system therefore, s_p slow earthquakes appear to be rare (non-existent). s_f events appear to occur more frequently, particularly after large earthquakes, but the total moment release is minimal compared that released seismically. Moment release for s_{NS} events may be larger than that from s_f events but in no case have we seen indications of events on multiple instruments with moments exceeding 10^{24} dyne-cm.

[3] LOCAL DIFFERENTIAL MAGNETIC FIELDS AT PARKFIELD, CALIFORNIA: JULY, 1985 TO JULY, 1991.

A differentially connected array of seven proton magnetometers has operated in the Parkfield region since 1985. Each magnetometer automatically measures total magnetic field intensity to an accuracy of either 0.25 nT or 0.125 nT every 10 minutes. The data are telemetered to Menlo Park, California for on-line processing and analysis to identify tectonomagnetic anomalies related to crustal deformational and/or earthquake processes. During this six year period only three unusual events with marginal amplitudes are observed; 1) from March 1987 to July 1987 a 0.7 nT magnetic field intensity decrease and subsequent increase back to normal is observed at magnetometer TFLM, 2) a 0.6 nT decrease is observed at magnetometer TFLM from the beginning of 1991 to the present, and 3) from about 1989 to the present a rate change of +0.5 nT/a is observed at magnetometer AGDM. The most significant systematic rate increase in seismic moment release in the Parkfield region occurred during the past year while two of the three magnetic events have occurred on two independent magnetometers. However, no seismic events with $M_L > 3.7$ have occurred. While there are suggestions of changes during mid-1987 and mid-1991 in the 2-color laser geodimeter line that monitors horizontal ground displacement near TFLM, these changes are either marginal or complicated by meteorologic effects. Changes in long-term creep rate are unremarkable during this time period. An exception is a change in creep rate at a single creepmeter during mid-1991, which is complicated by meteorologic effects. A model of differential fault slip with little stress and strain redistribution until 1990, but perhaps increasing since then, would best describe these various data at this time.

[4] EARTH STRAIN NOISE FROM DEEP BOREHOLES NEAR THE SAN ANDREAS FAULT SYSTEM FROM 0.01 SECONDS TO 100 MEGASECONDS

Records from an array of borehole strainmeters along the San Andreas fault system are used to determine comparative ground noise over ten decades of frequency (100 to 10^{-8} Hz) in a variety of locations. In particular, we search for differences in response between instruments in 1) fault locked and fault creeping

sites, 2) near-fault and far-fault sites, and 3) near-fault sites and sites in a volcanically active region. Also, we make an initial identification of strain noise attenuation with depth. The eight borehole instruments used are all installed at approximately 200 m depth. Contrary to some expectations, the general characteristics of power spectral density estimates obtained at all sites are similar. With the exception of about 10 dB microseismic noise peaks and 30 to 40 dB peaks at earth tidal frequencies, the spectra decrease from about -80 dB at a frequency of 10^{-8} Hz (100 megaseconds) to about -220 dB at a frequency of 10 Hz (0.1 seconds) in roughly an f^{-2} dependence on frequency. Strain in deep boreholes can thus be measured as well in these different tectonic and volcanically active regions as in aseismic regions. Strain transients are observed infrequently on near-fault instruments, particularly where it is actively creeping, but these do not contribute significantly to noise power spectra determined from long record sections. Initial comparison with near-surface (2m) and intermediate-depth (30m) strain instruments indicates a 10 dB reduction in noise from 2m to 30m and a another 10 dB reduction in noise from 30m to 200m.

[5] BOREHOLE STRAIN ARRAY IN CALIFORNIA

A network of 15 borehole strainmeters along the San Andreas fault zone and in the Long Valley Caldera continue to be monitored and maintained. All instruments are installed at depths between 117-m and 324-m and all are between 1-km and 5-km from the the surface trace of the fault. High frequency dilatometer data in the frequency range 0.005 Hz to 100 Hz are recorded on 16-bit digital recorders with least count noise less than 10^{-11} . Low frequency data from zero frequency to 0.002 Hz are transmitted through the GOES satellite to Menlo Park, CA, using a 16-bit digital telemetry system. At the USGS in Menlo Park the data are displayed in "almost real time" and are continuously monitored with detection algorithms for unusual behavior. Least-count noise is about $5*10^{-12}$ for the on-site digital recordings, and about $2*10^{-11}$ for the satellite telemetry channels. Earth strain tides, strain transients related to fault creep and numerous strain seismograms from local and teleseismic earthquakes with magnitudes between -1 and 6 have been recorded on these instruments. Static moments and total earthquake moments are determined from the co-seismic strains and total strain changes observed with the larger events.

[6] CROWLEY LAKE AND SAN ANDREAS LAKE WATER LEVEL MONITORING

Water level monitoring sites have been installed on Lake Crowley in the Long Valley/ Mammoth Lakes region and San Andreas lake on the San Andreas fault just south of San Francisco. These data provide differential water level measurements (tilt) with a measurement precision of less than 1 mm on baselines of 5 to 8 kilometers. Monthly averages of the data from San Andreas lake between 1979 and 1989 indicate a tilt rate of 0.02 ± 0.08 microradians/yr (down S34°E).

[7] DIFFERENTIAL MAGNETOMETER ARRAY IN CALIFORNIA

We continue investigations of local magnetic fields and relationships to crustal strain and seismicity in the Parkfield region and in southern California. The network consists of 9 stations which are all sampled synchronously every 10 minutes and transmitted with 16-bit digital telemetry to Menlo Park, CA through the GOES satellite. Data are monitored daily with particular attention to the seven stations operating in the Parkfield region of central California and the three stations operating in the Long Valley caldera. At these latter sites a magnetic field anomaly first became obvious in late 1989 and in continuing to the present in concert with anomalous 2-color geodetic strain measurements and spasmodic swarms of minor earthquakes.

[8] **CONTINUOUS HIGH PRECISION BOREHOLE STRAIN MEASUREMENTS NEAR THE LOCKED AND CREEPING SECTIONS OF THE SAN ANDREAS FAULT**

Deep-borehole strainmeters have been operating since 1984 at sites near the northern and southern creeping/locked transition zones and in the "Big Bend" region of the San Andreas fault in northern and southern California, respectively. These instruments resolve strain changes to better than 1 part per billion (ppb) over periods of months to minutes. The last five years of strain data show long periods of uniform crustal strain, infrequent episodes of aseismic strain sometimes resulting from aseismic fault creep, and high frequency straingrams and strain field offsets generated by local earthquakes. Whereas simple views of the earthquake rupture process have suggested that: 1) substantial non-linear deformation occurs prior to rupture, 2) the scale of this deformation exceeds the eventual earthquake rupture dimensions, and 3) the properties of near-fault materials may vary with time and location, these high resolution borehole strain recordings indicate: 1) minimal short-term non-linear precursive strain occurs, 2) the size of fault patches that initiate failure are probably less than a few hundred meters in size while the eventual earthquake rupture dimensions can be several tens of kilometers, 3) no evidence of variations in near-field material properties, and 4) strain offsets from local earthquakes that are largely transmitted elastically despite complex geology and fault geometry. In the case of the recent October 18, 1989, M_L 7.1 Loma Prieta earthquake, strain data from two instruments near San Juan Bautista, 5 km to 10 km southeast of the final southern extent of the rupture, indicate that any precursive failure in the hypocentral region (with a form similar to that during the earthquake) was at least a 1000 times smaller in the minutes to months before the earthquake. This, in turn, constrains the maximum amount of horizontal or vertical displacement in the hypocentral region to be at most, a few millimeters, if any occurred at all. As more borehole strainmeters are installed, these data will continue to place increasingly tighter constraints on physical processes that occur at the earthquake source.

[9] **ULTRA BROAD BAND DATA FROM AN ARRAY OF DEEP BOREHOLE STRAINMETERS ALONG THE SAN ANDREAS FAULT SYSTEM**

Records from an array of borehole strainmeters along the San Andreas fault system are used to determine comparative seismic response over nine decades of frequency (100 to 10^{-7} Hz) for local earthquakes, teleseismic earthquakes and "slow" earthquakes. The dynamic range of the borehole instruments exceeds 140 dB. Comparison of the short-period portion of the earth-strain noise spectrum (20 to 500 seconds) with average spectra determined from pendulum seismometers suggest that the observed seismic noise is predominately dilational energy. Simultaneous strain and seismic velocity measurements of incident P- and S-wave amplitudes are used to estimate wavefield inhomogeneity, free surface reflection coefficients, and local P velocity. Estimates of these parameters for moderate magnitude ($M_W \approx 6$) earthquakes agree well with those calculated from an anelastic half-space model with incident inhomogeneous waves. Total seismic moments determined from zero frequency strain steps for approximately 40 moderate magnitude earthquakes are approximately 20% greater than seismic moments determined from displacement spectra from instrument corrected seismic velocity data. This would indicate that only minimal aseismic moment release accompanies seismic moment release for these earthquakes.

Reports

Mueller, R. J., M. J. S. Johnston, and J. O. Langbein, 1991, Possible Tectonomagnetic Effect Observed from Mid-1989 to Mid-1990 in Long Valley Caldera, California. *Geophys. Res. Lett.* **18**, 601-604.

Hill, D. P., M. J. S. Johnston, J. O. Langbein, C. E. Mortensen, A. M. Pitt, and S. Rojstaczer, 1991, Response Plans for Volcanic Hazards in the Long Valley and Mono Craters Area, California. U. S. Geological Survey Open-File Report 91-270

Johnston, M. J. S., 1991, Recent Seismomagnetic and Volcanic Events: Implications for Physical Mechanisms, Abs for IUGG/IASPEI Meeting, August 11-24, Vienna, IASPEI Session SW11, p264.

Johnston, M. J. S., and A. C. Fraser-Smith, 1991, On Physical Mechanisms Pertaining to the Loma Prieta Earthquake ULF Electromagnetic Emissions, Abs for IUGG/IASPEI Meeting, August 11-24, Vienna, IASPEI Session SW11, p262.

Johnston, M. J. S., 1991, Earth Strain Noise from Deep Boreholes Near the San Andreas Fault System from 0.01 Seconds to 100 Megaseconds. *Trans. Am. Geophys. Un.*, **72**, 292.

Linde, A. T., M. T. Gladwin, and M. J. S. Johnston, 1991 Tidal Strain Response Before the 1989 Loma Prieta Earthquake: An Unsuccessful Search For Variations in Mechanical Properties. *Geophys. Res. Lett.* , (in press).

Johnston, M. J. S., 1991, Slow Earthquakes Within the San Andreas Fault System. *Trans. Am. Geophys. Un.*, **72**, 484.

Johnston, M. J. S., G. D. Myren, A. T. Linde and M. T. Gladwin, 1991. High Precision Continuous Strain Measurements near the Locked and Creeping Sections of the San Andreas fault. Joint US/China Workshop on Focused Earthquake Prediction Experiments. San Juan Bautista, California, 16-19 September, 1991.

Johnston, M. J. S., R. D. Borcherdt, G. D. Myren, and G. Glassmoyer, 1992. Ultra Broad-band Data from an array of Deep Borehole Strainmeters along the San Andreas Fault System, Workshop on "Frontiers of Broad Band Seismology", Seismographic Station, U.C. Berkeley, January 9-10, 1992.

**Marine Seismic Investigations
of the East Bay Faults
14-08-0001-G2123
01 Aug 91-31 Jul 92**

David L. Jones and Thomas V. McEvilly
Seismographic Station
Dept. of Geology and Geophysics
University of California
Berkeley, CA 94720

Phone: (510) 486-7347
FAX: (510) 486-5686
e-mail: tvmcevilly@lbl.gov

Project Description

This UC/USGS cooperative project supported the acquisition of nearly one million traces of multichannel airgun seismic profiling data from the Sacramento river delta through Carquinez strait into San Pablo and San Francisco bays, and then out to sea nearly 100 km beyond the Golden Gate. The primary purpose of the survey, now known as BASIX (Bay Area Seismic Imaging Experiment), is an investigation of the crustal structure and fault geometries within the complex plate boundary in the Bay Area. The survey, conducted in September, 1991, employed the USGS research vessel S.P. Lee with a source array of 12 airguns, and a 120-channel buoyed, telemetered receiver array which was moved each day along the line. The USGS contribution to the project was the ship and crew, the airguns, navigation, and the DFSV recording system. The UC Berkeley contribution was the subcontract to the commercial geophysical contractor for the telemetry system, at a cost which exhausted the funds provided in the award. We have asked for a supplement and no-cost extension to the award for FY92 to allow processing and interpretation of the data acquired.

FY91 Accomplishments (01-30 September)

Despite only two month's activity in FY91 under this award, much was accomplished, and the total funding was expended:

Survey execution The survey was conducted in September. Data reduction is very involved due to the non-coincident source and receiver lines (and the fact that the ship traversed each line segment in both directions, on different courses), and the current-induced shift of the buoyed receivers during a night's recording. Navigation by GPS and Del Norte must be recovered from the onboard computer disks and merged with the DFSV records. This merging of the full geometry and trace data will not be completed before year's end. We have extracted one night's trace data (spread 108) and a receiver gather of that night's shots is presented in Figures 1 and 2.

Complementary studies Land receiver arrays were deployed, supported by other resources, by UC Berkeley, USGS, and Stanford scientists, to complement the marine data and to extend survey coverage to wide angle. An example of land recording is illustrated in Figure 3 in a relatively short offset land-receiver gather for the same source array shown in Figure 2 for a marine receiver. A large number of land sites were occupied throughout the survey. High-resolution data also have been acquired.

AGU Poster session A special poster session has been arranged at the Fall AGU Meeting on the BASIX experiment. All aspects of the project will be featured.

FY92 Schedule

The FY91 effort exhausted the available funding, as reduced in the actual award, with the data acquisition subcontract. No support remains with which to reduce, analyze and interpret the data - researchers participating in the experiment and data reduction until now have been supported by other projects. Assuming the supplement request is granted, we will be able to devote the necessary human resources to the study in FY92.

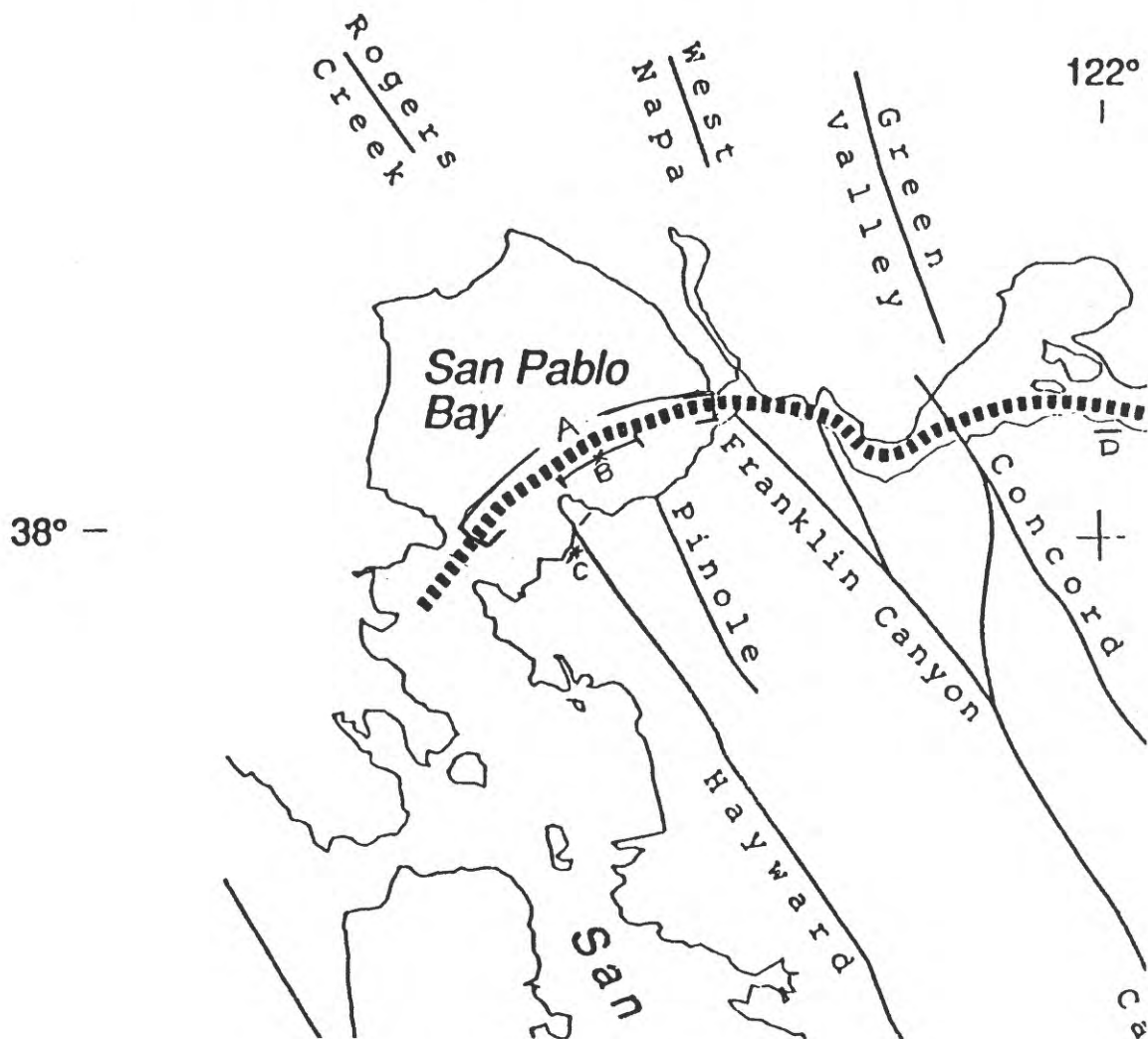


Figure 1. Map of early BASIX survey line, showing line 108 (track 'A', one night's shooting, some 700 shots) illustrated in Figures 2 and 3. Segment 'B' is the receiver spread for line 108. Figure 2 is a marine receiver gather from near the center of the spread. Figure 3 is a receiver gather from a land sensor array on Point Pinole (segment 'C'), near the western end of line 108. Segment 'D' is another land array deployed for that portion of the survey crossing the Antioch and Concord faults.

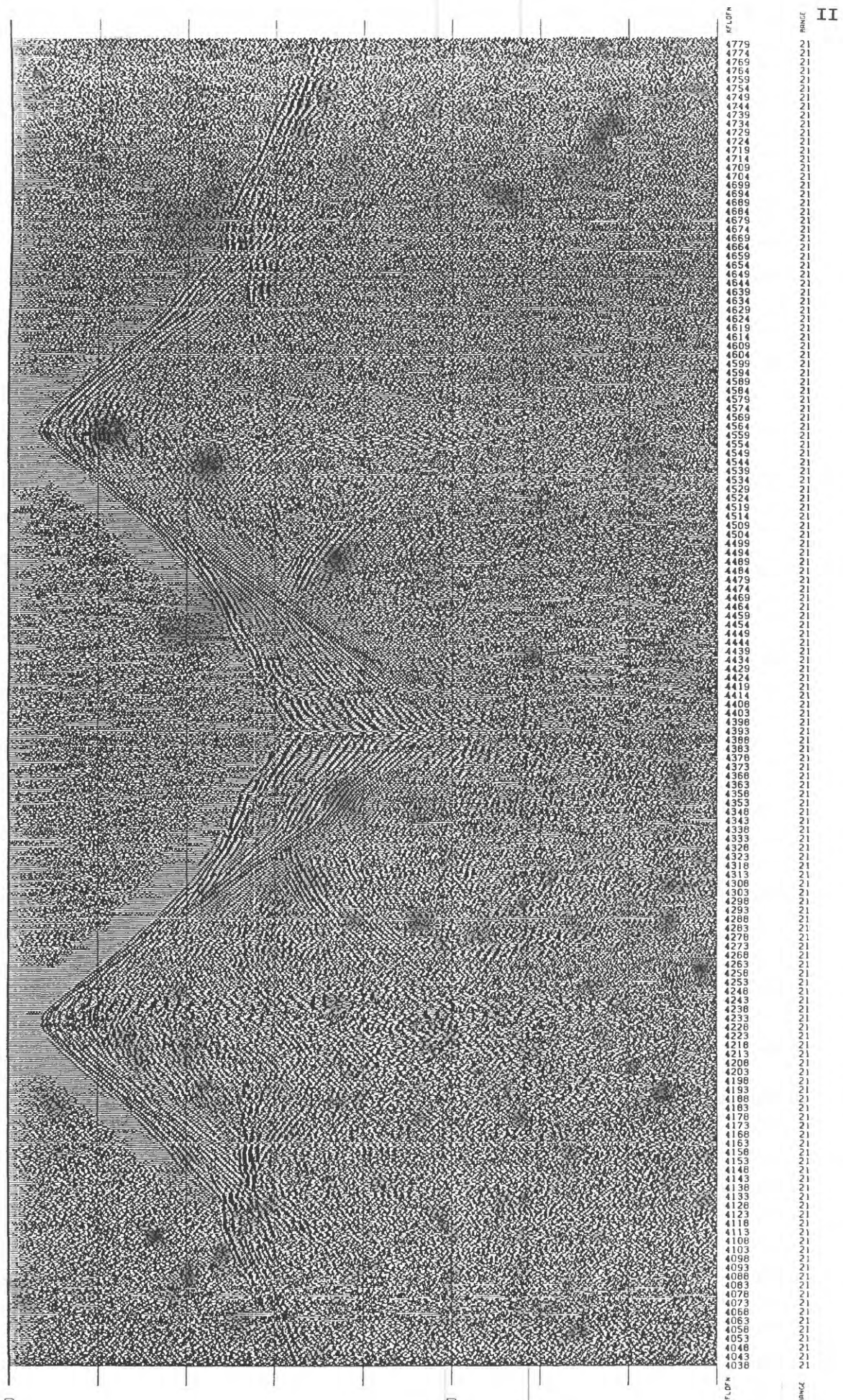


Figure 2. Receiver gather for a sensor near the center of spread 108. Eight seconds of data are shown. Apparent symmetry of the gather reflects the 'two-way' shooting of the line segments each night. The receiver array was fixed and the ship in the course of each night's shooting ran upstream and downstream tracks.

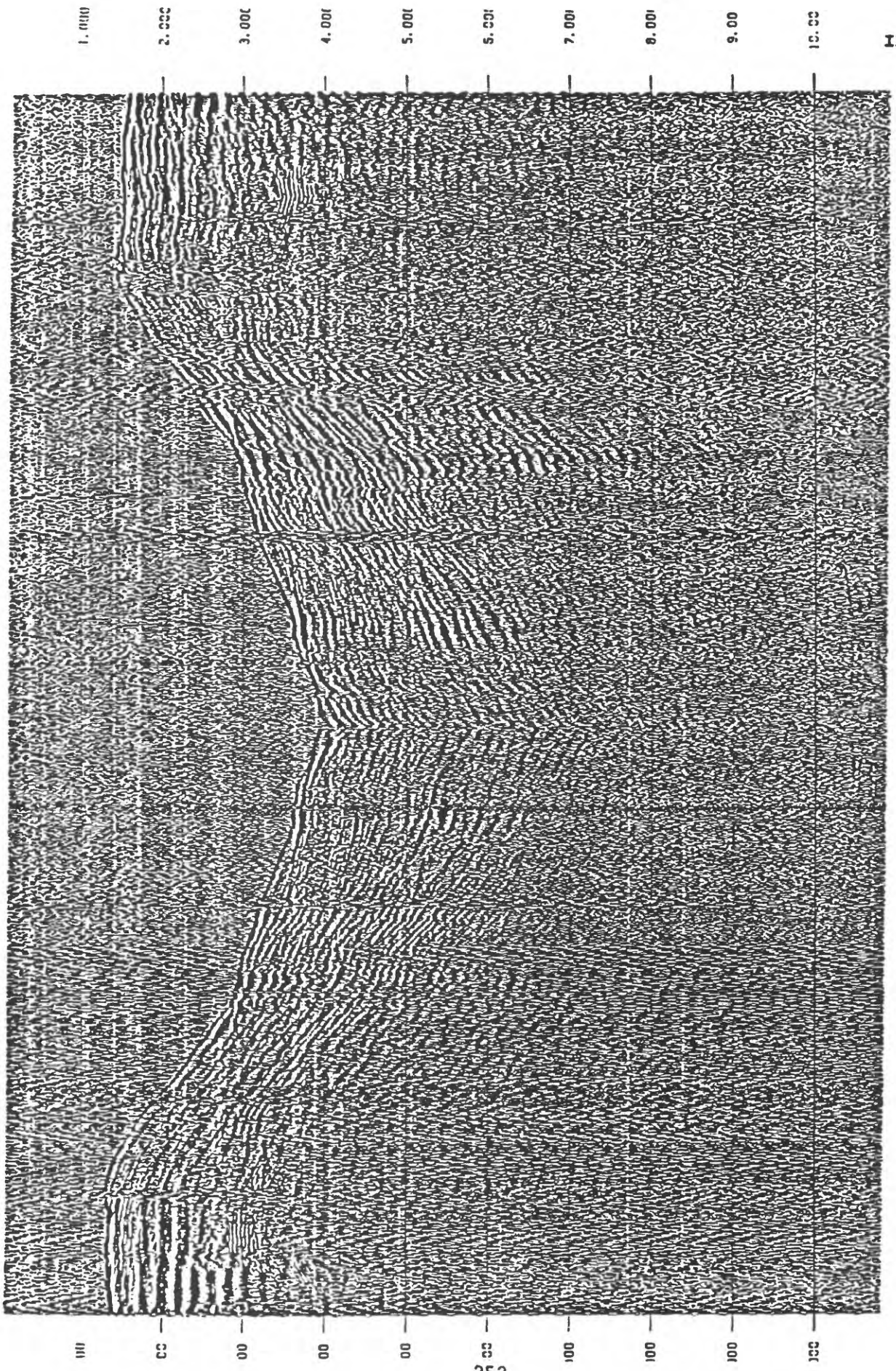


Figure 3. Receiver gather for a land sensor from the Point Pinole (west) array which was deployed as the ship traversed the Hayward fault crossing in San Pablo Bay. This sensor was located on land near the west end of the marine receiver array, where the ship track turns south, on a course roughly equidistant from the receiver, explaining the near-constant offset at the ends of the symmetrical gather.

Tectonics of the Chabot-Mission faults.

Award Number: 14-08-0001-G2136

David L. Jones

Department of Geology and Geophysics

University of California

Berkeley, CA 94720

415-642-2514

Investigations undertaken in FY 1991.

This investigation of the Chabot-Mission fault system is aimed at increasing our understanding of an important seismogenic zone along which slip apparently is being transferred from the Calaveras fault to the Hayward fault. Despite active seismicity along this transfer zone, no surface rupture has been detected, and neither the Chabot nor the Mission faults are included in Alquist-Priolo zoning. Because the tectonic history of these faults is so poorly understood, we are currently unable to evaluate their potential for producing damaging earthquakes in the future, nor has the style of expectable fault movement (e.g., strike slip, dipslip, or oblique slip) been clearly established.

The specific aims of this study are to: 1) determine the width of the zone of deformation that can be attributed to movement along the Chabot-Mission faults, and attempt to delineate the principal strand(s) along which the latest detectable movement has occurred; 2) establish the structural style of deformation across the entire width of the fault zone to provide long-term strain indicators necessary to establish the kinematic history of the faults; 3) search for stratigraphic and structural ties across the fault zone that will permit an assessment of the long-term history of displacement along the seismogenic zone; and 4) search for evidence that will establish the youngest episode of movement along these faults.

Preliminary investigations of the Chabot-Mission fault system commenced in August, 1991, with reconnaissance field studies in the Niles Canyon, Morrison Canyon, and Alum Rock Creek regions, in order to characterize the style of deformation within the fault zone and to collect samples for paleontologic examination. Based on these scattered and incomplete observations, the following tentative conclusions can be drawn:

1. The Mission fault system is a wide and complex fault zone that exhibits a significant component of west-vergent thrust displacement that locally places strata of Cretaceous age over Plio-Pleistocene deposits;
2. Several important contacts between stratigraphic units that previously were interpreted as depositional, are, in fact, significant faults, so the number of recognized fault strands within the fault zone has increased.

BASIX Seismic Reflection Lines and Wide-angle Recordings

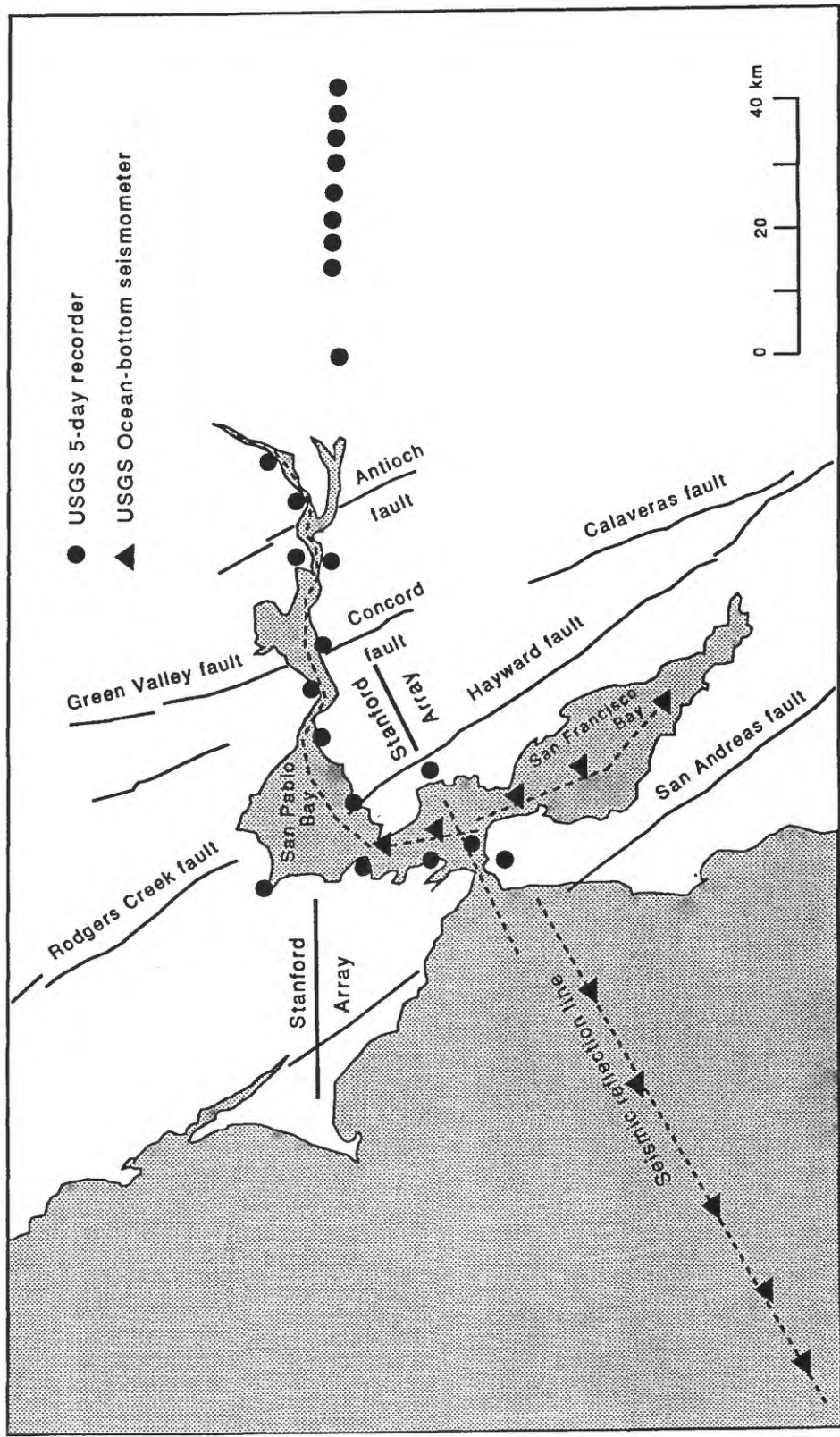


Figure 1. Index map showing location of seismic reflection lines and wide-angle recorders. CALNET stations, which also recorded the airgun signals, are not shown in this figure.

Results

1. Deep-penetration Multichannel Seismic Reflection Profiling in San Francisco Bay

The vast amount of multichannel seismic reflection data recorded by the S.P. Lee are in the process of being demultiplexed and edited at the DISCO Seismic Reflection Processing Center in Menlo Park. The data, recorded as common shot gathers, are being sorted to common receiver gathers to facilitate the editing and processing of the data. About 30% of the data have been played out, we expect to complete the processing of these data in FY92. Preliminary analysis of these data indicate the presence of several reflections in the upper 6 s of the crust (see example in Figure 2), which we expect to help us delineate the subsurface geometry of the major faults in the Bay Area.

2. Wide-angle Seismic Reflection and Refraction Profiling

Data from ten OBS wide-angle stations recorded by the USGS have been reduced and plotted. Five of these stations recorded along the offshore California margin. The data recorded are of high-quality (see Figure 3) and will be used to constrain the velocity and crustal structure of the continental margin. The remaining OBS profiles were acquired in San Francisco Bay. These profiles show mid- to lower-crustal reflections which will be important for the evaluation of the along-strike continuity of crustal reflectors.

Data recorded by the USGS five-day recorders are in the initial stage of playback. Preliminary plots of selected portions of these data indicate that signals generated by the airgun array are observed to ranges in excess of 140 km, and these data should allow resolution of the crustal structure and velocities in the vicinity of the East Bay faults (Figure 4). Due to the high-density of five-day stations along the Bay, we also plan to construct a low-fold seismic reflection profile along the multichannel reflection data to determine whether recording the airgun signals onshore produces a higher-quality reflection image of the middle to lower crust.

Wide-angle data recorded by Stanford University using PASSCAL Reftek recorders are also in the initial stage of analysis. Preliminary plots show that the quality of these data is similar to that recorded by the five-day recorders, and should provide important constraints on the existence of major structural changes across the main seismogenic faults in the Bay Area.

Wide-angle data recorded by the CALNET array is in the process of being dubbed and analyzed. We plan to invert the first arrivals on these data using tomography to obtain a 3-dimensional seismic velocity model of the crust in the Bay Area. Data from selected CALNET stations will also be used to supplement the recordings made by the USGS OBSs and five-day recorders as well as those obtained by the PASSCAL Refteks deployed by investigators from Stanford University.

3. High-Resolution Seismic Reflection Profiling

These data were acquired to determine the Neogene stratigraphy and deformation patterns in the San Francisco and San Pablo Bays. The analog data are in the process of being analyzed for the AGU Meeting in December, but reveal a number of important, if currently poorly understood, structures in the Neogene record. The tilting and geometry of observed reflections in San Pablo

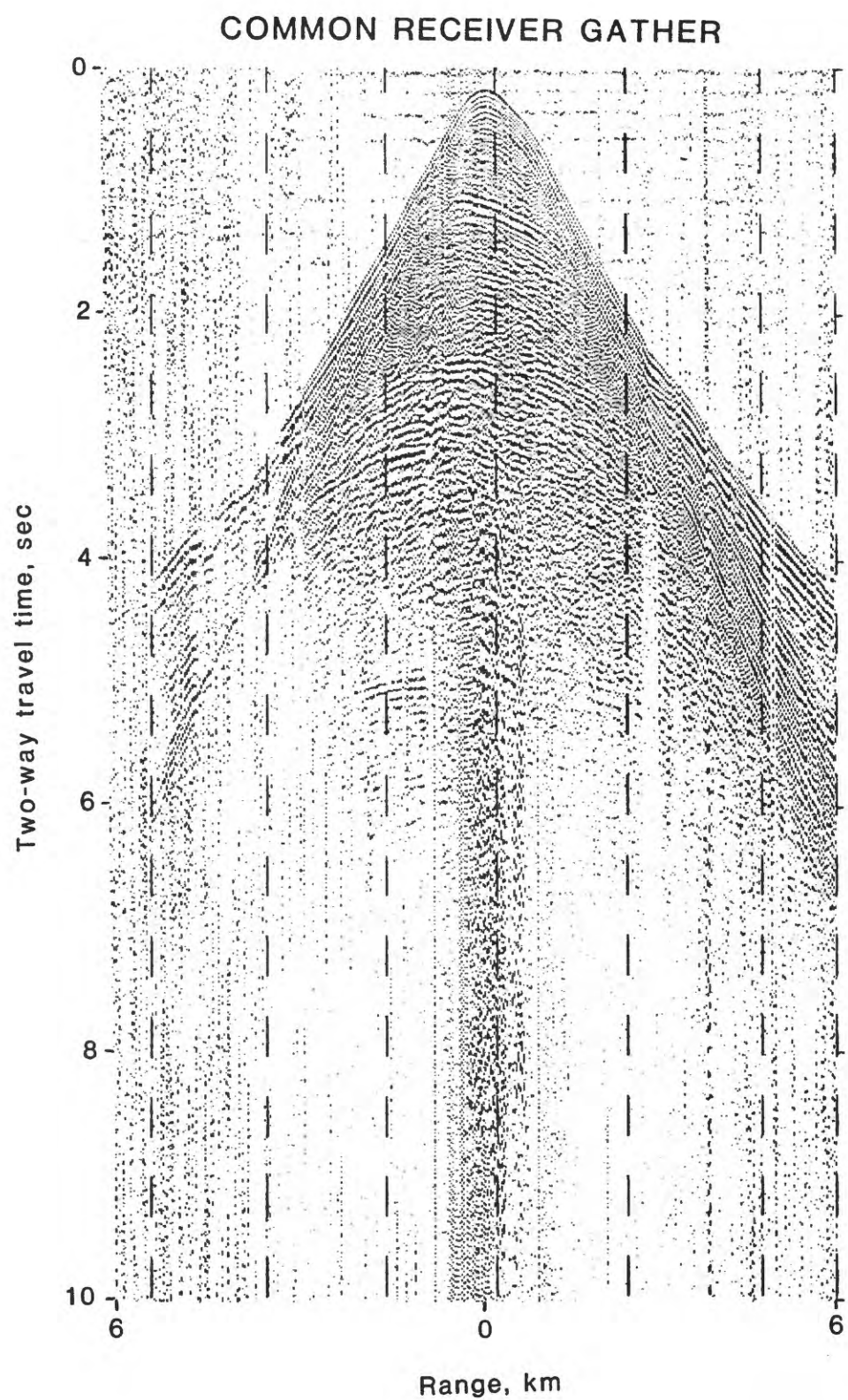


Figure 2. Example of seismic reflection gather acquired using tethered hydrophones recorded on the S.P. Lee.

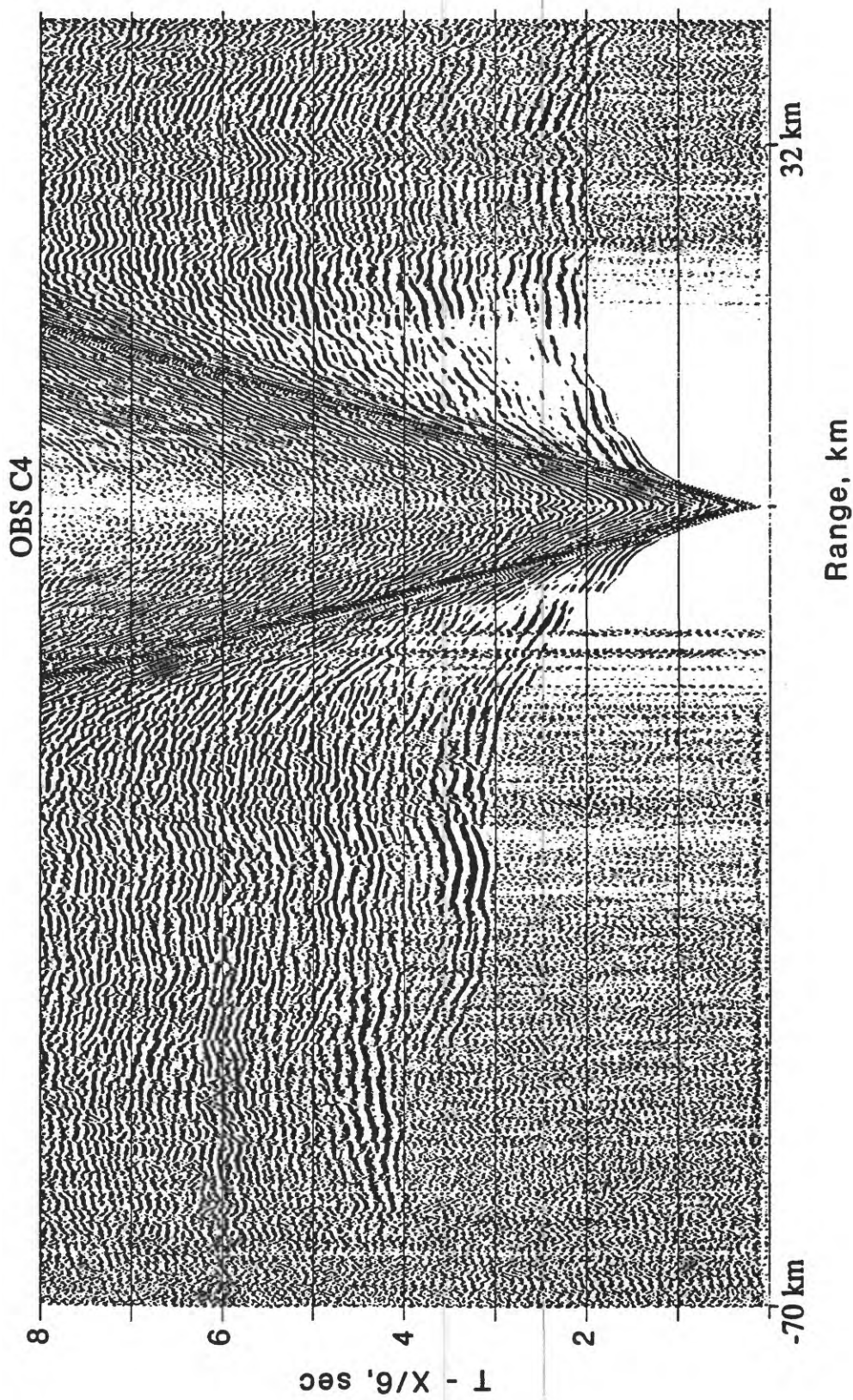


Figure 3. Example of an ocean-bottom seismometer recording from the offshore seismic reflection profile of the California continental margin.

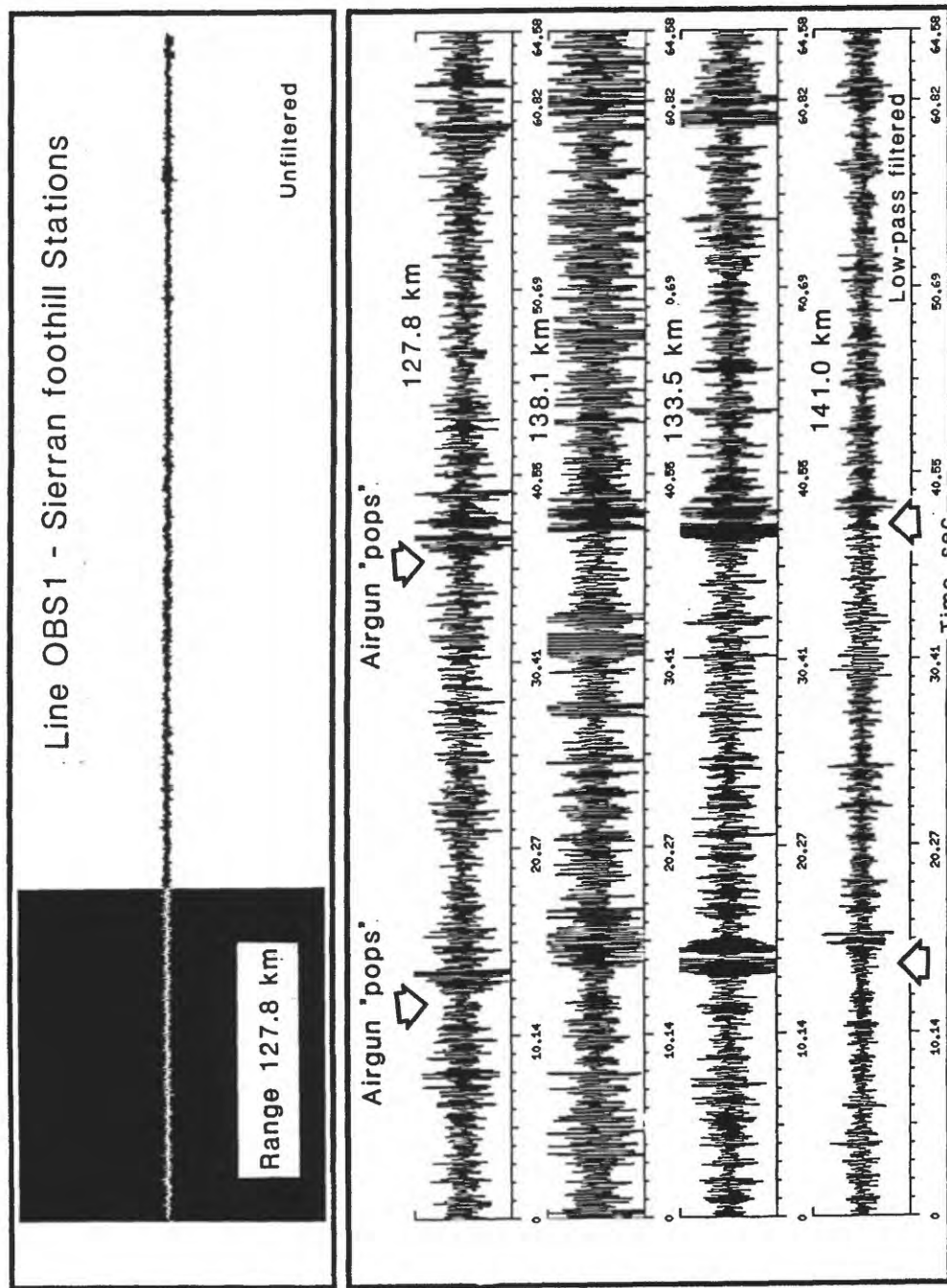


Figure 4. Example of data recorded by 4 different USGS five-day recorders in the western Sierran foothills (near Copperopolis) from airgun shots in San Francisco Bay along the OBS deployment. There is a dramatic improvement in signal levels after simple low-pass filtering.

Bay correlate with interpretations of the prominent gravity anomaly over this bay. Basin-filling sediments thicken westward while clear evidence of faulting and disruption can be observed on the eastern side of the bay in the vicinity of the Rodgers Creek fault. Faulting along the Hayward fault is observed, although the offsets are subtle and will require much more analysis before the observed deformation can be fully understood. Observed scour and fill near Pittsburg can be related to the last glacial lowstand, and provide the basic framework to understand the original shape of the bay and recent stratigraphy. The digitally recorded high-resolution data are being processed, mainly to suppress multiple reflections.

Reports

Anima, R., and P. Williams, High resolution marine-profiling in BASIX: Complex structures of major East Bay faults, EOS Trans. AGU, 72, 446, 1991.

Brocher, T.M., S.L. Klemperer, U.S. ten Brink, and W.S. Holbrook, Wide-angle seismic profiling of San Francisco Bay Area faults: Preliminary results from BASIX, EOS Trans. AGU, 72, 446, 1991.

Furlong, K.P., J. McCarthy, T. McEvilly, Geometry and kinematics of the Pacific-North American plate boundary in the San Francisco Bay Area: A testable model for BASIX, EOS Trans. AGU, 72, 445-6, 1991.

Hart, P.E., and R. Clymer, Geometry of San Francisco Bay Area faults: Preliminary results from BASIX, EOS Trans. AGU, 72, 446, 1991.

Holbrook, W. S., and U. S. ten Brink, Preliminary cruise report - San Francisco Bay and Margin Seismic Experiment, Ocean Bottom Seismometer Operation, Sept. 1991. 17 pages, 11 figures, Sept. 1991.

Jones, D.L., A.J.H. Lomax, and T.V. McEvilly, BASIX Motivation: Tectonics of a transpressive plate boundary - A new paradigm for the Central California Coast Ranges, EOS, Trans. AGU, 72, 446, 1991.

Klemperer, S.L., and BASIX Working Group, Bay Area Seismic Imaging eXperiment: Fan-profiling to Image the maximum depth of penetration of the San Andreas, Hayward, and Calaveras faults, EOS, Trans. AGU, 72, 446, 1991.

ACTIVE MARGIN TECTONICS, PACIFIC NORTHWEST REGION

9910-04492

P. A. McCrory

Branch of Engineering Seismology and Geology
U. S. Geological Survey
345 Middlefield Road, MS 977
Menlo Park, California 94025
(415) 329-5677 or (FTS) 459-5677

Investigations undertaken

FY91 research focused on the record of late Cenozoic tectonism preserved along the northwestern Pacific margin. Current work involves detailed study of sedimentary sequences in coastal southern Washington selected to obtain as complete a time record as possible and to document regional variation in the amount of vertical tectonic movement. FY89 field investigations identified several sites along coastal Washington with geomorphic and stratigraphic evidence of youthful folding, faulting, uplift or subsidence. Strata at these sites are being measured and sampled in detail for tephra, microfossil, depositional facies, and geohistory-backstrip analyses.

Geologic field investigations during this reporting period included stratigraphic measurement, description, and sampling of the North Pratt Cliffs, Cape Elizabeth, and Whale Creek-Raft River sections of the Quinault Formation.

Construction of a geologic cross-section of the tilted and faulted Pleistocene deposits exposed in the sea cliffs in the Raft River area to quantify the amount of tectonic shortening.

Field reconnaissance in the Raft River area for evidence of recent tsunami-subsidence occurrence. Submission of fossil wood material for ^{14}C age dating of a possible tsunami-subsidence deposit.

Collection of peat and fossil shell material from an upper Pleistocene deposit in the Kalaloch area for Ur-series and ESR age dating.

Lab investigations during this reporting period included microscope analysis of microfossil material from sedimentary rock samples collected in FY89 and processed in FY90 and FY 91.

Results obtained

1. The three sedimentary sequences measured and described during FY91 display evidence of syndepositional deformation such as slumping, liquification, sand venting which may be related to seismic shaking. Contacts between the Quinault Formation and the underlying accretionary prism rocks (Hoh Formation) suggest active diapirism during deposition of the Quinault Formation. There is some evidence that diapirism continued into the late Quaternary.
2. Documented offsets of an upper Pleistocene deposit at several sites along the coast. Some offsets clearly reflect tectonic activity, others may be caused by landsliding.
3. Rock samples collected in FY89 have been reprocessed to concentrate microfossils for analyses of age and uplift data.
4. Continued analyses of sedimentary rock samples collected in southern Washington in FY89 for age and uplift data.

Reports published

None this reporting period.

SEISMIC WAVE MONITORING AT PARKFIELD, CALIFORNIA

14-08-0001-G1703

T.V. McEvilly, R. Clymer, T. Daley, B. Foxall, E. Karageorgi, A. Michelini
 Seismographic Station, University of California, Berkeley, CA 94720
 and
 Earth Science Div, Lawrence Berkeley Lab, Berkeley, CA 94720

INTRODUCTION

Three programs of seismic wave analysis continue: Earthquake recording with the high-resolution seismic network (HRSN), begun in December, 1986; controlled-source monitoring with HRSN begun in June, 1987; and controlled-source experiments with the Varian well vertical array (VWVA), begun in November, 1987.

The HRSN (Figure 1) consists of ten, 3-component, borehole seismometers surrounding the 1966 Parkfield epicenter. Data-acquisition features digital telemetry with 125-Hz bandwidth and 16-bit resolution, and can operate in external-trigger (*i.e.*, controlled-source) or event-trigger (earthquake) modes. Network characteristics are shown in Table 1.

The VWVA extends to 968m depth at a site 2 km from the San Andreas fault (Figure 1), close to the nucleation zone of the expected magnitude 6 Parkfield earthquake. Early vertical seismic profile (VSP) results indicating local anisotropy were shown in Daley and McEvilly, 1990. Data have been recorded on a Sercel 338 96-channel reflection system.

INVESTIGATIONS

1) *Earthquakes.* Local microearthquakes of magnitude about -0.5 to about +2 are routinely recorded on scale. A 3-D velocity model and a high-precision relative hypocenter location procedure for clustered events with similar waveforms have been developed, and are now being used for high-resolution analysis of local earthquakes. Clustered events are being studied for evidence of temporal changes in fault zone processes and properties, including anisotropy, in cooperation with R. Aster of U.C. San Diego. Relocated events are being used to study failure processes, fault zone structure, and material properties within the Parkfield nucleation zone.

2) *Controlled-source monitoring with HRSN.* From June, 1987 through August 1991, the HRSN has been illuminated 36 times with S-waves of three polarizations at eight source positions throughout the study zone, using a shear-wave Vibroseis source, in an on-going monitoring program. The resulting data contain a temporal record of wave propagation characteristics throughout the nucleation zone. Albeit complexly encoded, the wave fields recorded contain the evidence for any nucleation-induced changes in velocities, attenuation or anisotropy. Data reduction is accomplished at the University of California's Lawrence Berkeley Laboratory (LBL), at LBL's Center for Computational Seismology (CCS). A paper summarizing this study is presently in press.

3) *Controlled-source monitoring with VWVA.* Analysis of local anisotropy and velocity structure using short-offset VSP's and 3-D generally anisotropic models is an ongoing topic of research at CCS in collaboration with several European scientists, and VWVA VSP data sets are prominently featured in this effort.

DATA COLLECTED

- Full-time, event-triggered recording of earthquakes has continued in the past year. Event data are archived as IEEE-format binary files on magnetic tape with simple headers.
- Five vibrator data sets have been collected and the data reduced in FY91. Data after routine processing (edit, stack, correlation, gather by source site) are archived in SEGY format on magnetic tape.

RESULTS

1) *Earthquake studies*:

- A final 3-D velocity model has been established, and a paper on the modeling process and results has been published.
- A graduate student working with Parkfield earthquake data and 3-D modeling has completed his studies.
- Local Parkfield events have been picked and relocated with the 3-D model through December, 1990.
- In a major effort, we have defined, gathered, and archived clusters of events with similar waveforms through 1989. About 500 events were relocated through the 3-D model for analysis. The result is 70-80 clusters defined within our network (Fig 1), with 2-18 events/cluster. About two-thirds of the total events are clustered. Many clusters span the three years of data collection.
- We have completed the automated picking of relative P and S arrival times within clusters (using B. Foxall's cross-correlation, cross-coherence procedure), and high-precision relative relocation of cluster events. Many of the relocated clusters span only 100-200m (Fig 2).
- Procedures have been developed to efficiently add post-1989 data to the clusters.
- In the work with R. Aster, we are studying S-wave polarization variations within the clusters, and the implications for anisotropy.

The archived clusters will be the basis for further studies: of rupture processes on small patches of the fault using either theoretical or empirical Green's functions (Foxall).

2) *Controlled-source studies - HRSN*. The final working data sets for analysis are "time gathers": one source into one receiver gathered across calendar time, producing 720 files, each containing, at present, 35 similar traces. The time gathers are then examined for variations in waveform parameters.

Most displays to date show only seasonal variations in various properties (travel time, amplitude, spectral properties). Seasonal variations are due to very near-surface moisture changes under the vibrator (Clymer and McEvilly, 1981). The magnitude of the variation varies considerably from site to site. This is illustrated for two paths in Figure 4 for spectral amplitude. The path from vibrator position (VP) 2 to MMN shows an overall trace amplitude change - the shear-wave vibrator couples to the ground better in the dry summer - but little change in the shape of the spectrum, or (not shown) in the travel time. Path 4-MMN data, on the other hand, show a significant change in the shape of the amplitude spectrum, with higher frequencies being increased relative to low frequencies in the dry months when the vibrator couples better, and in travel time (not shown).

A paper on the controlled-source work has gone through final revisions and is in press.

Figure 5 illustrates a travel-time anomaly that appears on paths that pass through the vicinity of VP 2, south-west of the 1966 epicenter. The figure shows grey-scale displays of relative travel-time change (correlation lag) across time gathers in a moving window. Several paths show relative advances in travel time of 30-60 msec for a band of late phases (the dark zones at late times), beginning in mid-1988. This effect is particularly well developed on most paths from source site 2, although it is seen from other source sites as well. Path 6-FRO, on a north-west azimuth, does not show the effect. Energy on this path may preferentially refract through the intact granites lying south-west of the SAF, and thus not sample the area of VP2. Data from the path from VP2 to SMN, to the north-west, similarly do not show the effect. Figure 6 shows windowed travel-time changes of individual prominent late phases from various source sites into VCA. All the arrivals examined show a significant advance, with the exception of those from sites to the north-west.

Figure 6 summarizes the paths examined to date. The wide solid and narrow dashed lines indicate paths that respectively show and do not show the anomaly. There is an indication of a zone of anomalous velocity south-west of Middle Mountain.

References

Clymer, R.W., and McEvilly, T.V., 1981. Travel time monitoring with VIBROSEIS, *Bull. Seism. Soc. Amer.*, **71**, 1902-1927.

Daley, T.M., and T.V. McEvilly (1990). Shear Wave Anisotropy in the Parkfield Varian Well VSP, *Bull. Seis. Soc. Am.*, **80**, 857-869.

Published Papers, Reports, Abstracts

Clymer, R.W., E.D. Karageorgi, A. Michelini, and T.V. McEvilly, 1991. Anomalies in Controlled-Source Waveform Parameters at Parkfield, *Seis. Res. Letts.*, **62**, 46. -abstract

Daley, T.M., and T.V. McEvilly, 1991. Update of shear-wave anisotropy measurements at the Parkfield Varian well, *Seis. Res. Letts.*, **62**, 46. -abstract

Karageorgi, E., R. Clymer and T.V. McEvilly, 1991. Shear-wave monitoring at Parkfield with Vibroseis, *Seis. Res. Letts.*, **62**, 46. -abstract

Karageorgi, E., R. Clymer and T.V. McEvilly, 1992. Seismological studies at Parkfield: II. Search for temporal variations in shear wave propagation using Vibroseis, *Bull. Seism. Soc. Am.*, in press.

Michelini, A. (1991). Fault zone structure determined through the analysis of earthquake arrival times, PhD. Thesis, Univ Calif, Berkeley.

Michelini, A., and T.V. McEvilly (1991). Seismological studies at Parkfield: Simultaneous inversion for velocity structure and hypocenters using cubic B-splines parameterization, *Bull. Seis. Soc. Am.*, **81**, 524-552.

Table 2. Parkfield HRSN Instrumental Description

STATIONS (Since 13 Jan 1988)	Station Name	Lat. ¹ [N]	Long. ¹ [W]	Surface Elev. ^{1,2} [m]	Sensor Elev. ^{1,2} [m]	Polarities ³ H1	Polarities ³ H2	Sensor
EAD	35.89522	120.42262	503	258	D	170°	260°	L22 5
FRO	35.91095	120.48688	549	265	D	338°	248°	L22
GHI	35.83225	120.34728	427	364	U	out	?	L22
JCN	35.93897	120.43112	567	343	D	0° 4	27.0°	L22
JCS	35.92117	120.43400	488	333	U	300°	210°	HS1 6
MMN	35.95650	120.49600	735	514	D	175°	265°	L22
RMN (GP)	36.00087	120.47772	1198	1125	D	310° 4	40° 4	L22
SMN	35.97297	120.57988	732	450	D	120°	210°	L22
VAR	35.92608	120.44705	509	-63	U	15	285	1023 7
VCA	35.92162	120.53392	789	589	D	200°	290°	L22

1 Sites located with GPS; datum = NAD84. (Conversion to NAD27: +0.000004° latitude, -0.00101° longitude.)

2 Height above mean sea level. (Conversion to height above ellipsoid: -34m.)

3 Direction of ground motion (east from true north) producing positive digital counts as recorded on SEG-Y tape in field and as archived at Berkeley

4 These channel polarities are reversed on archive tapes generated by UCSB/Duke

5 Mark Products, 2 Hz, 5.5 KΩ, 0.7 damping, 0.60 v/cm/s

6 Geospace, 4.5 Hz, 125Ω coils, 0.49 v/cm/s open circuit; 0.6 damping with 2500Ω shunt resistance; vertical = 1660Ω (8 phones, 2 parallel stacks of 4 in series), 1.30 v/cm/s; horizontals = 830Ω (single phones), 0.33 v/cm/s

7 Litor, 4.5 Hz, 670Ω, 0.7 damping, 0.39 v/cm/s

SIGNAL CONDITIONING & TELEMETRY

Digitizers: RefTek 24, 3-component, DC coupled, 80 dB gain, 125 Hz 12-pole Butterworth anti-alias filters, 16-bit conversion, 500 samples per second per channel, asynchronous sampling clocks among sites.

Telemetry : Digital, RefTek radios, 216-220 MHz, 38.4 Kbaud, RefTek44 multiplexer (Interface to recorder).

RECORDING SYSTEM

WESCOMP II: LS11-based VSP recording system, 32 channels, SEG-Y output tape, for event and Vibroseis recording.

HRSN Specs

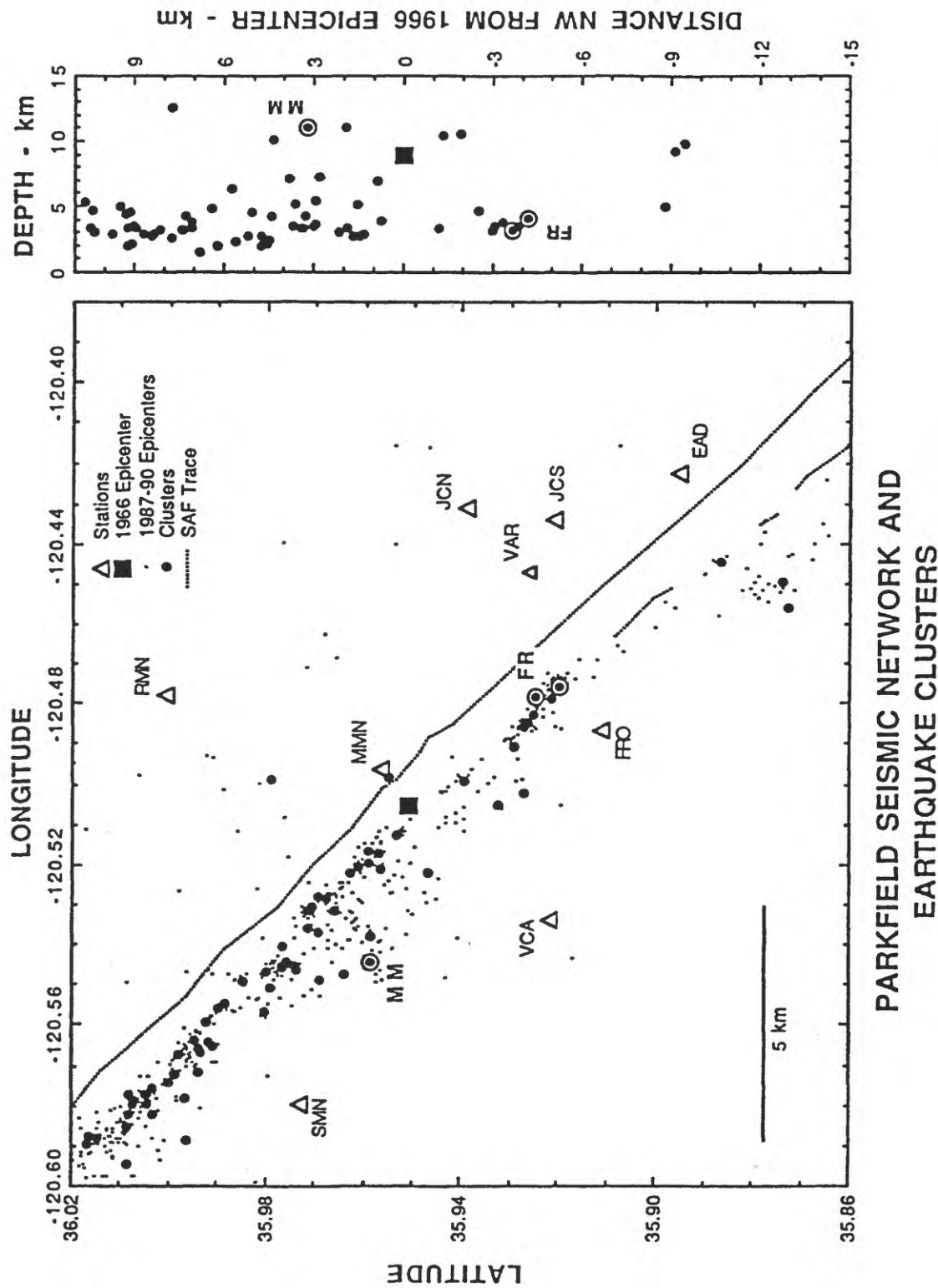


Figure 1. Parkfield location, showing the High-Resolution Seismic Network (HRSN), and 6/87-12/90 seismicity as relocated through the UCB 3-D velocity model, with identified clusters.

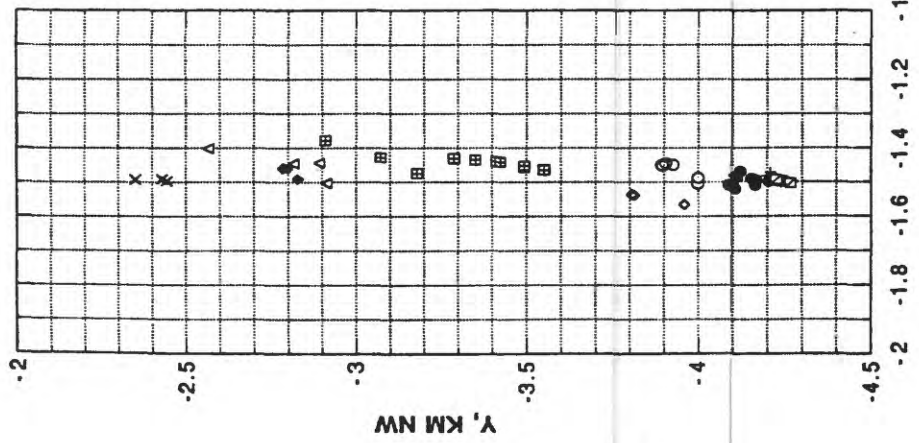
FRO Clusters**a****b****c**

Figure 2. Microearthquake clusters in the vicinity of HRSN station FRO. a) map view, with X- and Y-axes perpendicular and parallel to the local strike of the San Andreas fault (SAF), and center of coordinates at the epicenter of the 1966 Parkfield earthquake. b) and c) are cross-sections parallel and perpendicular to the SAF. Note the changes in scale.

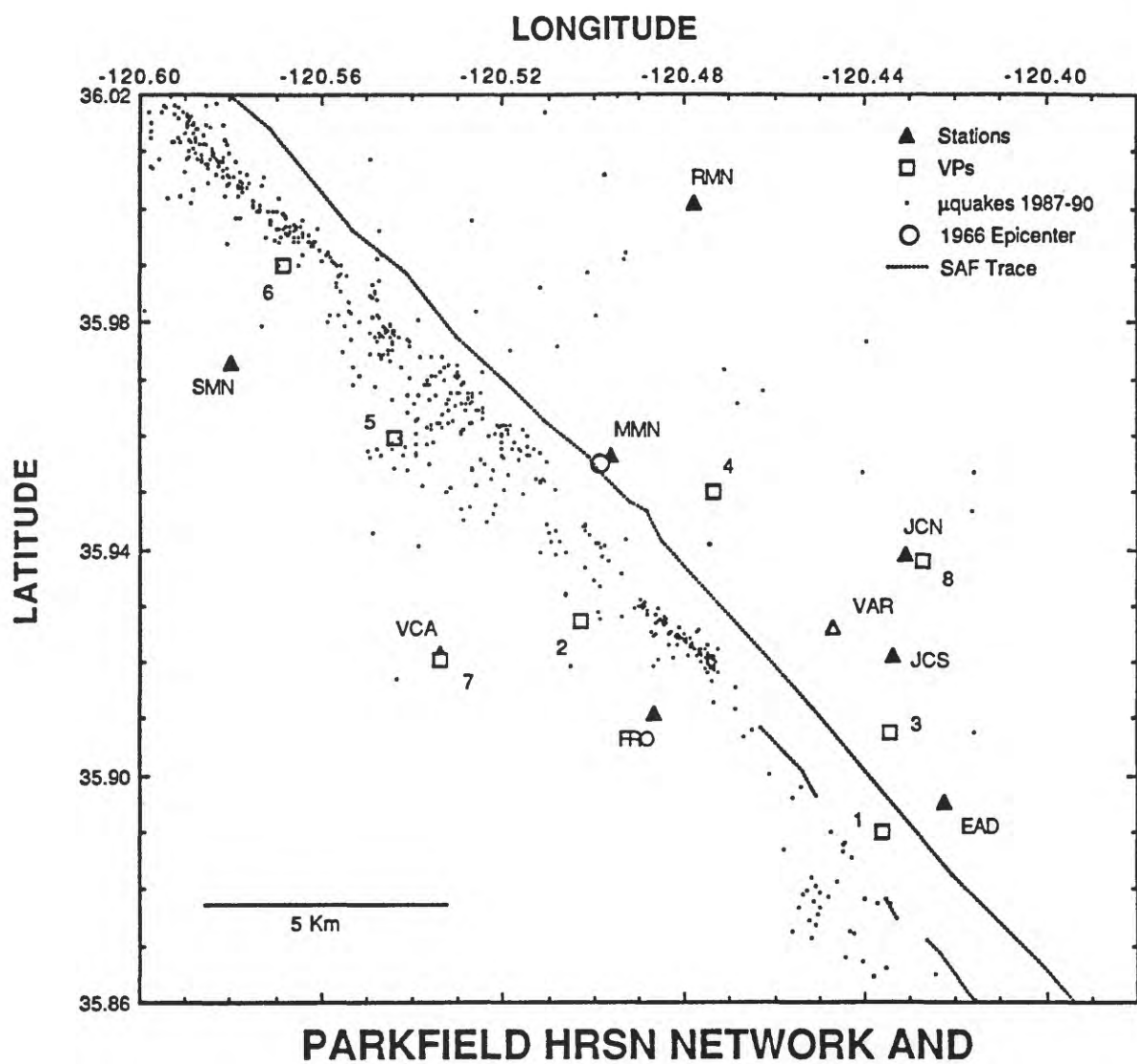


Figure 3. Location map, showing the vibrator monitoring sites and the HRSN.

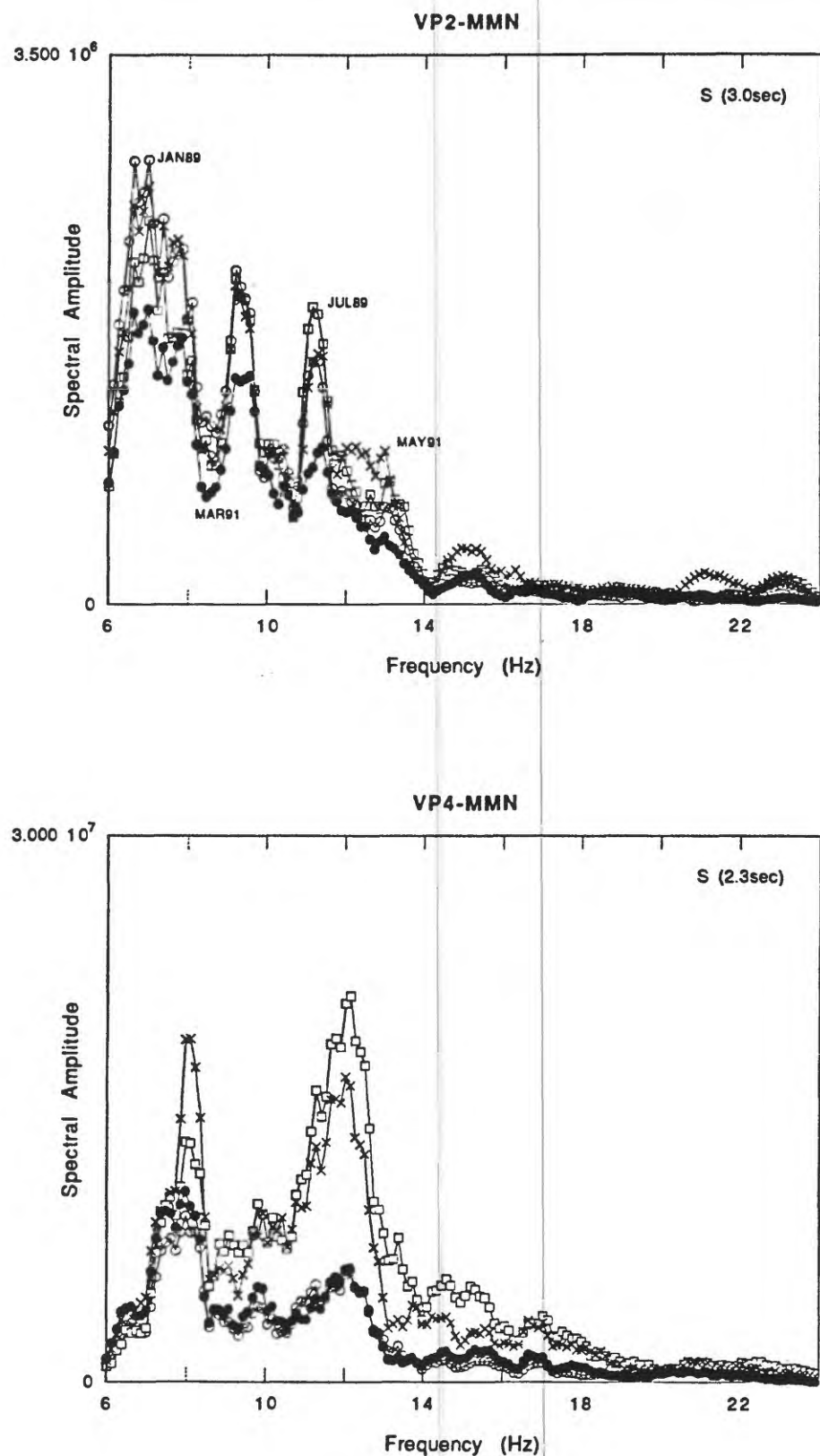


Figure 4. Amplitude spectra, showing seasonal variations in frequency content of the direct S arrival on two paths.

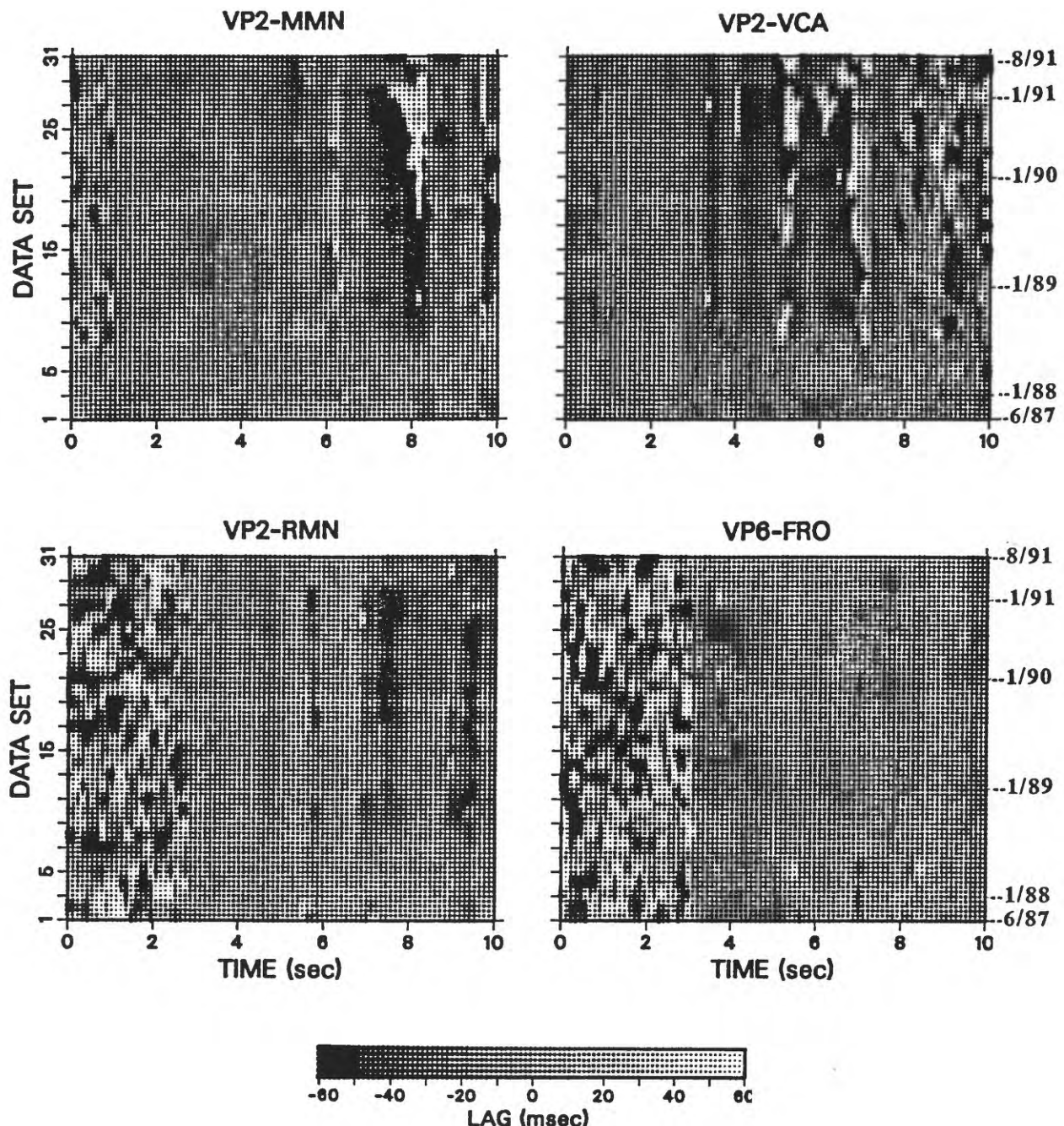


Figure 5. Travel-time change relative to data set 6 (April '88) by cross-correlation in a moving time window. Three of these show the late 30-60msec advance (dark zones) beginning in mid-1988, as discussed in the text.

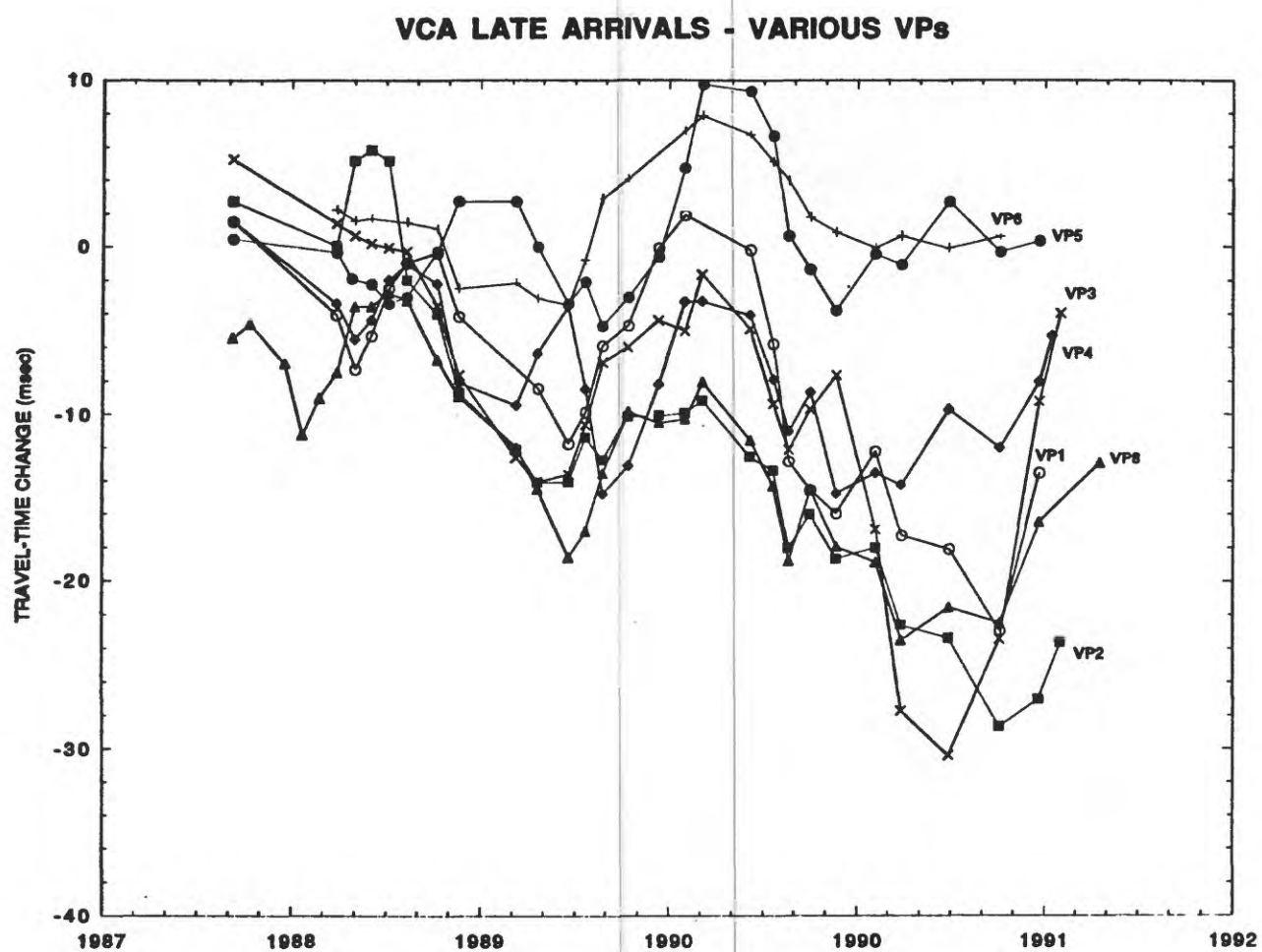


Figure 6. Relative travel-time variations measured on paths into VCA from several source sites, calculated by a cross-correlation, cross-spectral technique in fixed time windows centered on prominent late phases .

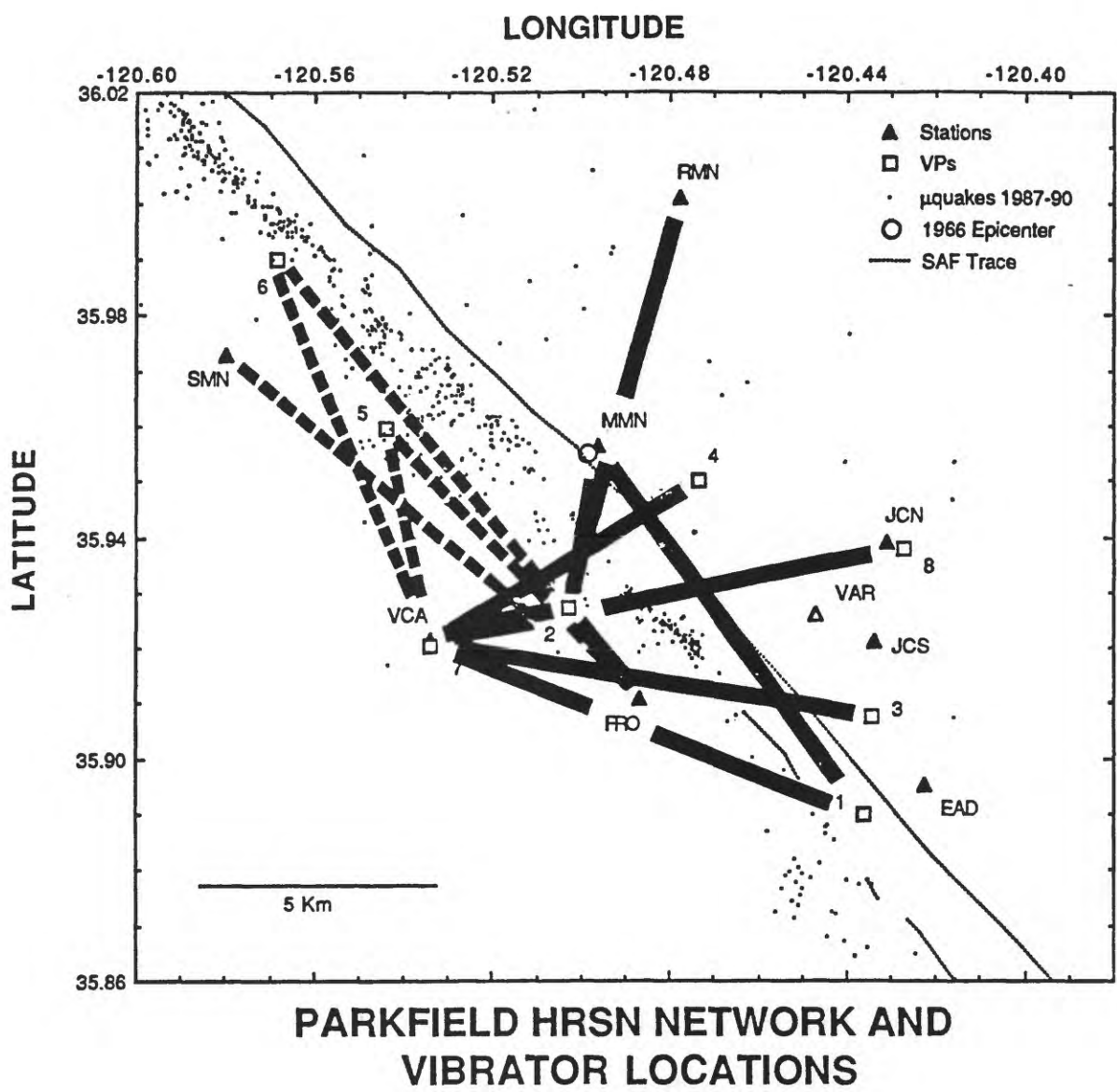


Figure 7. Base map showing source-receiver pairs that have been examined for late-phase travel-time anomalies. Wide solid and narrow dashed lines indicate time gathers with and without anomalies.

Bay Area Digital Seismic Network**14-08-0001-G2122****01Sept91-30Sep92**

Thomas V. McEvilly and Barbara Romanowicz
Seismographic Station
Dept. of Geology and Geophysics
University of California
Berkeley, CA 94720

Phone: (510) 486-7347
FAX: (510) 486-5686
e-mail: tvmcevilly@lbl.gov

Project Description

This UC/USGS cooperative project is the installation of a new digital seismographic network in the San Francisco East Bay region along the full length of the Hayward fault (Ellsworth on the southern half - UC the north). The purpose is to achieve a substantial improvement in the resolution with which we can monitor seismicity to very small magnitudes and fault-zone processes on the Hayward fault. Ultimately some 24 stations are planned with wide dynamic range and frequency bandwidth (>20 bits, 250 Hz), with on-scale recording to 0.5 g. Current funding will allow installation of perhaps 12-16 initial stations.

FY91 Accomplishments (01-30 September)

Despite only one month's activity in FY91 under this award, a substantial startup effort was mounted:

Borehole sensor installations. Existing geophones from UC/LBL stock were provided to Malcolm Johnston in order to insure that his pilot exploratory holes for the borehole strainmeter project, which are immediately cemented upon completion, would be equipped with downhole sensors for the digital network. Other 'off-the-shelf' borehole seismometers were supplied from USGS. (Drilling costs for installing network seismometers were deleted from the UC award, so holes of opportunity are being used wherever possible. A borehole sonde was developed for deployment of multi-component sensors downhole to 1000 ft depth. Experience at other sites (Parkfield, the Geysers, Long Valley) and the known Bay Area noise levels render surface sites there only marginally effective as high-resolution, high-frequency stations.) Boreholes of opportunity have also been found in Alameda (Kyle Rollins project), at the east approach to the Bay Bridge (courtesy of CALTRANS) and on the Berkeley/LBL grounds (three holes exist). Figure 1 summarizes the installation progress as of mid-November. So far, most hole depths are around 500 ft. We would prefer emplacement depths of 800-1000 ft.

Sensor selection. Tests were initiated on appropriate sensors for the network. The high-frequency operation planned for the network calls for better noise characteristics above 15Hz than are available in conventional 2 or 4.5 Hz velocity geophones. We are testing low-noise accelerometers, and one such comparison is presented in Figure 2. Presently we are leaning to a 4-component (three accelerometers and a redundant vertical velocity sensor) instrument package.

Data acquisition system. Specifications were developed for the network data acquisition systems and a request for bids was issued. The system will sample at up to 1000 sps and telemeter continuously a data substream, using Pacific Bell's new digital network. On-site backup will exist and central site event triggering will be a possible mode of operation. At mid-November a vendor has not yet been selected.

Schedule. Sensors and data acquisition equipment will be ordered in December. Station sites will continue to be sought and instrumented throughout the year. Telephone lines will be arranged for definite sites. Central site software and hardware will be purchased/developed early in 1992. In the late spring the prototype remote sites will be activated and the telemetry system tested under real operation.

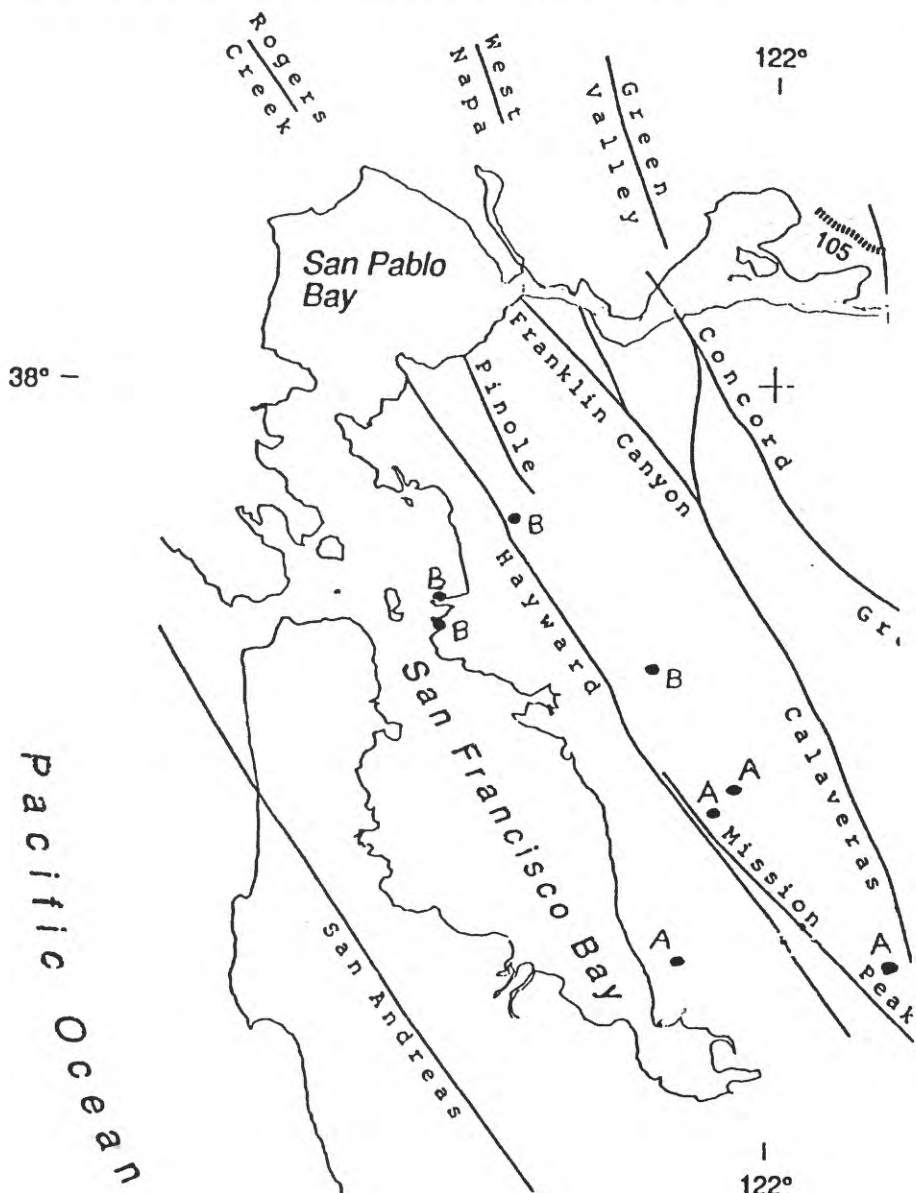


Figure 1. East Bay network station sites with (A) borehole sensors installed, as of mid November, 1991. (B) sites are presently available or planned borehole sites to be used when available.

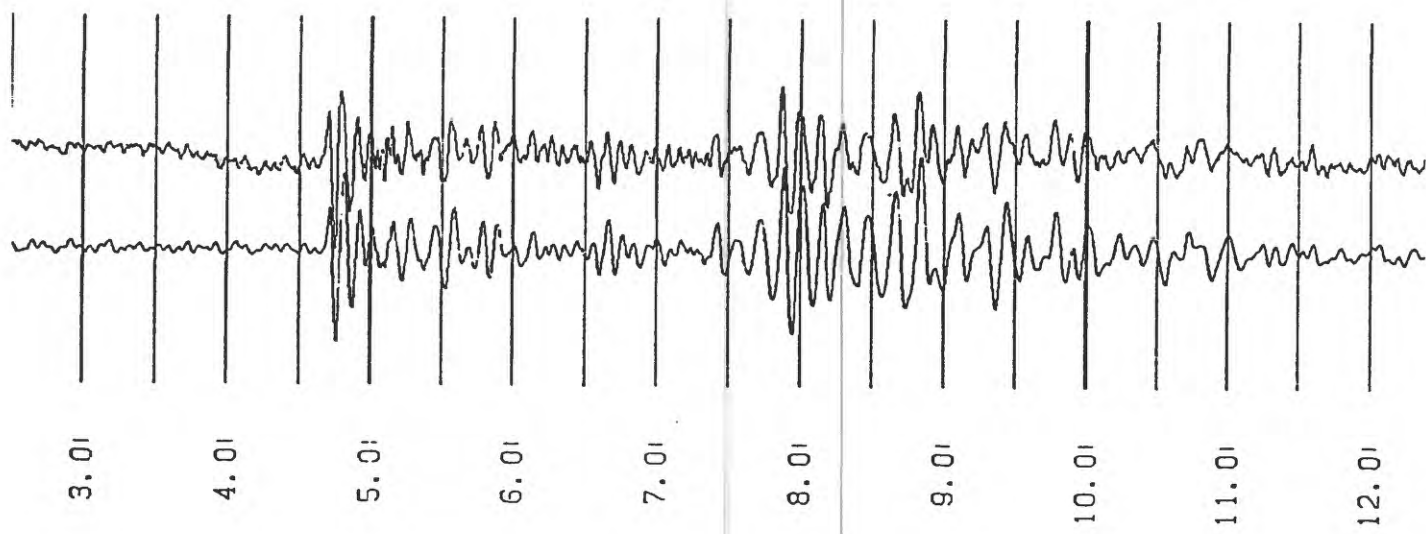


Figure 2. Preliminary sensor comparison between conventional 4.5 Hz velocity geophone (lower trace) and wide-band (0.1- 600 Hz) accelerometer, integrated to velocity (both sampled at 1000 sps with 250 Hz anti-alias filter), for the recording of a $m=1.2$ event about 25 km from the sensors, which were installed in a common sonde at the bottom of a 550-ft borehole on the fault at the stadium on the UC Berkeley campus. 60 Hz noise and the presence of tube waves degraded this comparison somewhat, and the experiment will be repeated more carefully. Initial results suggest that the 0.5g full-scale accelerometer will serve well as the detector for the small microearthquakes, particularly at frequencies above 10 Hz.

Parkfield Earthquake Prediction Experiment: Earthquake Seismology

9930-02098

Andrew J. Michael
Branch of Seismology
U.S. Geological Survey
345 Middlefield Road, MS/977
Menlo Park, California 94025
(415)329-4777

Investigations:

The principal subject of investigation is an attempt to understand the structure and behavior of the seismogenic zone at Parkfield, California in order to better understand the physical processes that control the earthquake generation cycle in that area. In addition we have been attempting to apply these ideas to other areas to determine if we have uncovered processes that are generally applicable or if they are specific to the Parkfield area. To accomplish this we have maintained a detailed catalog of Parkfield hypocenters and focal mechanisms and determined a three-dimensional velocity model of the Parkfield region. This velocity modeling work is in collaboration with Donna Eberhart-Phillips.

In order to test the ideas we have developed at Parkfield we have also been determining a three-dimensional velocity model for the Loma Prieta, California area. To provide greater control of the model and hypocentral locations with respect to surface features a series of six calibration shots were recorded on the CALNET array and a distributed deployment of portable receivers in May of 1991.

In September of 1991 I participated in Jill McCarthy's marine seismic reflection experiment that aimed to determine fault structures under the San Francisco Bay and associated waterways. My involvement with the experiment was to coordinate the recording of the airgun blasts on the CALNET array. This data will be analyzed during fiscal year 1992.

Other research includes further studies of the stress state surrounding in the Loma Prieta and Whittier Narrows regions in order to better understand the coseismic effect of the mainshocks.

Results

The most important result to come out of this project is the discovery of relations among fault behavior and the material properties of the rocks that contact the fault at seismogenic depths. Regions of high moment release appear to correlate with high seismic velocities whereas rupture initiation or termination may be associated with lower seismic velocities. These relations point toward a physical understanding of why faults are divided into segments that can fail independently, an understanding that could improve our ability to predict earthquakes and strong ground motion.

The use of three-dimensional velocity models to understand the processes that result in fault segmentation could be very important because other work at Parkfield,

CA has shown that surface fault geometry is not simply related to the fault geometry at seismogenic depths. The offset in Cholame Valley is one of the largest on the San Andreas Fault and has often been cited as the feature that terminates the rupture of the Parkfield earthquakes. However, the use of the three-dimensional velocity model to relocate both background seismicity and the 1966 aftershocks has shown that this offset does not exist at seismogenic depths. Thus the offset in the fault may be limited to the upper 1 to 3 kilometers. The one unusual feature observed in the Cholame Valley seismicity is the existence of some normal faulting mechanisms. However, they are not distributed throughout the valley as might be expected but instead lie in the same plane of hypocenters as strike-slip mechanisms that define a planar San Andreas fault.

Preliminary results from the Loma Prieta calibration shots have been used to calculate station corrections for the CALNET stations with respect to the three-dimensional velocity model. However the relationships between the shallow Loma Prieta aftershocks and the surface faults is still enigmatic.

The efforts to unravel the very heterogeneous stress state left by the Loma Prieta earthquake are still ongoing. Currently we are testing a variety of methods to compare the aftershock focal mechanisms to the stresses imposed by the mainshock in order to find a method that is sufficiently robust with respect to errors both in the mainshock rupture pattern and the aftershock hypocenters and focal mechanisms. Some of the stress inversion techniques being used at Loma Prieta were developed and tested on the Whittier Narrows aftershocks sequence. There we were able to show that the stress state during the aftershocks had a significant component of spatial heterogeneity but were unable to relate this to the mainshock rupture. However, tests using simulated data suggested that the errors in the data were large enough to mask the effects of the mainshock's dislocation. At Loma Prieta the errors are comparable, but the mainshock is larger and the simulations suggest that we should be able to define its effects.

Reports:

Michael, A. J. , 1990, Energy constraints on kinematic models of oblique faulting: Loma Prieta versus Parkfield-Coalinga, abstract, EOS, 71, 1646.

Aviles, C.A. and Michael, A. J., 1990, Complications at the southern end of the 1966 Parkfield rupture zone, abstract, EOS, 71, 1473.

Michael, A. J., 1991, Spatial variations in stress within the 1987 Whittier Narrows, California, aftershock sequence: new techniques and results, J. Geophys. Res., 96, 6303-6320.

Michael, A. J., and Eberhart-Phillips, D. M., 1991, Relationships between Fault Behavior, Subsurface Geology, and Three-Dimensional Velocity Models, Science, 253, 651-654.

Eberhart-Phillips, D. M., Michael, A. J., and W. D. Stanley, 1991, Overpressure in the Parkfield Preparation Zone?, abstract, Seismology Research Letters, 62, 46.

Some tidal-wetland soils, however, may have been submerged and buried by non-tectonic processes. Peaty soils are commonly interbedded with mud in intertidal sequences of mid-latitude passive continental margins. Examples of non-tectonic processes that can produce such sequences include rapid changes in the rate of regional sea-level rise combined with changing sedimentation rates, or changes in the configuration of bars and channels in tidal inlets that led to local changes in tidal range. Tidal-wetland soils can be assumed to have been submerged by coseismic subsidence only where the abrupt upper contact of a widely-mapped, peaty soil gives strong evidence of a sudden, substantial change (>0.5 m) in water depth.

Precise radiocarbon dating can help distinguish soils buried following regional plate-interface earthquakes from soils buried during local upper-plate earthquakes or by non-tectonic processes. Synchronous ages for soils submerged along hundreds of kilometers of coast would be consistent with great plate-interface earthquakes, some perhaps as large as M 9. Non-synchronous ages would indicate lower magnitude plate-interface earthquakes with coseismic subsidence of much more limited extent, moderate-magnitude earthquakes on shallow structures in the upper plate, or soil submergence and burial by non-tectonic processes.

Each of the above processes may have submerged and buried tidal-marsh soils in the Coos Bay region of southern Oregon. This area includes the distal part of the active accretionary wedge of the North America plate. Analogies with deformation during great earthquakes in Chile, Japan, and Alaska indicate that regional uplift of as much as several meters and/or differential movements across folds and faults may occur in the accretionary wedge during great plate-interface earthquakes. In southern Oregon, late Holocene coseismic deformation has been inferred on shallow, upper-plate faults and folds in the South Slough arm of western Coos Bay. Surface deformation associated with these structures might be reflected as submergence or emergence events of 0.5-2 m in the tidal-marsh stratigraphic record. Many localized deformation events are probably coincident with plate-interface earthquakes, but shallow earthquakes of moderate to large magnitude (M 6-7 3/4) on smaller structures (<30 km long) in the overriding plate might also produce localized areas of coseismic subsidence or uplift.

The frequency of submergence events and the precision with which suddenly submerged soils can be radiocarbon dated determine if closely spaced submergence events can be distinguished from site to site. But in the Coos Bay region the precision of conventional ^{14}C ages on peaty tidal-marsh soils is too low and the recurrence intervals between events are too short to distinguish local from regional submergence events (Nelson, in press).

The precision of age estimates for events in southern Oregon can be improved by averaging multiple accelerator-mass-spectrometer (AMS) ^{14}C analyses of rigorously selected and pretreated plant macrofossils at the abrupt upper contacts of tidal-marsh soils. An initial test of this method in South Slough shows that standard deviations on AMS ages can be reduced to ± 25 -40 years (Fig. 1). However, consideration of the total analytical errors in AMS analysis and age differences due to changes in the rate of ^{14}C production in the atmosphere over time indicate that 95% confidence limits on calendar-corrected ages for submergence events range from 50 to 400 years (Fig. 2). Events that occurred only 100 years apart may be distinguishable if their ages fall on favorable parts of the ^{14}C calibration curve. In other cases, we may not be able to identify events that occurred as much as 400 years apart at different sites.

In FY91, Nelson, Brian Atwater (USGS), Wendy Grant (USGS), Lee-Ann Bradley (USGS) and Mark Darienzo (Portland State University) collected multiple AMS samples from buried soils in marshes in southwestern Washington and northern Oregon (Fig. 3). Samples from one or two of the best developed soils were collected at the best sites at each locality. A staged program of multiple AMS analysis of macrofossils from these soils over the next two years should show whether or not correlated soils were submerged during the same 50-400 yr period at each site.

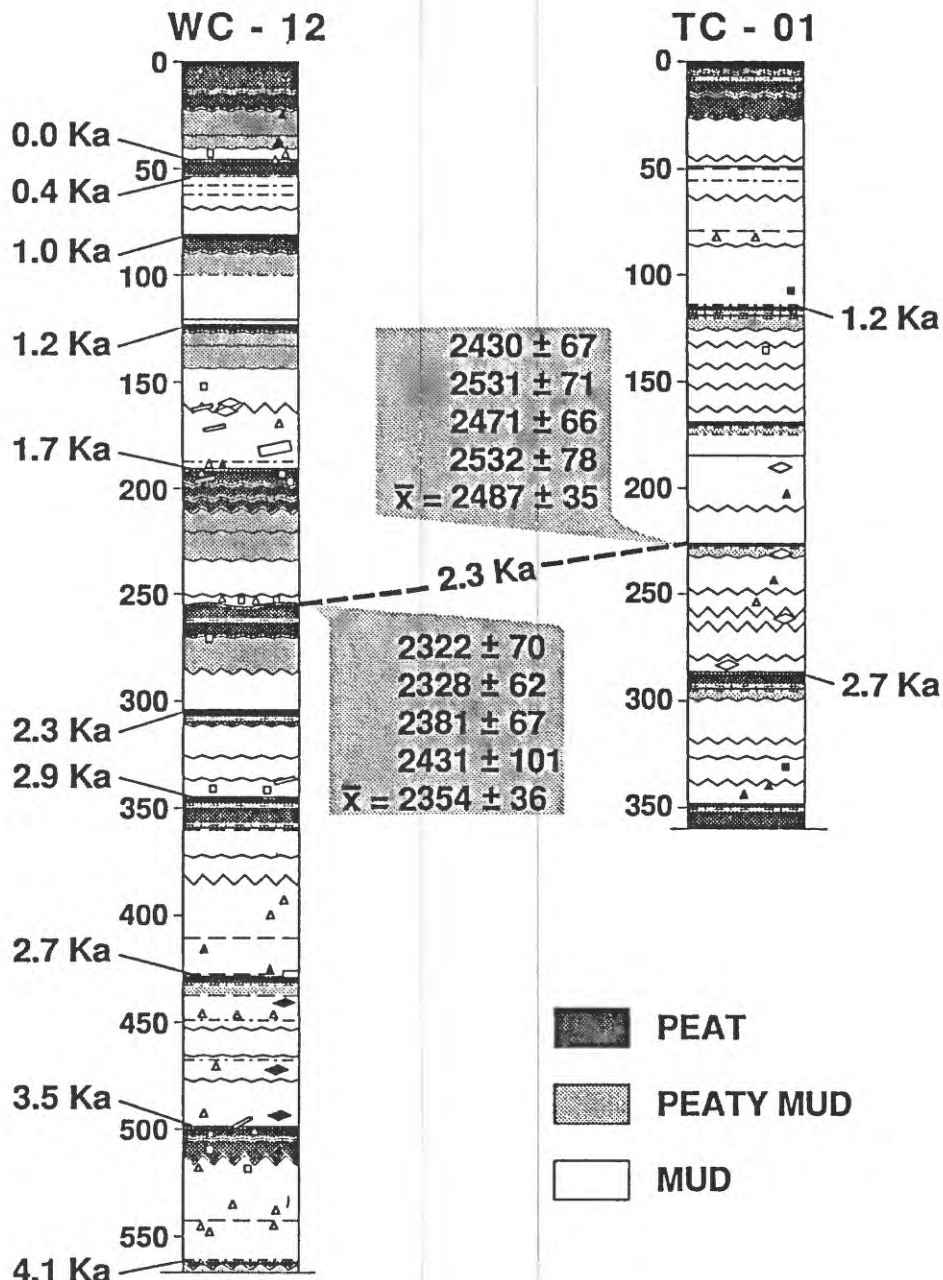


FIG. 1.-- General lithologies and age estimates (in thousands of ^{14}C years) for the tops of peaty units in two cores along Winchester Creek (WC-12) and Talbot Creek (TC-01) in separate arms of South Slough, Coos Bay, Oregon. Approximate age estimates shown to left of core WC-12 are based on 20 conventional ages and seven AMS ages from that core (Nelson, in press). Approximate age estimates shown to right of core TC-01 are based on single AMS ages. Four ages from carefully selected and pretreated samples collected from the same soil (2.3 ka) in both cores are shown with the mean age (\bar{x}) and combined standard deviation of the mean age next to each core.

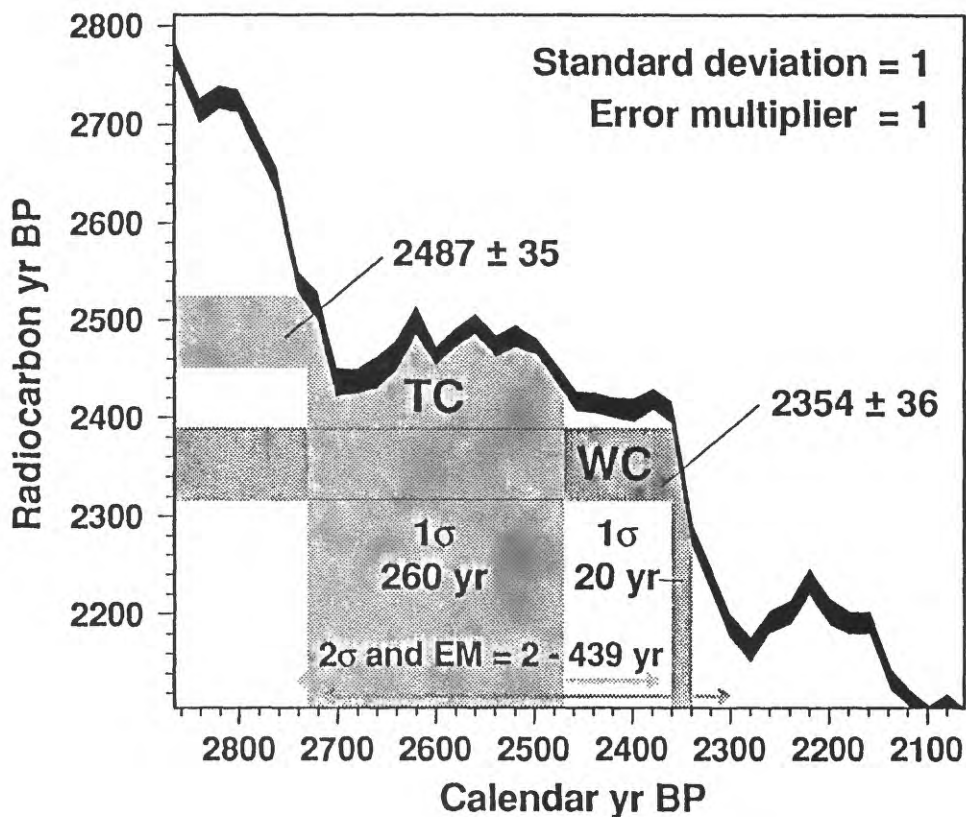


FIG. 2.-- Calibration of the mean ^{14}C ages from core WC-12 and TC-01 (Fig. 1) from radiocarbon years to calibrated years (approximately calendar years) at one standard deviation. At one standard deviation the mean age from core TC-01 corresponds to a calibrated-yr time interval of 260 yr. The mean age from WC-12, which falls on a much more favorable portion of the calibration curve, corresponds with a calibrated-year time interval of only 20 yr. At one standard deviation the calibrated age intervals do not overlap. But if a more reasonable error multiplier of two is used ($\text{EM}=2$), the calibrated ages from the cores overlap considerably at two standard deviations (overlap shown by arrows above the calendar yr BP axis). Because of the overlap we cannot infer that the soils in both cores were submerged at different times.

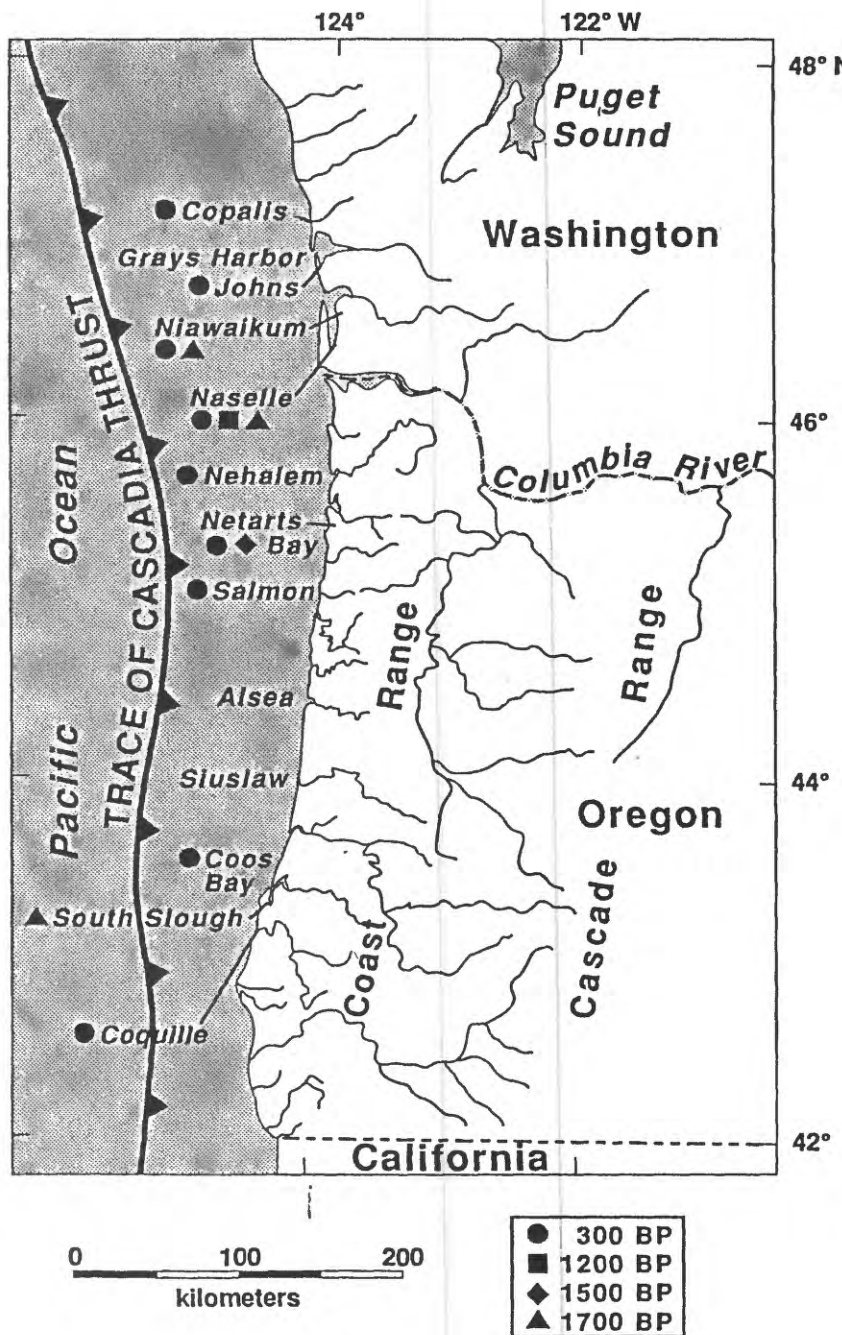


FIG 3.-- Location and approximate age of macrofossil samples collected from the tops of peaty soils at selected sites in estuaries in Washington and Oregon. Most samples consist of stems and leaf sheaths of the marsh plants *Juncus balticus*, *Carex lyngbyei*, or *Potentilla pacifica*. The stems were rooted in the tops of abruptly buried soils and the stems extended 2-40 mm into the overlying mud or sand. The samples from the tops of the soils at Coos Bay and South Slough consist of detrital above-ground plant parts and may differ more in age from the time of soil submergence and burial than the rooted plant fossils. More than eight samples were collected from each soil at each site. Following extensive cleaning and pretreatment of the samples we will select five from each soil at each site for AMS analysis.

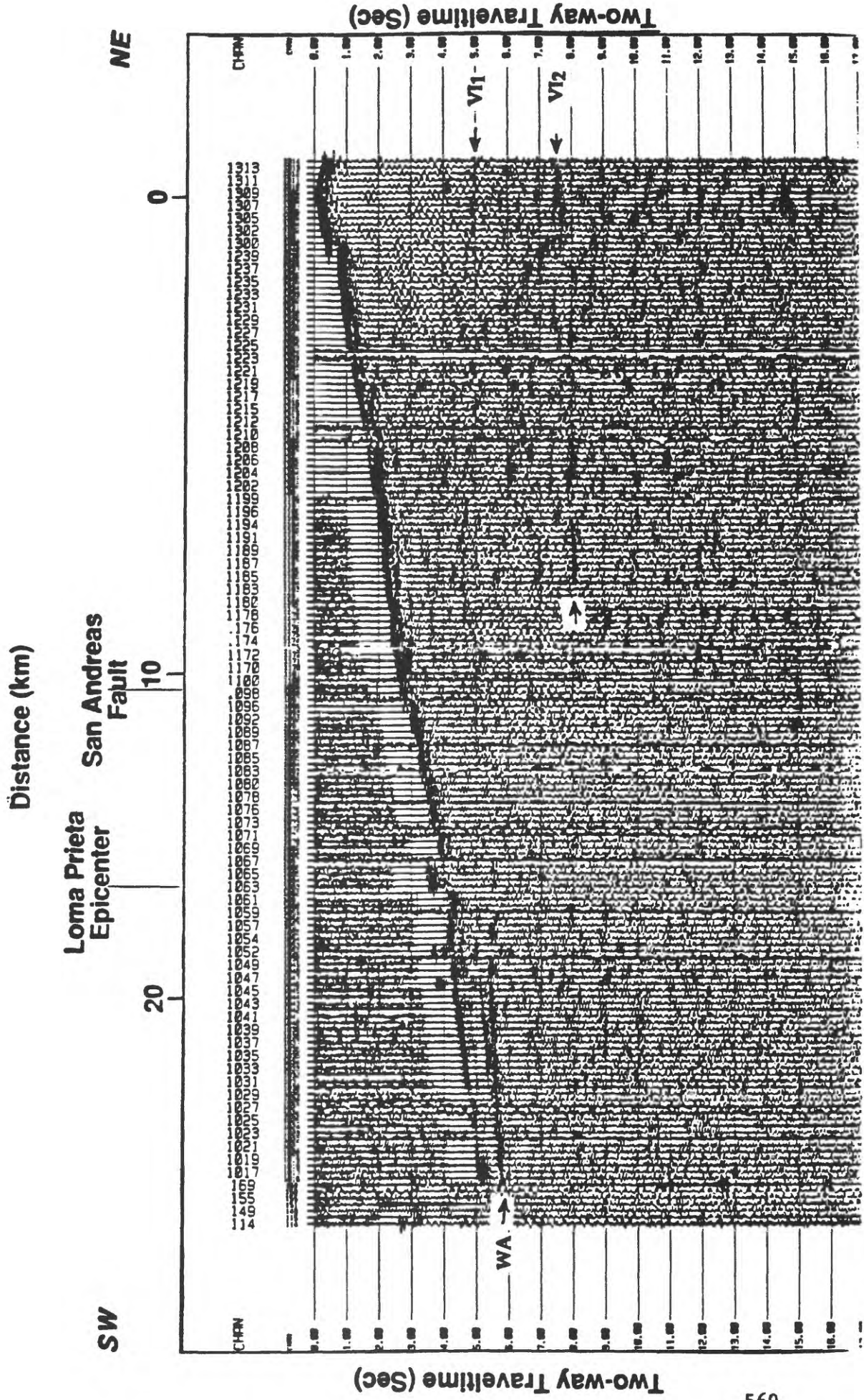


Fig. 2 (a) An unprocessed shot gather from the May 1991 seismic profile (LP line) across the epicenter of the 1999 Loma Prieta earthquake. Distance is about 26 km and time (sec) is about 17 sec. The strongest deep reflectors occur at wide angles (- 6 sec at about 20 km offset; labeled WΛ).

These may correlate with a weak vertical-incidence reflector at 5 s (labeled VII). The bottoming points for W1 lie beneath the surface trace of the SAF. At about 7 to 8 sec at near-vertical incidence (between 18 and 20 km depth, the approximate depth of the 1999 Loma Prieta hypocenter), one sees a stronger reflector (labeled VI2).

Analysis of Crustal Deformation Along the Southernmost Segment of the San Andreas Fault System, Imperial Valley, California: Implications for Earthquake Prediction

14-08-0001-G1679

R.E. Reilinger
Earth Resources Laboratory
Dept. of Earth, Atmospheric, and Planetary Sciences
Massachusetts Institute of Technology
Cambridge, Massachusetts 02142
(617) 253-7860

INVESTIGATIONS

This project involves using geodetic observations in conjunction with other geophysical and geological information to investigate contemporary tectonic processes along the southernmost segment of the San Andreas fault system. Our primary efforts during the present contract period include:

1. Completing a multi-institutional GPS campaign along an approximately 500 km section of the Pacific-North America plate boundary from northeast of Los Angeles, California to the Gulf of California, northern Mexico.
2. Continuing analysis and interpretation of 1986 to 1991 GPS measurements in the Imperial Valley-Salton Trough with emphasis on temporal and spatial patterns of regional strain accumulation, and strain release associated with the 1987 Superstition Hills earthquakes.

RESULTS

1. From 7 March through 3 April 1991, a consortium of universities, and state and federal agencies, undertook an extensive Global Positioning System measurement campaign along a 475 km section of the Pacific-N. American plate boundary from the Gulf of California, Baja, California, Mexico to the Big Bend segment of the San Andreas fault northeast of Los Angeles, California (Figure 1). Participating institutions included Caltech, CICESE, L-DGO, M.I.T., NGS, Riverside County Flood Control, San Bernardino County Survey, UNAVCO, University of Mexico, University of Texas at Dallas, and USGS. A total of 23 Trimble 4000 SST and 4 Ashtec receivers were used to observe 108 stations. In addition, simultaneous observations were made by the Orange County Survey using 8 dual frequency Ashtec receivers (sites not shown in Figure 1).

The primary objective of the 1991 STRC GPS campaign was to continue monitoring the spatial and temporal distribution of crustal strain along this seismically active segment of the plate boundary. Towards this end, most sites observed in the Coachella Valley-Riverside County portion of the network have a history of GPS observations dating to 1988, and all sites

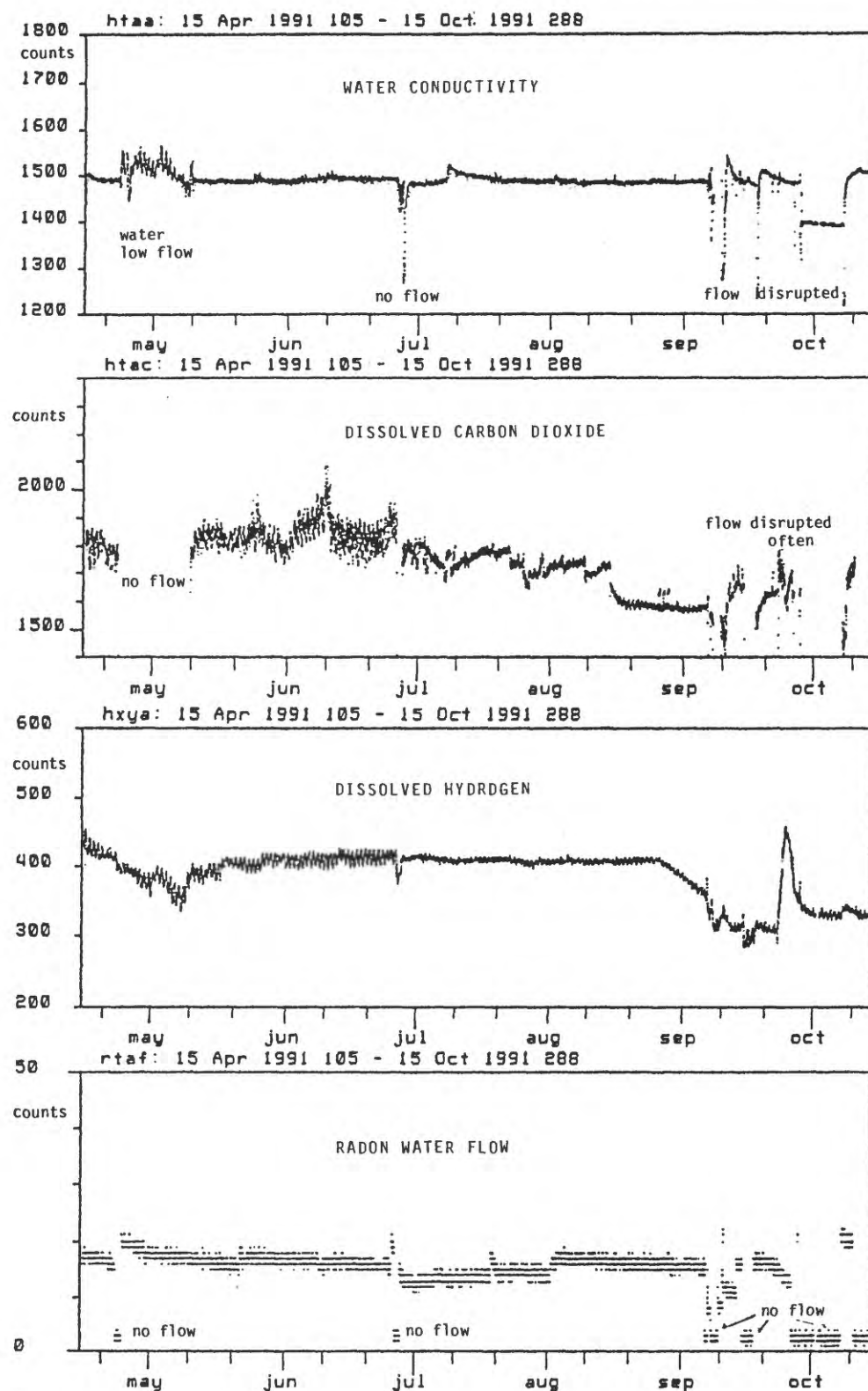


(Fig. 2) Water geochemistry data recorded at the Taylor Ranch site between April 15 and October 15, 1991.

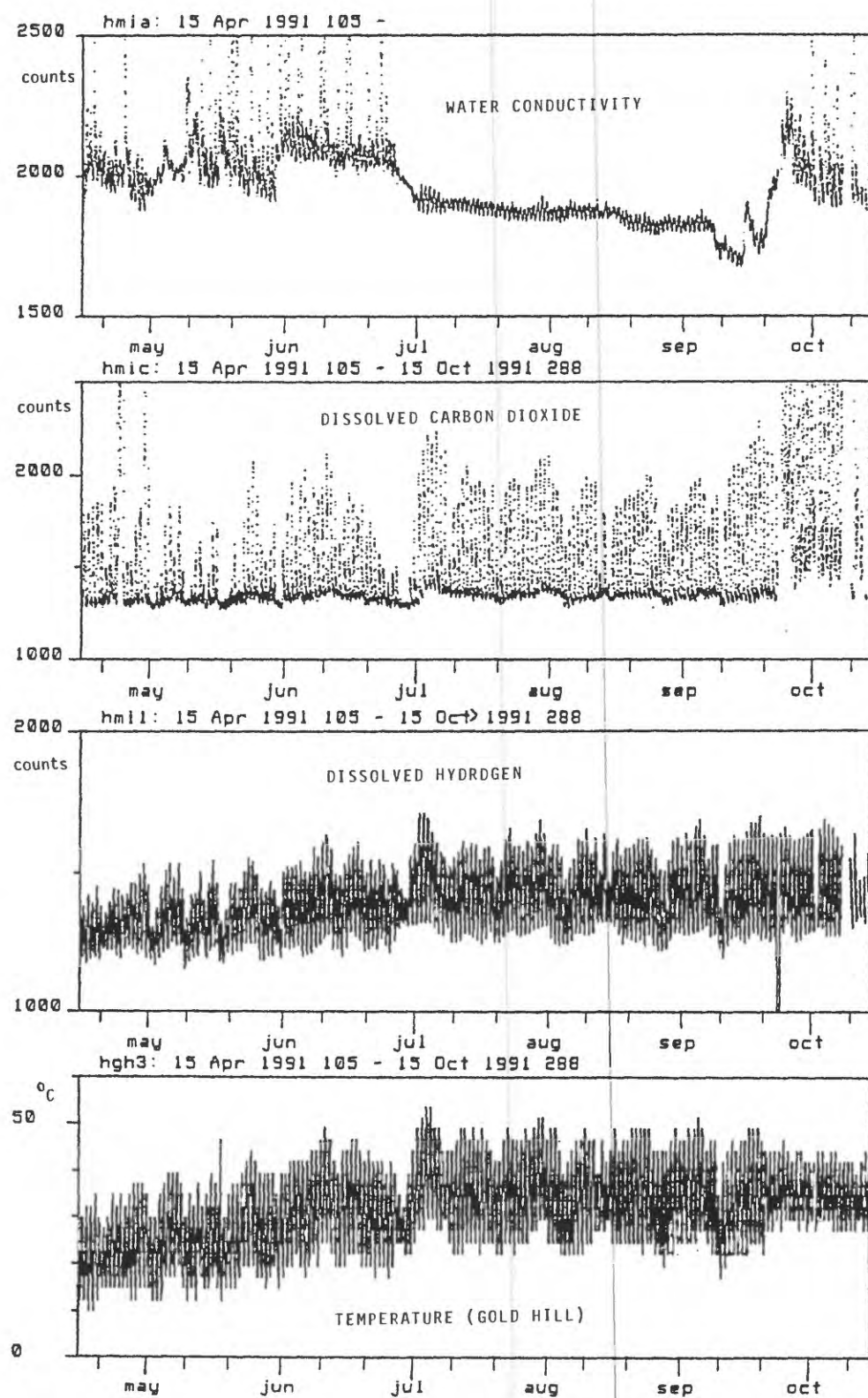


(Fig. 3) Water geochemistry data recorded at the Miller Ranch site between April 15 and October 15, 1991.

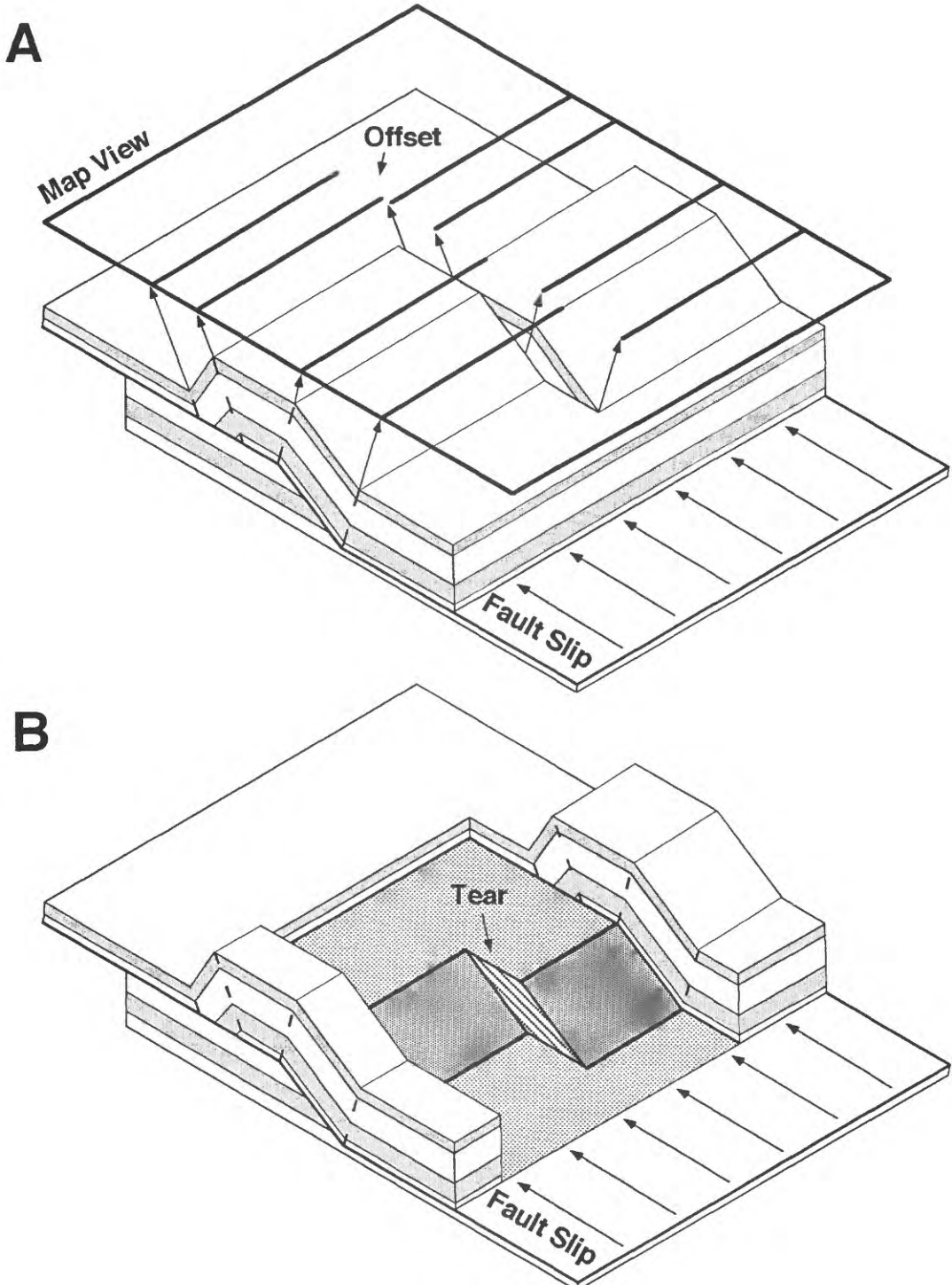


Figure 1: A balanced 3-dimensional models of fault-bend folds which have grown during slip on an underlying non-planar thrust fault. In (A), axial surfaces projected to the surface run parallel in map view above fault ramps with constant slip. However, axial surface pairs are offset above subsurface fault tears, shown in the cut away of (B).

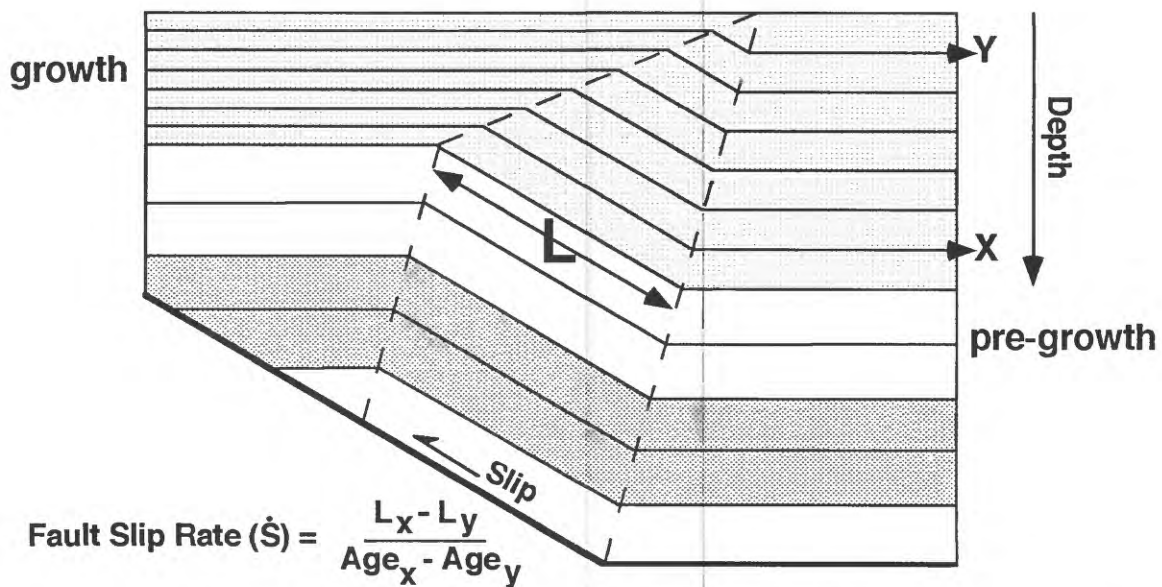


Figure 2: A fault-bend fold model in which a kink band forms above a bend in the underlying thrust. Syntectonic, or growth, sediments deposited atop the fold form a narrowing upward kink band or growth triangle, as sediments deposited earlier in the slip history record a wider kink band width than do sediments deposited later. In cases where the age of selected horizons (x,y), are known, the fault slip rate can be determined.

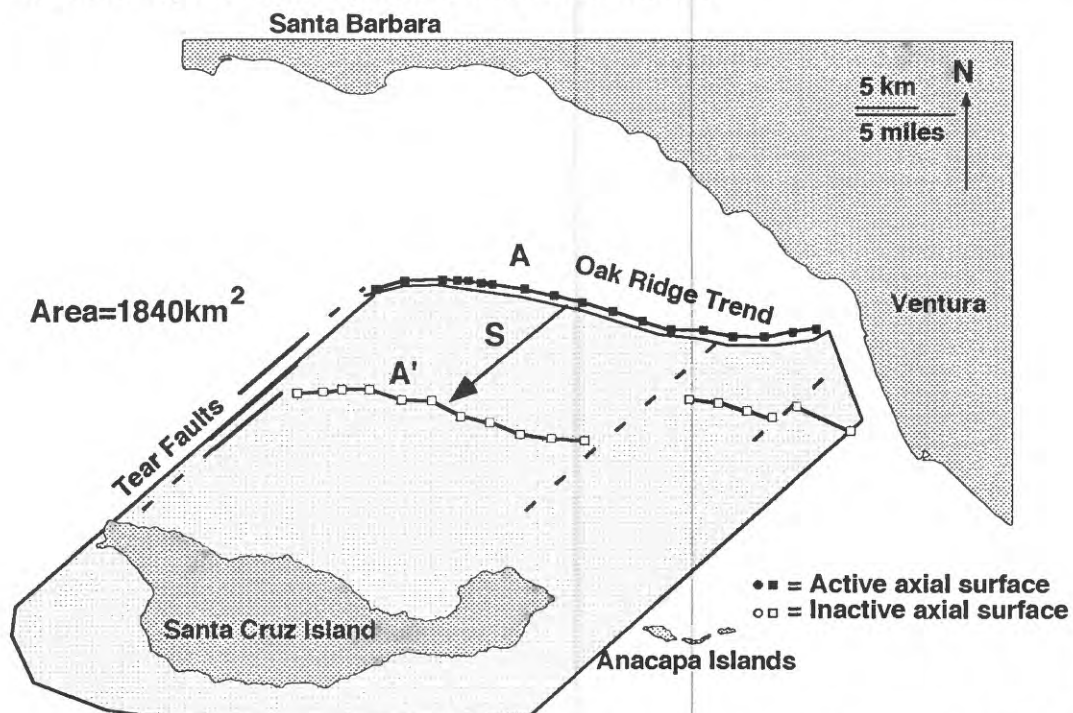


Figure 3: A map of axial surfaces in the eastern Santa Barbara Channel, California. The axial surfaces bound a kink band formed during Pliocene and Quaternary motion on an underlying oblique, right-lateral blind thrust. Continuity of the active axial surface (A) suggests that the underlying fault ramp, which approaches the surface south of Santa Cruz Island, is continuous over an area of at least 1840 square km.

Reports Published

Byrd, J.O.D. and R.B. Smith, 1991, Paleoseismicity, near-surface fault geometry, and segmentation of the Teton fault, Wyoming, (abs), Eos Trans. Amer. Geophys. Union, 72, 316.

Byrd, J. O. D., 1991, Paleoseismicity of the Southern Section of the Teton Fault, Wyoming, 1991 Abs. with Prog., 1991 Annual Meeting, Geol.Soc.Amer., 23, 5.

Meertens, C. M. and R. B. Smith, 1991, Crustal deformation of the Yellowstone caldera from first GPS measurements: 1987-1989, Geophys.. Res. Lett., 18, 1763-1766.

Sylvester, A.G., J.O.D. Byrd and R.B. Smith, 1991, Geodetic evidence for aseismic reverse creep across the Teton fault, Teton Range, Wyoming, Geop. Res.Lett, 18, 6, 1083-1086.

Smith, R. B. and W. J. Arabasz, 1991, Seismicity of the Intermountain Seismic Belt, in Seismicity of North America, editor E.R. Engdahl, Decade of North American Geology, Bull. Geol. Soc.Am. (in press).

Smith, R.B., J.O.D. Byrd, and D.D. Susong, 1991, Quaternary History, Neotectonics, and Earthquake Hazards of the Teton Fault, Wyoming, submitted to "The Geology of Wyoming", A. Snoke and J. Steidtmann *eds*, published by Wyoming Geological Association, submitted.

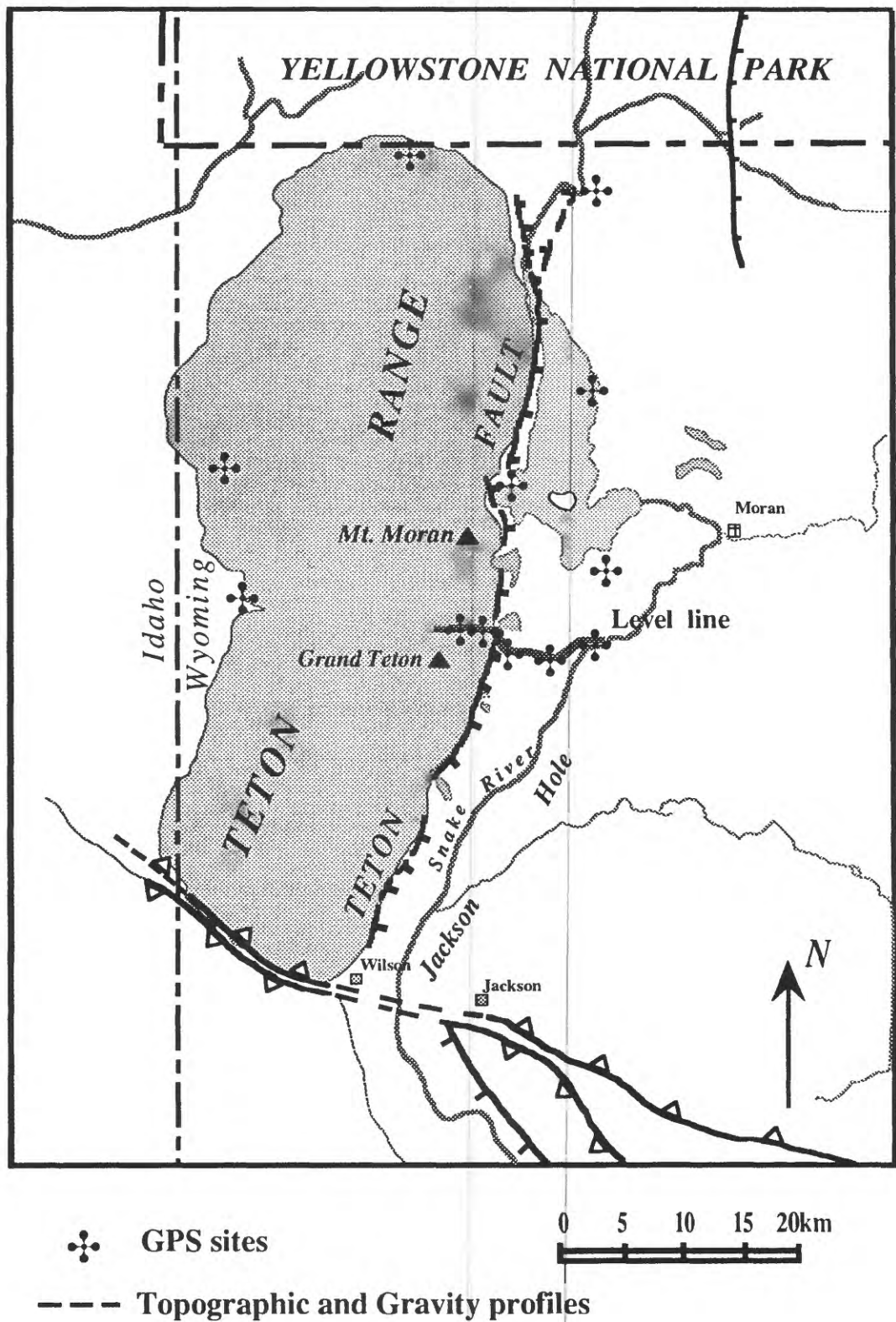


Figure 1: Location map showing major geographic features and the trace of the Teton fault, 1st order level line, GPS sites, topographic and gravity profiles

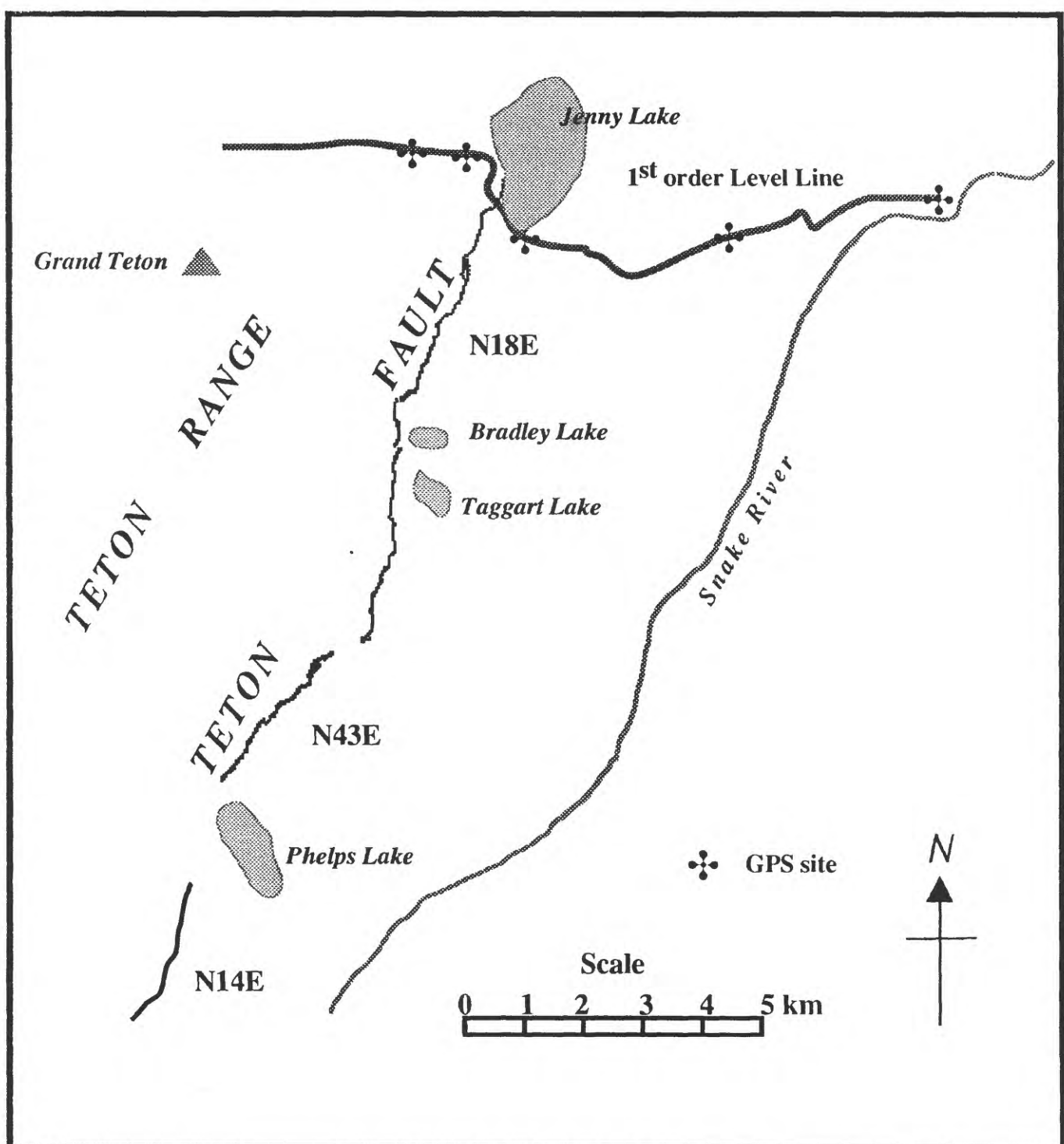


Figure 2: Area covered by detailed three dimensional survey of the Teton fault and locations of GPS sites along the 1st order level line. Western GPS sites were established in 1991. Geographic points are included for reference.

Teton Range

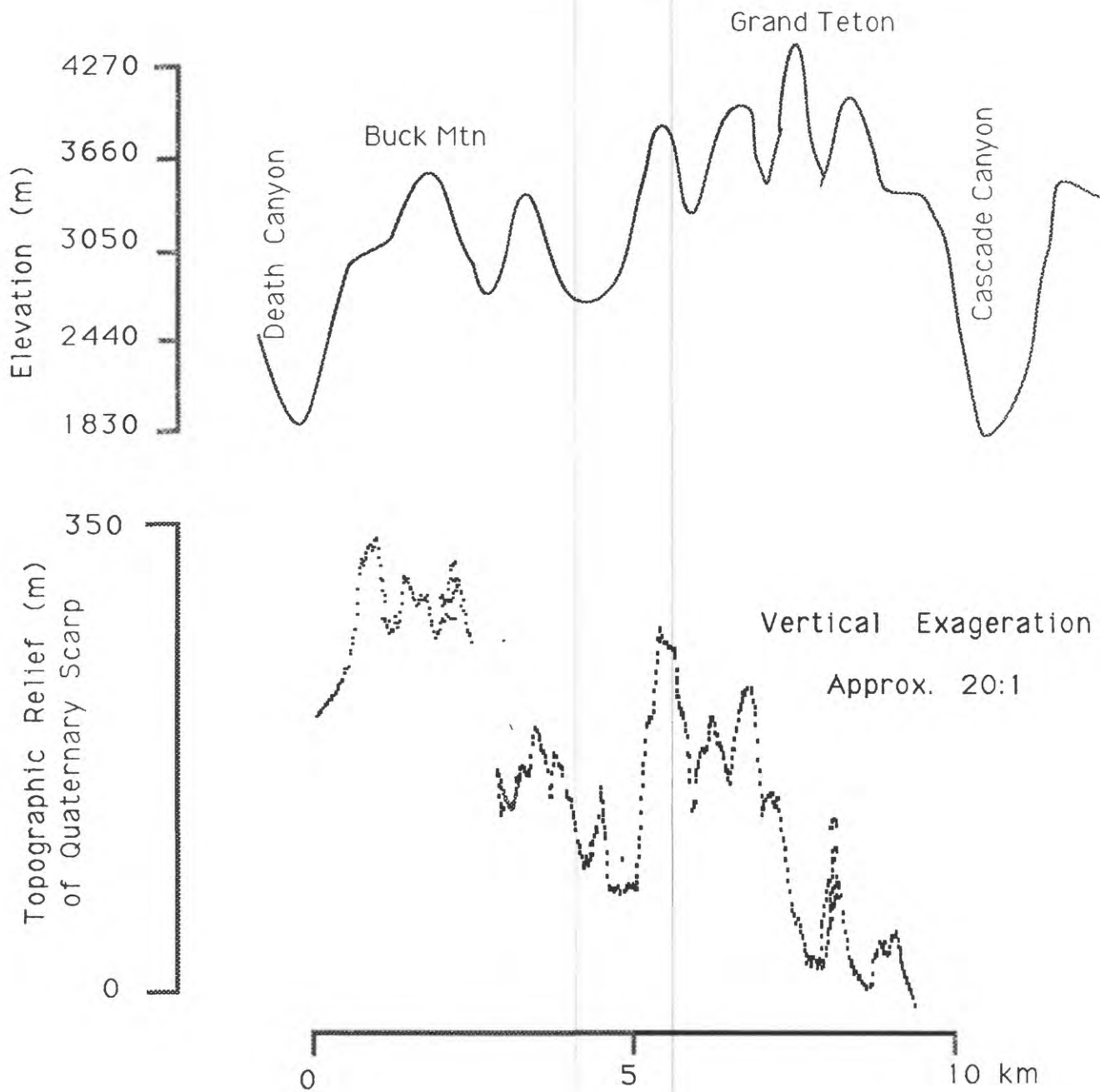


Figure 3: General topography of the crest of the Teton Range and "up-dip" expression of the surface trace of the Teton fault (note vertical exaggeration) along a portion of the detailed three dimensional survey of the fault. Note apparent self-similar character of the wave form of the fault.

ONSHORE-OFFSHORE NEOTECTONICS - NORTH COASTAL ZONE OF OREGON

9460-11032

P.D. Snavely, Jr., Ray E. Wells
 Branch of Pacific Marine Geology and Western Regional Geology
 U.S. Geological Survey
 345 Middlefield Road, MS-999
 Menlo Park, California 94025
 (415) 354-3081
 FTS 459-3081

Investigations

Drowned marshes and forests of coastal Oregon and Washington may record coseismic subsidence of the shoreline during large subduction zone earthquakes (e.g., Atwater, 1987, *Science*, v. 236, p. 942-944; and others). However, new bedrock geology of the northern Oregon coast (Snavely et al., 1990; Wells et al., in prep.) shows that Tillamook Bay, Netarts Bay, and possibly other estuaries are structurally controlled by major late Cenozoic fault zones that trend northwest onto the continental shelf. Estuaries lie on the downthrown block in each case. Some of these structures may correlate with features observed on a USGS seismic-reflection line 76-6 that parallels the coast, about 10 km offshore (fig. 1). A surprising amount of late Cenozoic deformation can be seen on this profile on structures that are apparently transverse to the margin. Deformation on these transverse fault zones may in part control the subsidence history of adjacent downdropped estuaries.

Our investigations address the timing and style of young faulting along northwest coastal Oregon through onshore mapping of Quaternary thrust faults exposed in seacliffs and through interpretation of the offshore seismic lines. The correlation of the onshore and offshore tectonic framework may place constraints on interpretations of workers concerned with co-seismic events as disclosed from studies of submerged estuary deposits along this coastal zone. Areas of supposed co-seismic subsidence could be of regional extent, or may in part be due to local downwarping or downdrop blocks along observed north-trending antithetic faults.

Results1. *Coastal seacliff mapping.*

At the north end of Netarts Bay near Happy Camp (fig. 1), Wells, Snavely, and A. Niem (Oregon State University) have mapped in detail a 200-m-long and 20-m-high seacliff exposing middle Miocene (15 Ma) Columbia River Basalt flows which are cut by a group of northeast-dipping low-angle thrust faults (fig. 2). These faults offset Pleistocene gravel-filled channels and tilt the channel fills up to 25° to the northeast. A later nested Pleistocene channel containing abundant logs and other carbonaceous material interbedded in sand and gravel is also cut by the thrust faults. The top of the cliff appears to be a fluvial or marine terrace which is warped and uplifted over the thrust faults. A buried soil at the top of the cliff appears to be thicker on the downthrown side toward Netarts Bay. Dune sand obscures fault relationships in the Holocene part of the section. Samples for C^{14} dating were collected from the youngest buried soils and channel fills.

2. Offshore seismic reflection profiles.

Snavely completed geologic interpretations of three N-S multichannel seismic-reflection lines off northern Oregon. USGS line 76-6, which is parallel to the coast and about 10 km west of Netarts Bay, indicates that a master thrust underlies folded and faulted strata which may correlate in part with the section studied in the seacliffs north of the bay (fig. 3). The onshore projection of this master thrust may be contributing to the episodic downwarping of Netarts Bay. However, high-resolution seismic profiles on the inner shelf are required to establish this correlation.

The west-northwest trending Quaternary thrusts exposed in the seacliff are consistent with N-S compression axes determined from present-day crustal earthquakes and well borehole breakouts in the Pacific Northwest (references in Snavely and Wells, 1991) and suggest that late Cenozoic north-south shortening of the Coast Range is an important element of the present tectonic regime.

Reports

Niem, A.R., N.S. MacLeod, P.D. Snavely, David Higgins, J.D. Fortier, J. Meyer, and A. Seeling, in press, Onshore-offshore geologic cross section, northern Oregon Coast Range to continental slope, *Oregon Department of Geology and Mineral Industries Oil and Gas Investigations* ___, 38 p., 2 plates.

Snavely, P.D., N.S. MacLeod, and D.L. Minasian, 1990, Preliminary map of the Nestucca Bay quadrangle, Tillamook County, Oregon, *U.S. Geological Survey Open-File Report 90-202*, scale 1:24,000.

Snavely, P.D., N.S. MacLeod, and D.L. Minasian, 1990, Preliminary geologic map of the Neskowin quadrangle, Lincoln and Tillamook Counties, Oregon, *U.S. Geological Survey Open-File Report 90-413*, scale 1:24,000.

Snavely, P.D., N.S. MacLeod, and D.L. Minasian, 1991, Preliminary geologic map of the Dolph quadrangle, Lincoln, Tillamook and Yamhill Counties, Oregon, *U.S. Geological Survey Open-File Report 91-277*, scale 1:24,000.

Snavely, P.D., and R.E. Wells, 1991, Cenozoic evolution of the continental margin of Oregon and Washington, *U.S. Geological Survey Open File Report 91-441-B*, 34 p.

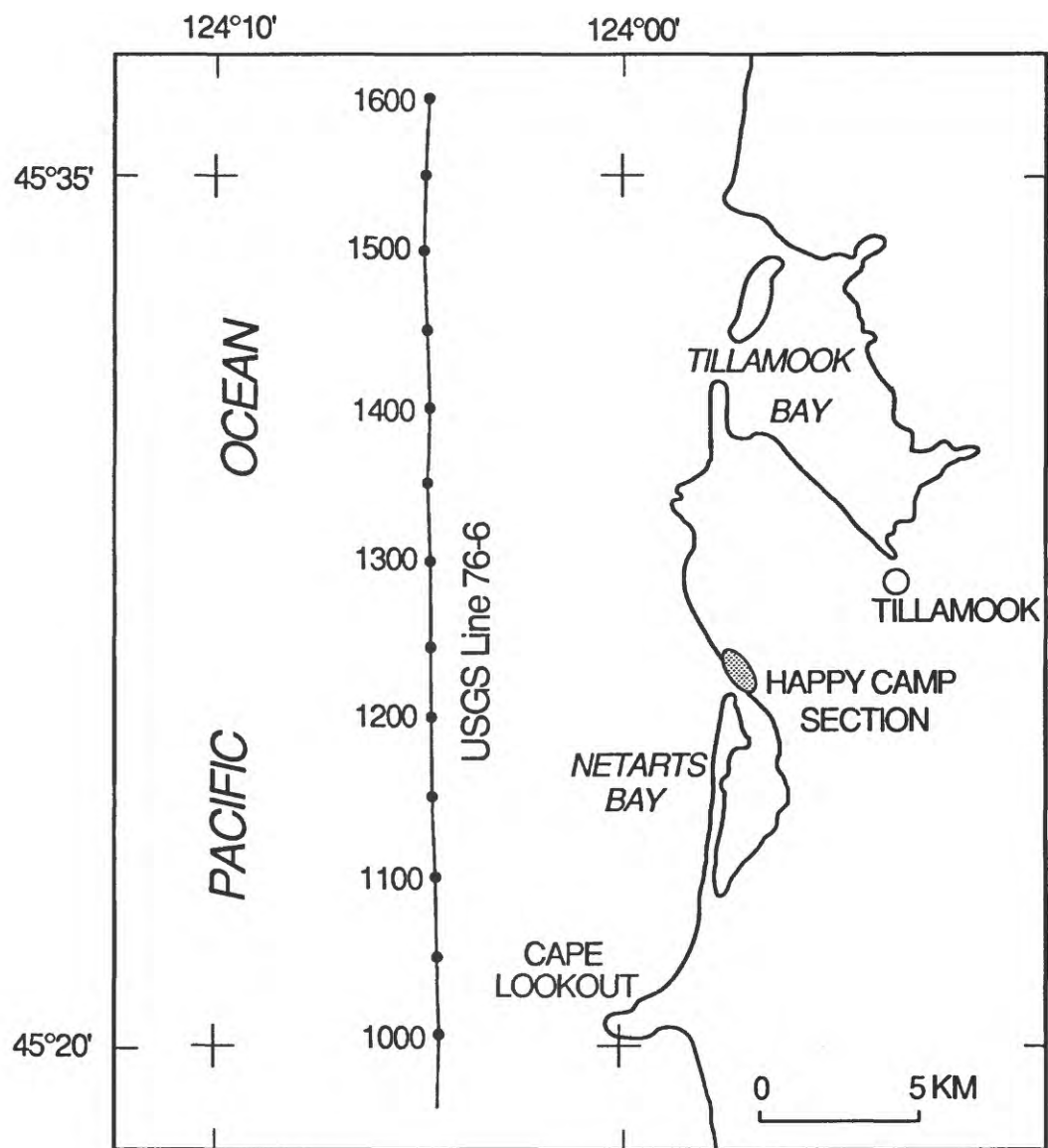


Figure 1. Map of northwest Oregon showing location of Happy Camp seafloor exposure and location of USGS seismic-reflection line 76-6. Shot points along seismic line correlates with those shown on interpreted section, figure 3.

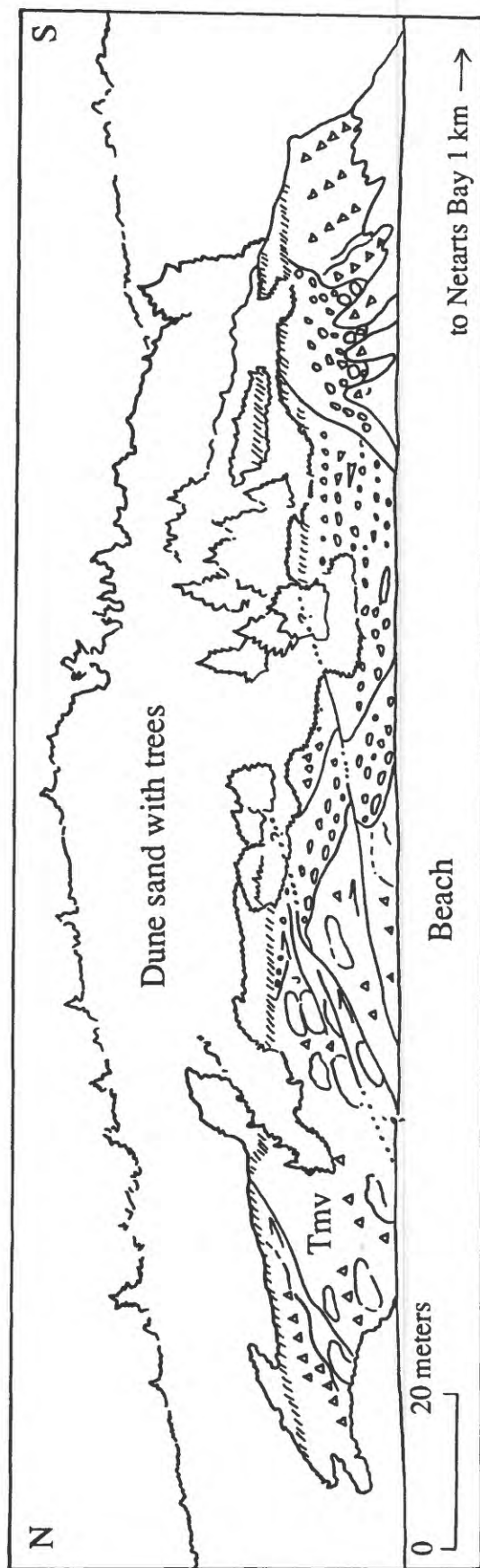


Figure 2. Line drawing of 200-m-long and 20-m-high seacliff exposure near Happy Camp, north of Netarts Bay, Oregon. Tmv is Miocene (15 Ma) Columbia River Basalt pillows and breccia (triangles). Thrust faults cut basalt and Pleistocene channel fills (gravel symbols) containing wood fragments. Hachured lines indicate buried soils.

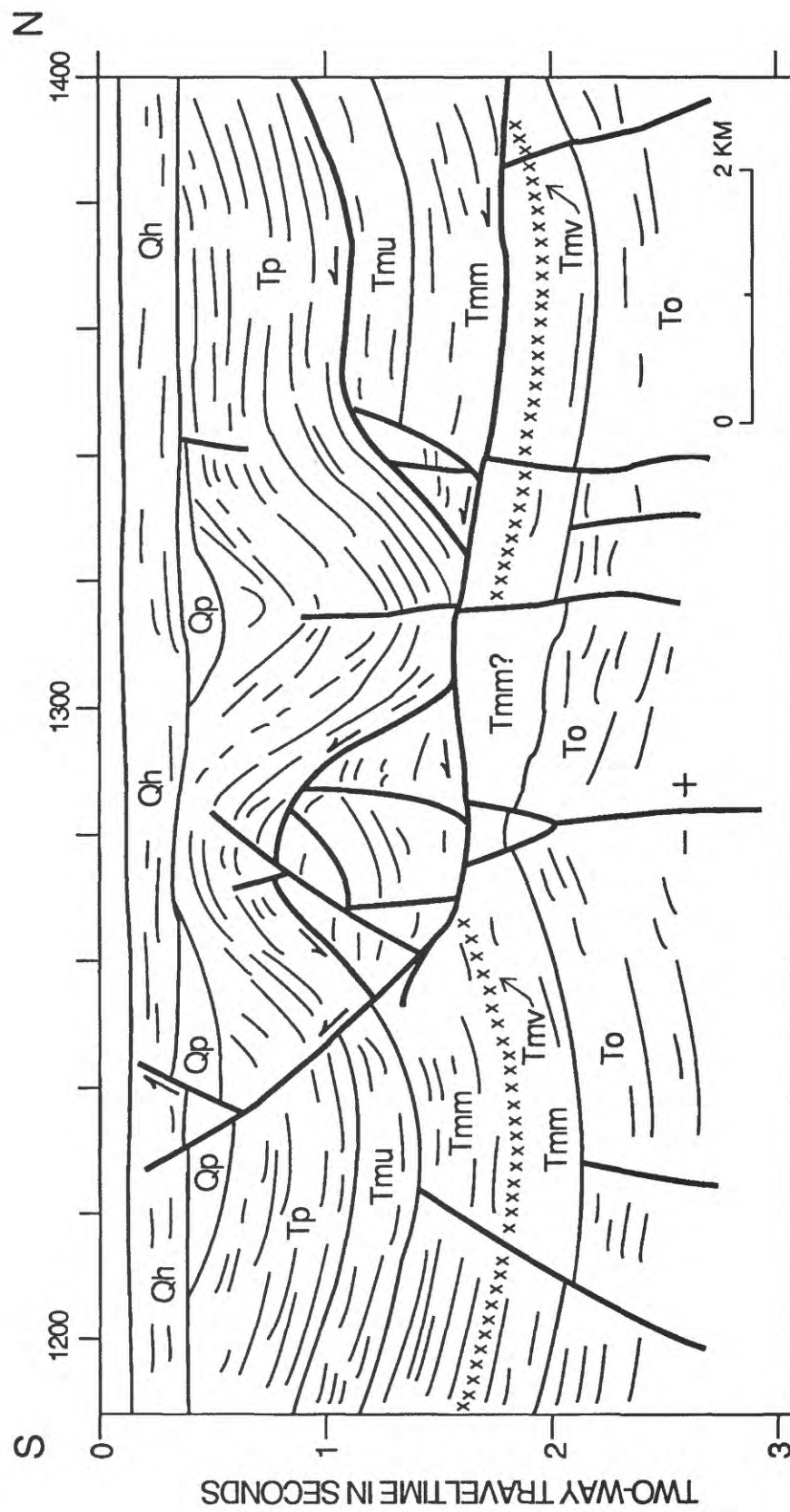


Figure 3. Geologic interpretation of a segment of USGS multichannel seismic-reflection profile 76-6. Symbols: Qh, Holocene; Qp, Pleistocene; Tp, Pliocene; Tmu, upper Miocene; Tmm, middle Miocene; To, Oligocene; small x's with symbol Tmv, middle Miocene (15 Ma) basalt flow; faults, half arrows indicate direction of movement on thrust faults.

Annual Technical Report XXXIII

Modeling and Monitoring Crustal Deformation 9960-01488

Ross S. Stein, Wayne Thatcher, and Grant A. Marshall
Office of Earthquakes, Volcanoes, and Engineering
345 Middlefield Road, MS 977
Menlo Park, California 94025
Tel 415/329-4840, FTS 459-4840
Fax 415 329 5163

INVESTIGATIONS

1. We investigated extensional tectonics in continental, mid-oceanic ridge and trench outer rise settings.
2. We studied the mechanics of blind thrust faults in the Los Angeles basin, concentrating how isolated faults in elastic media interact with the free surface.
3. Analysis and interpretation of tidal gage data relevant to interseismic deformation at the Nankai Trough, Japan, subduction zone.

RESULTS

Extensional and conjugate fault geometries. Examination of data bearing on fault initiation and evolution in diverse extensional environments has illustrated their common and contrasting features. Earthquake fault plane solutions show that continental and mid-ocean ridge pure normal fault dips are concentrated near 45° , while trench outer rise normal faults dip about 55° . The absence of significant lithospheric extension near oceanic outer rises suggests, as simple faulting theory implies, that normal faults initiate near $\sim 60^\circ$ dip and undergo little rotation, while continental and mid-ocean ridge faults rotate and coalesce into major seismogenic features as they evolve and are deactivated for dips less than about 45° . At mid-ocean ridges the degree to which fault-related topography develops depends on magma supply rate fluctuations and spreading rate. A simple model of faulting, lithospheric flexure and rotation produces synthetic bathymetric profiles that can reproduce tectonically-generated relief at slow-spreading ridges. (W. Thatcher and D. Hill)

Mechanics of Blind thrust faults. This is a continuation of work in press by *Stein and Ekström*, which analyzed blind thrusting in the San Joaquin Valley. Geodetic and geological evidence has revealed that the crust beneath the Los Angeles basin is contracting at a rate of ~ 8 mm/yr in a north-south direction, and that a suite of blind reverse and thrust faults underlies the basin to accommodate this contraction. We seek to understand the deep fault geometry in the Los Angeles basin, to deduce or constrain the fault slip rates and, where possible, earthquake repeat times. In addition, we seek to understand the earthquake cycle on the blind faults, and to learn how adjacent blind faults interact as they are stressed and relaxed during the cycle. We investigated the shear and dilatation fields associated with

tapered slip on blind faults, since patterns of aftershocks furnish a means to test whether the predicted strain changes are observed in the earth. We examined a suite of fault geometries that are found or are believed to exist in the Los Angeles basin, studying the effects of fault dip and the proximity of the fault to the free surface. When the fault is deeply buried, a high shear strain halo encircles the fault, with slightly concentrated strain at the fault ends. When the depth of the fault tip was less than the fault's down-dip width, ground-surface interaction significantly modifies the shear and dilatant strain fields, and the halo breaks up into several isolated zones of high shear strain. These zones correspond to sites of high-angle reverse faults and aftershocks found in the cores of many active anticlines, which lie above the fault tip. If the rocks at this shallow depth are strong enough to store elastic strain, the increased shear will promote secondary failure [see Figure] (J. Lin, R. Stein, and G. King).

Interseismic Deformation at Subduction Zones. Uplift along the coast of southwestern Japan following the 1944 Tonankai ($M_S = 8.0$) and 1946 Nankaido ($M_S = 8.2$) earthquakes has been inferred from the 1950-1985 tide-gage records. Although uplift rates vary with geographic position, the temporal dependence at each site can be described as the superposition of an exponentially decaying time constant (~5 yr) transient, significant only in the first decade postseismic, and a steady interseismic rate. The steady interseismic uplift rate is defined only over the 1956-1985 interval, but the linearity in time of that uplift record is such that uplift over the remainder of the interseismic cycle (~80 yr) might reasonably be expected to occur at the same rate. Moreover, the spatial pattern and magnitude of the steady uplift rate is reasonably close to that predicted by a simple dislocation model of subduction. However, the currently observed steady uplift rate is not consistent with the uplift rate inferred from geodetic leveling for the final half of the previous earthquake cycle. Thus, either the hypothesis of a steady interseismic uplift rate after the first decade postseismic is wrong or the strain accumulation pattern for one earthquake need not be the same as for the preceding earthquake on the same segment. (J.C. Savage and W. Thatcher)

REPORTS PUBLISHED OR SUBMITTED DURING THIS PERIOD (excluding abstracts):

Ekström, G., R. Stein, J.P. Eaton, and D. Eberhart-Phillips, Seismicity and geometry of a 110-km-long blind thrust fault, 1, The 1985 Kettleman Hills, California, earthquake, in press, *J. Geophys. Res.*, 1991.

Hill, D.P., and W. Thatcher, A minimum energy criterion for frictional slip on misoriented faults, in press, *Bull. Seismol. Soc. Am.*, 1991.

Marshall, G.A., R.S. Stein, and W. Thatcher, Faulting geometry and slip from coseismic elevation changes: The October 17, 1989 Loma Prieta, California, earthquake, *Bull. Seismol. Soc. Am.*, 81, 1660-1693, 1991.

Savage, J.C., and W. Thatcher, Interseismic deformation at the Nankai Trough, Japan, subduction zone, *J. Geophys. Res.*, submitted, 1991.

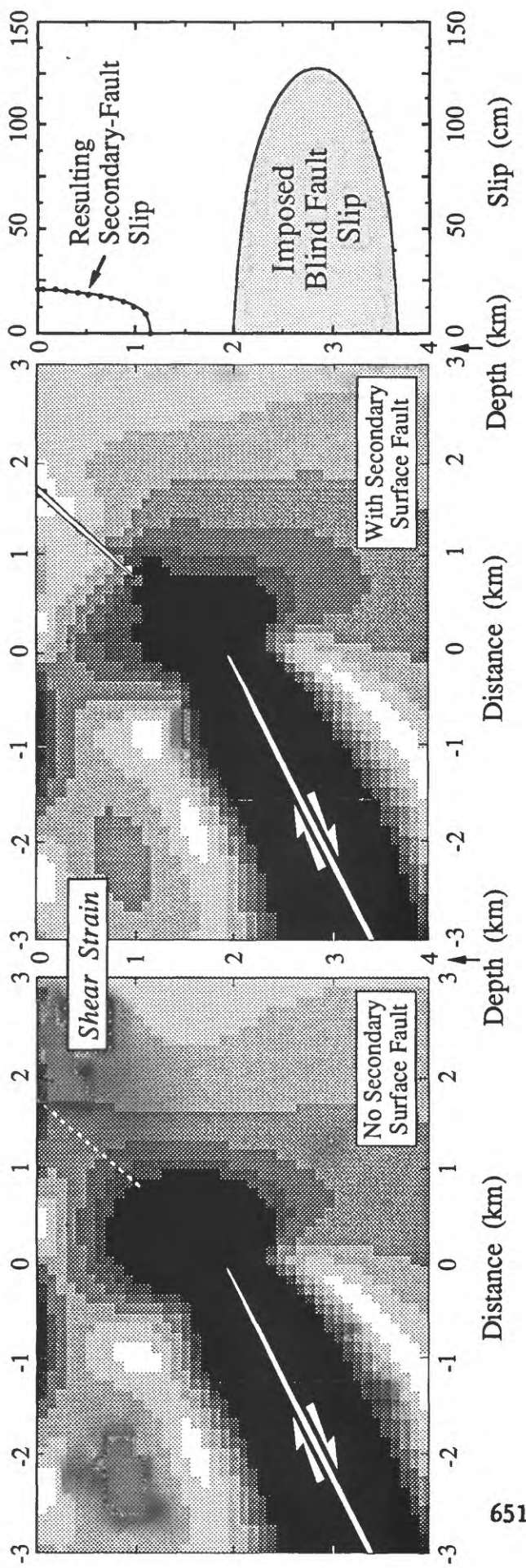
Stein, R.S., and G. Ekström, Seismicity and geometry of a 110-km-long blind thrust fault, 2, Synthesis of the 1982-1985 California earthquake sequence, submitted, *J. Geophys. Res.*, 1991.

Stein, R. S., P. Briole, J.-C. Ruegg, P. Tapponnier, and F. Gasse, Contemporary, Holocene and late Quaternary deformation of the Asal rift, Djibouti: Implications for the mechanics of slow-spreading ridges, in press, *J. Geophys. Res.*, 96, 1991.

Thatcher, W., and D.P. Hill, Fault orientations in extensional and conjugate strike-slip environments and its implications, *Geology*, 19, 1116-1120, 1991.

Yeats, R.S., A. Farah, M.A. Mirza, T. Nakata, M.R. Pandey, R.S. Stein, and K.S. Valdiya, The Himalayan frontal fault system, *Geological Character of Active Faults*, IGCP-206 Volume, Cambridge University Press, in press, 1991.

A Rootless Secondary Reverse Fault Relieves Strain Produced by Slip on a Blind Thrust



- Slip on a blind thrust produces high shear strain (dark zones) above the fault tip at the earth's surface.
- Secondary slip on a rootless reverse fault relieves strain in front of the blind thrust fault.
 - For this geometry, slip on the surface-cutting fault will be 25% of the blind thrust slip.

Consolidated Digital Recording and Analysis

9930-03412

S.W Stewart, R.S. Dollar, A.W. Walter
Branch of Seismology
U. S. Geological Survey
345 Middlefield Road, MS/977
Menlo Park, California 94025
(415) 329-5515

Investigations.

This project supports the Earthquake Hazards Reduction Program in the following ways. (1) It has developed and now provides automated hardware/software systems to enable the operation of large, regional seismic networks. For example, the CALNET Northern California Seismic Network and the Caltech/USGS Cooperative Southern California Seismic Network are producing masses of data in identical formats because they are using matched automated computer systems developed by this project. (2) It supports the focused monitoring experiment currently being carried out at Parkfield, California. The same software/hardware system used for large regional networks is used at the Varian and Haliburton monitoring sites at Parkfield.

There are between 25-50 regional seismic networks in the U.S., consisting of 1200-1500 seismic stations. The two largest regional networks are the Northern California Seismic Network (CALNET) operated by the USGS in central California, and the Southern California Seismic Network operated jointly by Caltech and the USGS. CALNET consists of more than 300 sites and 500 instruments, while the Southern California Seismic Network has at least 200 sites and 300 instruments. These two networks combined account for about one-half of the existing seismic stations and about three-quarters of the existing data volume of digitized waveforms from all regional seismic networks in the U.S.

This project has developed the hardware and software systems necessary to automate both the detection and processing of earthquakes occurring within these two regional networks.

Hardware for these systems is based upon the Digital Equipment Corporation (DEC) VAX series of micro-computers. Currently, this includes the VAX 750, microVAX II, and VAXstations 2000, 3100 and 3200.

Software is based upon the DEC/VMS operating system, the CUSP database system, and the GKS graphics system. VMS is a major operating system, well documented and developed, and has a rich variety of system services that facilitate our own system development. CUSP is a state-driven database system designed for systematically processing large numbers of earthquakes recorded by large local seismic networks. It was developed by Carl Johnson formerly of the USGS. GKS is an international-standard graphics analysis package that provides interactive input facilities as well as graphical output to a workstation. We use the DEC implementation of GKS.

Results:

1. All elements of a complete package for Realtime processing of Regional Seismic Network Data were completed and installed at the sites listed in (2) below. These elements are collectively referred to as the CUSP system, version 1.0, and include:

RT: the Real_Time data acquisition system; this system performs both online earthquake detection and pre-processing. The pre-processing steps include automatic P-phase picking and calculation of a hypocenter.

TIMIT: an interactive graphics program to process earthquake traces; this program can handle seismic waveforms recorded on different regional networks, merged from several sources, each with different digitizing rates and different instrument characteristics. For example, Quanterra 24-bit waveform data from Caltech can be merged and displayed along with 16-bit waveform data from the CALNET and Southern California earthquake networks. The former QED earthquake editor is a subset of the TIMIT system.

STNMAP: an interactive graphics program to display the station locations and epicenter of each earthquake. The analyst can select subsets of the stations and trial hypocenters for more detailed analysis.

2. The following networks (or network operators) are now using CUSP software:

Northern California Seismic Network (CALNET)
 Southern California Seismic Network
 Parkfield Prediction Experiment (Varian site)
 Parkfield Prediction Experiment (Haliburton site)
 University of Nevada (Reno)
 Idaho National Engineering Laboratories (INEL)
 University of Southern California

3. To make the CUSP data more easily available to the scientific community, we spent considerable time making general-purpose routines to convert seismic data from one format to another, including CUSP-to-SEGy, SEGy-to-CUSP, and CUSP-to-AH XDR format. The latter includes decimation filtering for processing teleseismic data. The CUSP-to-AH software is used extensively by other investigators in the Seismology Branch for teleseismic studies.

4. It is no longer necessary to convert CUSP digitized waveform data to other formats in order to use it. For example, a cross-correlation program used in the study of earthquake doublets was modified to read the CUSP seismogram files directly.

5. The RTP-to-CUSP software was re-written and is operating within the CALNET network. The net result is less demand on the CPU, more efficient error-handling, and more efficient maintenance and modification of the software.
6. This project continued its responsibility for providing general VAX/VMS computing services to the Branch of Seismology in Menlo Park.

Reports:

None.

INFLUENCE OF THE SOUTHERN WASHINGTON CASCADES CONDUCTOR ON VOLCANISM AND TECTONISM

9980-04028

Donald A. Swanson
Branch of Igneous and Geothermal Processes
U.S. Geological Survey
Department of Geological Sciences AJ-20
University of Washington
Seattle, WA 98195
(206) 553-5587

Investigations

The Blue Lake 7-1/2-minute quadrangle (figs. 1 and 2), near the eastern edge of the Southern Washington Cascades Conductor (SWCC; Stanley and others, 1987, 1990), was mapped geologically at a scale of 1:24,000. In addition, parts of the Tower Rock (Swanson, 1991), McCoy Peak (Swanson, 1992), and French Butte (Swanson, 1989) quadrangles were field checked and modified where necessary. The geologic map of the Blue Lake quadrangle will be released as an open-file report after chemical analyses and thin sections are received and evaluated, most likely in 1992.

This work is part of an ongoing cooperative effort with Roger Ashley and Russ Evarts (Branch of Western Mineral Resources, U.S. Geological Survey, Menlo Park) to define the development of the Cascade Range along an east-west transect in the Mount St. Helens area (fig. 1). The SWCC, an anomalous electrical conductor at intermediate depth within the crust, underlies that part of the transect area between Mount St. Helens and Mount Adams. One goal of the cooperative effort is to compare and contrast volcanism and tectonism above the SWCC with that beyond the limits of the SWCC.

Improved understanding of the nature and influence of the SWCC is important in order to define and evaluate earthquake hazards in the area. The western margin of the SWCC coincides with the St. Helens seismic zone (Weaver and Smith, 1983; Grant and others, 1984; Grant and Weaver, 1986), which "could, under certain assumptions, be capable of generating a magnitude 7.0 earthquake" (Weaver and Smith, 1983, p. 10,380). The northeastern margin of the SWCC includes a north-northwest-trending zone of seismicity near Mount Rainier (Weaver and Malone, 1987; Stanley and others, 1987) and the epicentral area of the 1981 Goat Rocks earthquake (magnitude 5.0; Zollweg and Crosson, 1981; Weaver and Smith, 1983).

Results

The Blue Lake quadrangle contains a suite of volcanic rocks ranging in age from late Oligocene to Quaternary. Lava flows, pyroclastic flows, and diamictites of andesite and basaltic andesite, with minor dacite and rhyolite, comprise the Tertiary section. These rocks were intruded by numerous dikes and related intrusions and then folded along a north-northwest-trending axis that crosses the quadrangle from its northwest corner to its southeast corner (fig. 2).

The folding took place before about 12 Ma, the approximate age (from zircon fission-track counts) of a suite of hornblende andesite-dacite and hornblende diorite-quartz diorite dikes and sills that intrude the older rocks (fig. 2). This hornblende-bearing suite forms a subvolcanic complex with a large radial dike swarm (Swanson, 1990, 1991) centered in the northeast part of the McCoy Peak quadrangle. The pattern of the radial dikes, and their systematic subvertical orientation, indicate that they were intruded after folding, which produced dips of 30–50°. In addition, several other bodies of

hornblende diorite in the Blue Lake quadrangle, though clearly part of the subvolcanic suite, may reflect the presence of other smaller volcanoes, all other evidence for which has been eroded away.

The distribution of the hornblende-bearing intrusive suite is of interest relative to the eastern limit of the SWCC. From reconnaissance work, no representative of this suite occurs much farther east than the eastern edge of the Blue Lake quadrangle, which roughly coincides with the margin of the SWCC (figs. 1 and 2). Future work in the adjoining Hamilton Buttes quadrangle will test this idea.

The hornblende-bearing intrusions in the Blue Lake quadrangle are restricted to the area south of the North Fork Cispus River (fig. 2). In the adjacent Tower Rock quadrangle, the intrusions are similarly restricted to the area south of the Cispus River downstream from the mouth of the North Fork. No significant faulting is evident along these rivers. The rather sharp northern limit in distribution of the hornblende-bearing suite might reflect some kind of crustal control not manifested at the surface, such as a blind fault or hidden structure in the SWCC.

Regional uplift and associated erosion followed intrusion of the hornblende-bearing suite. The timing and duration of the uplift is unknown but might be continuing today. My unpublished reconnaissance study of the paleogradient of the Tieton Andesite, an 80-km long, 1-Ma intracanyon flow in the Tieton River drainage on the east flank of the Cascades (fig. 1), suggests uplift of the Cascade axis of about 4.7 m/km in the past one million years. Whether this implies that uplift is continuing in the Blue Lake area is debatable.

The Pin Creek fault zone (fig. 2), a north-northwest-trending zone first recognized by Hammond (1980), cuts obliquely across the southwest corner of the Blue Lake quadrangle (fig. 2). The fault zone may control the course of the Cispus River for several kilometers upstream from the mouth of the North Fork Cispus River (Swanson, 1991). At least some of the motion within the Pin Creek fault zone was in a dextral sense, as indicated by subhorizontal slickensides on surfaces with stepped surfaces with minimal roughness in a right-lateral direction. Other surfaces show steeply plunging slickensides, however. A marked flattening of attitudes in the volcanic rocks on either side of the fault zone suggests that the zone may in part be a broken monocline on the west flank of the mapped anticline, perhaps a transpressional feature. The age of most recent movement in the fault zone is not known. All breccia zones contain calcite and zeolite and give the appearance of being of Tertiary age. Exposures are poor, however, and the possibility of Quaternary displacement cannot be discounted.

A moderate-size, partly subglacial volcano (Blue Lake volcano) composed of high- K_2O olivine basalt formed during the Hayden Creek Glaciation (probably about 140 ka) in the valley of the Cispus River in the western part of the Blue Lake quadrangle (fig. 2). Basalt of similar composition but probably slightly younger age erupted from several smaller vents just west and south of Blue Lake volcano (fig. 2). These vents lie near and within the Pin Creek fault zone.

The high- K_2O olivine basalt at Blue Lake volcano also lies at the northeast end of a zone of similar olivine basalt that extends southwestward from Blue Lake volcano to beyond the southern limit of the McCoy Peak quadrangle (fig. 2; Swanson, 1992). Significantly, this suite of basalt, which includes at least one flow containing aegirine-augite and a K_2O content of about 2.3 percent, is the most potassic known in the southern Washington Cascades except for the Simcoe volcanic, which is in a behind-the-arc setting. Whether the SWCC influences the composition of the basalt is a question for future work.

To summarize, work in the Blue Lake and adjacent quadrangles has found several features unusual for the southern Washington Cascades that may reflect the presence of the SWCC: an extensive hornblende-bearing suite of intrusive rocks; possible control by the SWCC on the distribution of this suite; and high- K_2O olivine basalt of late Quaternary age that is anomalous in this intra-arc setting. Continued study of the several quadrangles already completed, and of those targeted for future work, will address these issues.

Reports

Swanson, D.A., 1991, Geologic map of the Tower Rock quadrangle, southern Cascade Range, Washington: U.S. Geological Survey Open-File Report 91-314, scale 1:24,000, 26 p.

_____, 1992, Geologic map of the McCoy Peak quadrangle, southern Cascade Range, Washington: U.S. Geological Survey Open-File Report, scale 1:24,000, in preparation.

References Cited

Grant, W.C., and Weaver, C.S., 1986, Earthquakes near Swift Reservoir, Washington, 1958–1963: seismicity along the southern St. Helens seismic zone: *Bulletin of the Seismological Society of America*, v. 76, p. 1573-1587.

Grant, W.C., Weaver, C.S., and Zollweg, J.E., 1984, The 14 February 1981 Elk Lake, Washington, earthquake sequence: *Bulletin of the Seismological Society of America*, v. 74, p. 1289-1309.

Hammond, P.E., 1980, Reconnaissance geologic map and cross sections of southern Washington Cascade Range: Portland, Oreg., *Publications of Department of Earth Science of Portland State University*, scale 1:125,000.

Stanley, W.D., Finn, Carol, and Plesha, J.L., 1987, Tectonics and conductivity structures in the southern Washington Cascades: *Journal of Geophysical Research*, v. 92, p. 10,179-10,193.

Stanley, W.D., Mooney, W.D., and Fuis, G.S., 1990, Deep crustal structure of the Cascade Range and surrounding regions from seismic refraction and magnetotelluric data: *Journal of Geophysical Research*, v. 95, p. 19,419-19,438.

Swanson, D.A., 1989, Geologic maps of the French Butte and Greenhorn Buttes quadrangles, Washington: U.S. Geological Survey Open-File Report 89-309, scale 1:24,000, 25 p.

_____, 1990, Trends of middle Tertiary dikes in and north of the Dark Divide Roadless area, southern Washington Cascades: *Eos, Transactions of the American Geophysical Union*, v. 71, p. 1144.

_____, 1991, Geologic map of the Tower Rock quadrangle, southern Cascade Range, Washington: U.S. Geological Survey Open-File Report 91-314, scale 1:24,000, 26 p.

_____, 1992, Geologic map of the McCoy Peak quadrangle, southern Cascade Range, Washington: U.S. Geological Survey Open-File Report, scale 1:24,000, in preparation.

Weaver, C.S., and Malone, S.D., 1987, Overview of the tectonic setting and recent studies of eruptions of Mount St. Helens, Washington: *Journal of Geophysical Research*, v. 92, p. 10,149-10,154.

Weaver, C.S., and Smith, S.W., 1983, Regional tectonic and earthquake hazard implications of a crustal fault zone in southwestern Washington: *Journal of Geophysical Research*, v. 88, p. 10,371-10,383.

Zollweg, J.E., and Crosson, R.S., 1981, The Goat Rocks Wilderness, Washington, earthquake of 28 May 1981: *Eos, Transactions of the American Geophysical Union*, v. 62, p. 966.

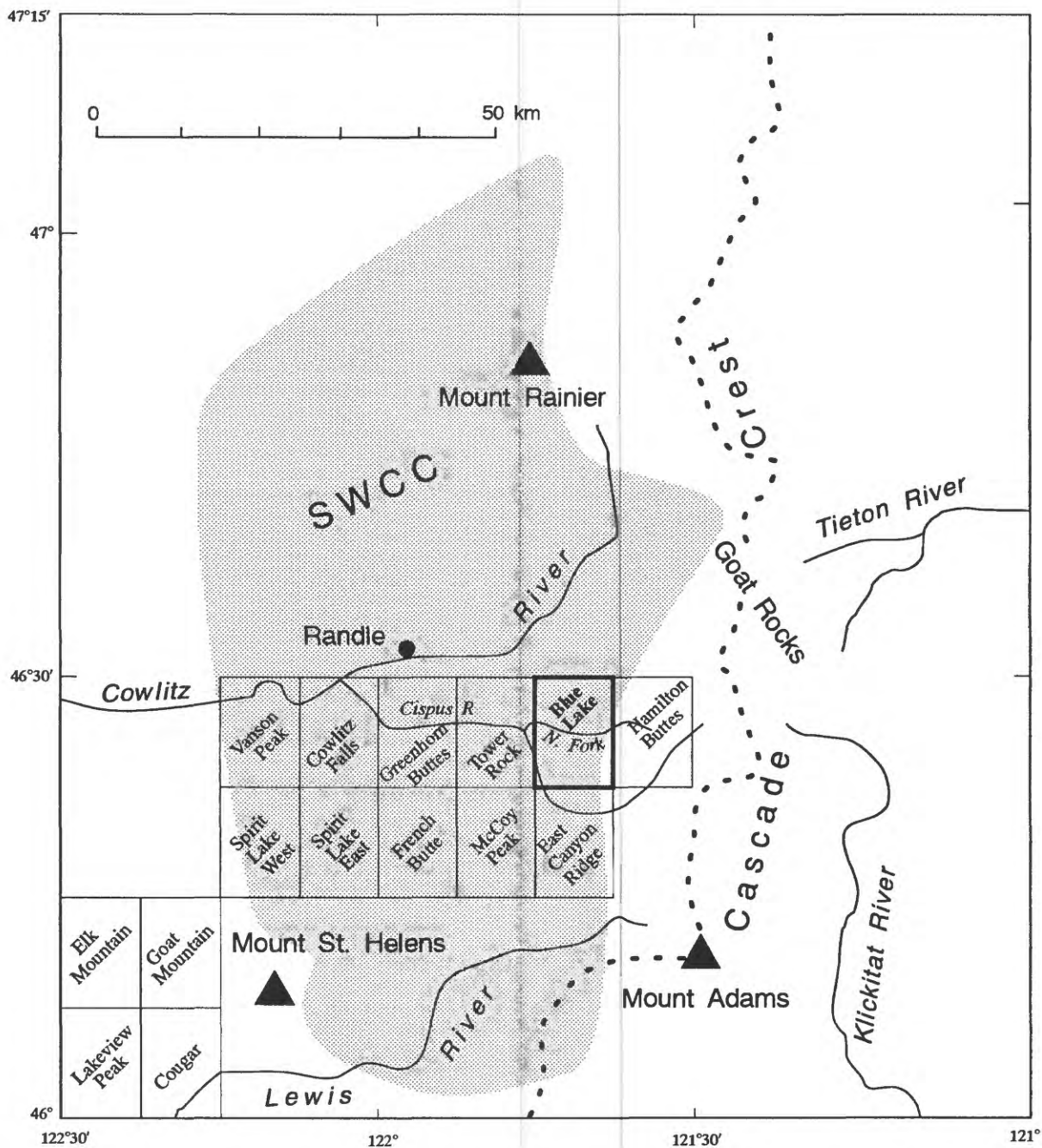


Figure 1. Map showing locations of Blue Lake quadrangle and other quadrangles being mapped in the southern Washington Cascades relative to the Southern Washington Cascades Conductor (SWCC). The quadrangles west of longitude 122° are being mapped by Russ Evarts and Roger Ashley (U.S. Geological Survey, Menlo Park), and those east of 122° by me.

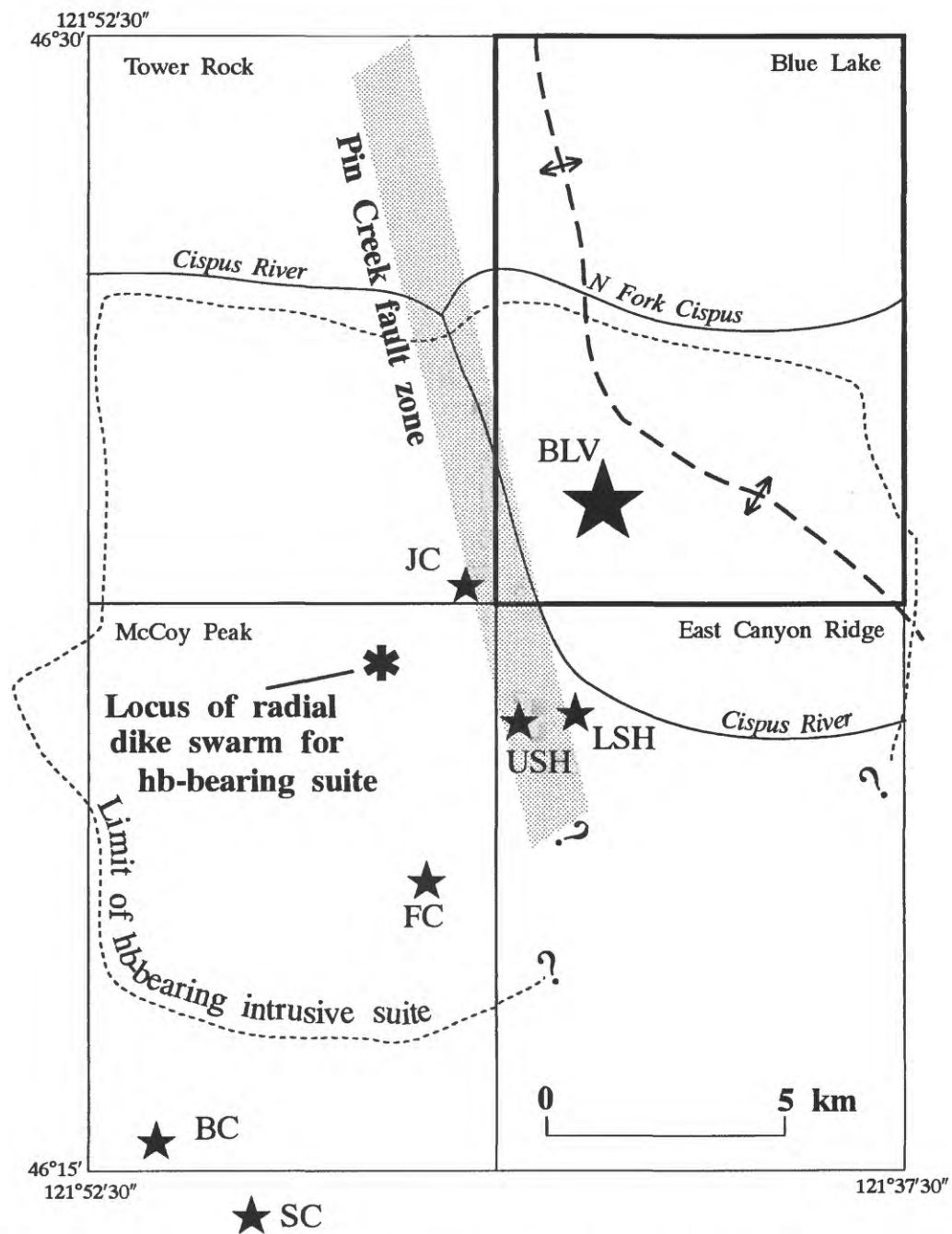


Figure 2. Sketch map showing location of several important geologic features mentioned in the text and possibly relevant to the SWCC. Stars indicate vents for Quaternary high- K_2O olivine basalt. BLV, Blue Lake volcano; JC, Juniper Creek; LSH, lower Spud Hill; USH, upper Spud Hill; FC, Falls Creek; BC, Basin Camp; SC, Snagtooth Creek.

Geometry, kinematics and evolution of pseudotachylyte-bearing rupture systems

Grant #: 14-08-0001-G2060

Mark T. Swanson
University of Southern Maine
Gorham, Maine 04038
(207) 780-5051

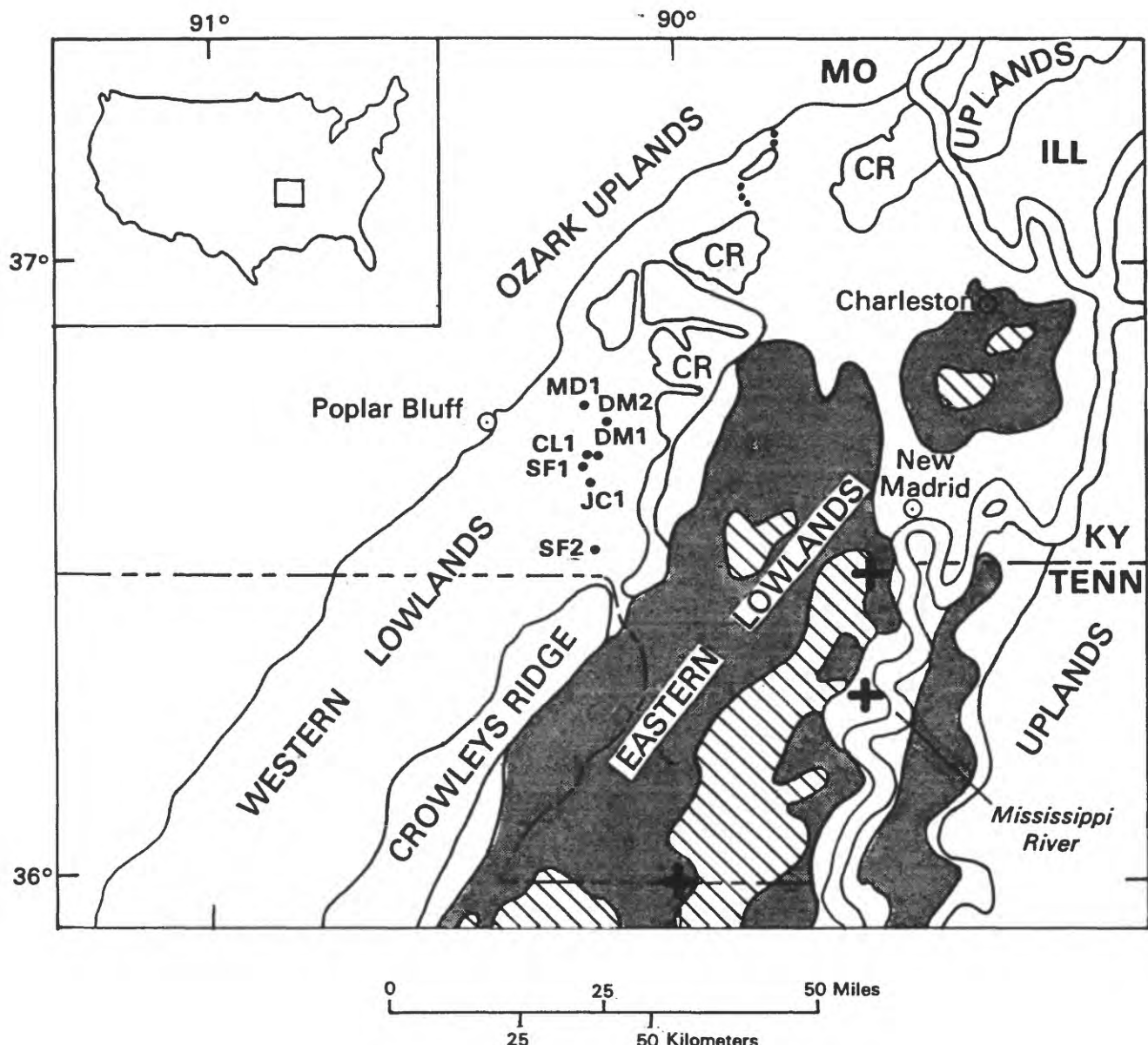
Investigations: Current research involves continuing efforts in the detailed outcrop mapping of brittle fault geometries within both ductile mylonitic and brittle cataclastic fault zones from two localities along the Maine coastal exposures that approximate lower to mid-levels within paleo strike-slip seismogenic zones.

Fort Foster Brittle Zone - Mapping has continued within this pseudotachylyte-bearing rupture system along the NW boundary extending the coverage of earlier mapping efforts. Mapping is conducted at a 1:15 field scale from photo mosaics of a coastal outcrop terrace. This phase of mapping has focussed on a 20 x 60 meter section to determine the pattern of major linking oblique dextral shears that tie the intense layer-parallel slip surfaces at the NW boundary with the interior of the brittle zone. Detailed structural analysis along with sampling and thin-section examination is continuing.

Richmond Island Fault Zone - Mapping in the Cape Elizabeth area of coastal Maine had been focussing on the detailed structural relations within the Two Lights cataclastic fault system, a series of en echelon dextral strike-slip fault zones that locally generated pseudotachylyte, both abrasive and adhesive wear features and abundant syn-kinematic quartz veining. Current mapping has moved on to a nearby exposure of a larger cataclastic fault zone exposed on Richmond Island just offshore from the Two Lights area. The Richmond Island fault zone was targeted for detailed study because of the higher displacements, more evolved fault zone structures and mechanisms and the apparent absence of both pseudotachylyte and significant syn-kinematic veins. Mapping has proceeded at a field scale of 1:1200 using an enlarged air photo base for a preliminary survey of the available exposures. Further more detailed mapping is focussing on a one kilometer coastal section with well exposed complicated fault geometries. Detailed mapping is continuing at a field scale of 1:240 using plane table-alidade surveying techniques to accurately depict the geometry of the exposed fault structures. Final detailing and analysis at the outcrop surface along with sampling and thin-section examination is continuing.

Results to date: The results of these field studies are preliminary at this point in the investigation in that mapping is nearing completion but supporting outcrop and thin-section analyses are only getting underway. However, some observations can be made as to the significance of the structures under study.

Fort Foster Brittle Zone - From the completed mapping the system of oblique slip surfaces in these exposures serves as a mechanism of extensional linkage between the intense system of layer-parallel slip surfaces along the NW boundary zone and the interior of the brittle zone. The layer-parallel surfaces are the largest pseudotachylyte generators, while only minimal pseudotachylyte is produced on these oblique dextral shears. Adhesive wear features, as meter-scale sidewall ripouts, is a dominant mechanism along the layer-parallel slip surfaces in the NW boundary zone but are quite rare along the numerous layer-parallel surfaces within



EXPLANATION

-  One to 25 percent of ground surface covered by 1811-12 sandblows
-  More than 25 percent of ground surface covered by 1811-12 sandblows
-  Epicenters for three largest 1811-12 earthquakes according to Nuttli (1979)
- Sites investigated
- ... Terrace riser
- CR Crowley's Ridge

Figure 1. Map showing locations of sites in the Western Lowlands of southeast Missouri where paleoearthquake and 1811-12 earthquake features have been identified. Distribution of 1811-12 sandblow deposits is from Obermeier (1990).

Table 1.
Archaeological and Radiocarbon Data Used to Establish Age Ranges
of Paleoliquefaction Events

Event	Site ¹	Archaeological data ²	¹⁴ C age (yr)	Laboratory no. (Teledyne)	Stratigraphic position	Material
F	DM1		22,750 \pm 650	I-16,459	35 cm below base of buried sandblow	Wood
	DM1		3,570 \pm 100	I-16,460	10-15 cm above bottom of paleochannel that truncates composite sandbar-sandblow	Wood
L	MD1		13,430 \pm 170	I-16,463	58-62 cm below base of buried sandblow	Carbonaceous clayey silt
	MD1	10,000-9,000 yr B.P.			Surface of braided-stream terrace	Early Archaic artifacts
R	DM1		12,570 \pm 200	I-16,462	25-30 cm below base of paleochannel	Mammal vertebra
	DM1		590 \pm 80	I-16,461	Base of paleochannel that truncates clastic dikes	Wood

¹DM1, Dudley Main Ditch site 1; MD1, Mingo Ditch site 1.

²Archaeological data from O'Brien and others (1989) and J.E. Price (1991, oral communication).

Hayward Fault Recurrence Behavior: Trenching Studies, Fremont and Oakland California

14-08-0001-G2115

1 July 91 - 30 June 92

Patrick L. Williams and David L. Jones
Department of Geology and Geophysics
University of California
Berkeley, California 94720

Phone: (510) 486-7156
FAX: (510) 486-5686
e-mail: plwilliams@lbl.gov

Recurrent motion of the Hayward fault is recorded by offset, tilt, and liquification of late Holocene pond and fluvial deposits at the northern end of Tule Pond, in Fremont, California. Tule Pond is contained in a 100-m-wide pull-apart graben cutting the Holocene alluvial fan complex of Alameda Creek. The pond is fault-bounded on the west and east. The eastern trace is not through-going and thus is unlikely to accommodate creep. During 1991 two trenches were excavated across the eastern trace (M3, M4) and a third trench (M5) cut adjacent to the fault. These and two trenches excavated during 1990 reveal evidence for up to five Hayward fault ruptures in the past 1700 years. Evidence for two additional events is equivocal and requires corroboration. Significant gaps in the sedimentary record were also identified, thus some late Holocene ruptures are almost certainly not recorded at this site. Two ruptures within the past \leq 320 years (events R, U) are suggested by 19° and 8° tilts of successive, originally flat-lying pond strata. A maximum southern Hayward fault recurrence time of 190 years is inferred from the \leq 320-year-age of the package of successively tilted strata and subtraction of the 133-year-age of historical rupture of this segment. Strata appear to have sustained warping with a vertical amplitude of about 2m during this period. Additional constraint of the faults *average* recurrence time is needed.

Results from radiocarbon analysis of individual detrital charcoal clasts show abundant old charcoal in the pond sediments. The ages summarized above are inferred from the youngest population of age determinations for given horizons. The younger detrital ages were indicated by 40% of our 1990 samples. All but one of a suite of 15 charcoal clasts submitted for radiocarbon analysis in 1991 were determined to be significantly older than the previously interpreted ages of their host beds. Because several stratigraphic inversions are indicated by the new dates, we suspect that our 1991 sampling picked a higher percentage of old charcoal than previously, or, that a systematic error was introduced during radiocarbon measurement. In order to exclude the latter possibility we are submitting four splits to a second AMS facility for confirmation. We are also considering whether the stratal ages at this site may be, in fact, older than previously interpreted.

FY1991 Accomplishments:

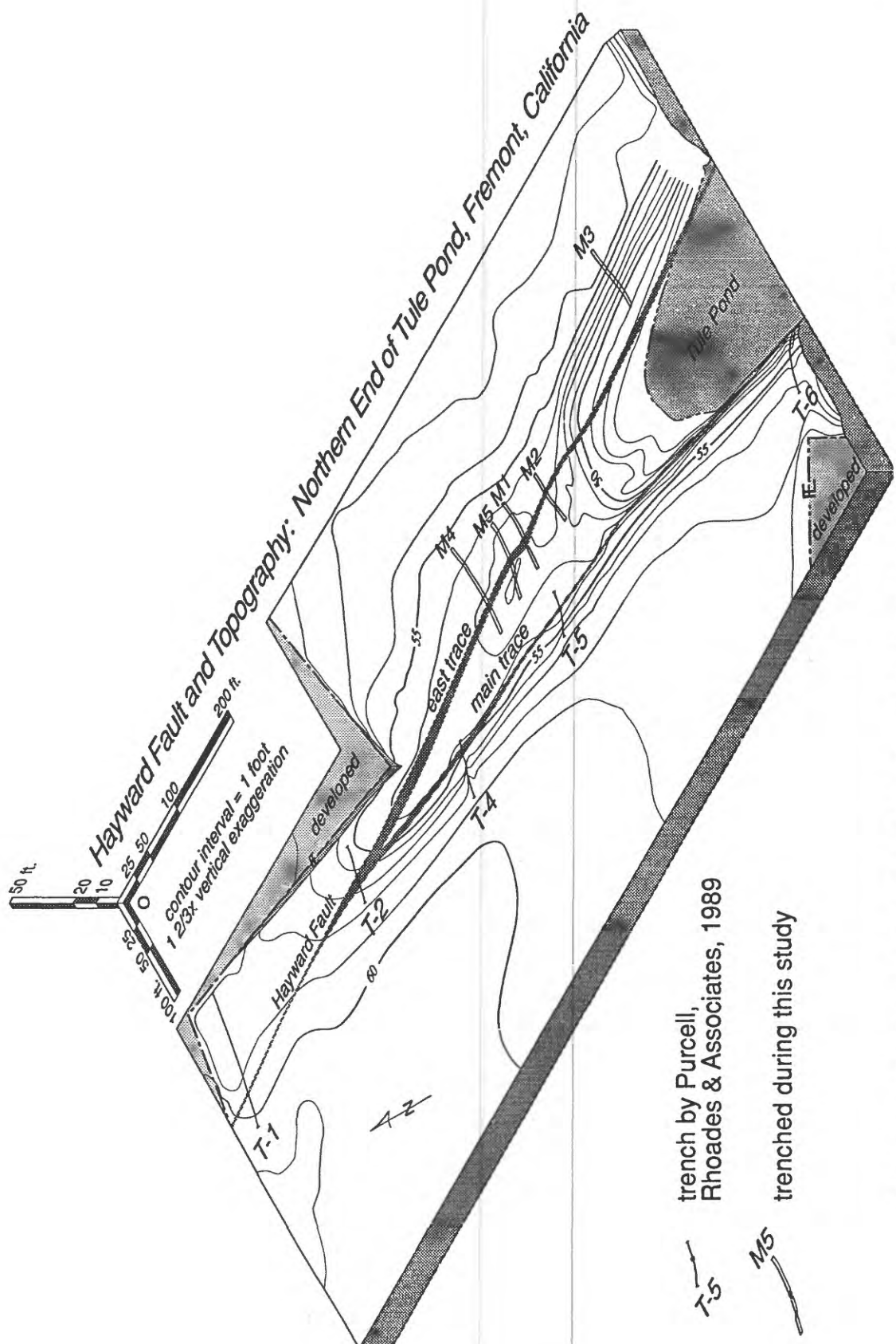
- a) Logging of three new trenches at the north end of Tule Pond;
- b) collection and archiving of over 200 charcoal, bone, and peat samples
- c) Submission of 16 samples for AMS ^{14}C analysis

Additional work planned

Three projects are planned for this funding period: 1) excavation of a trench 5 meters south of M2; 2) collection of several cores to a depth of 5m along the M1 to T5 transect to extend and tie those records; and 3) submission of additional charcoal and other carbon-rich material for dating.

Acknowledgments

Research Assistants T. Black, P. Holland, A. Hosokawa, and M. Thibodeau contributed to field and laboratory investigations.



Orthometric view map of north Tule Pond site. Map shows the topographic expression of the northern end of the Tule Pond graben. The graben results from extension across a right double-bend of the west trace. Artificial fill subdues topographic expression of the graben north of the 47' contour. Pre-fill topography illustrates that the graben is crisply outlined by the mapped fault traces. Trenches M1 and M2 excavated in 1990; M3 and M4 excavated in 1991 in cooperation with William Letts and Associates, M5 excavated by us in 1991.

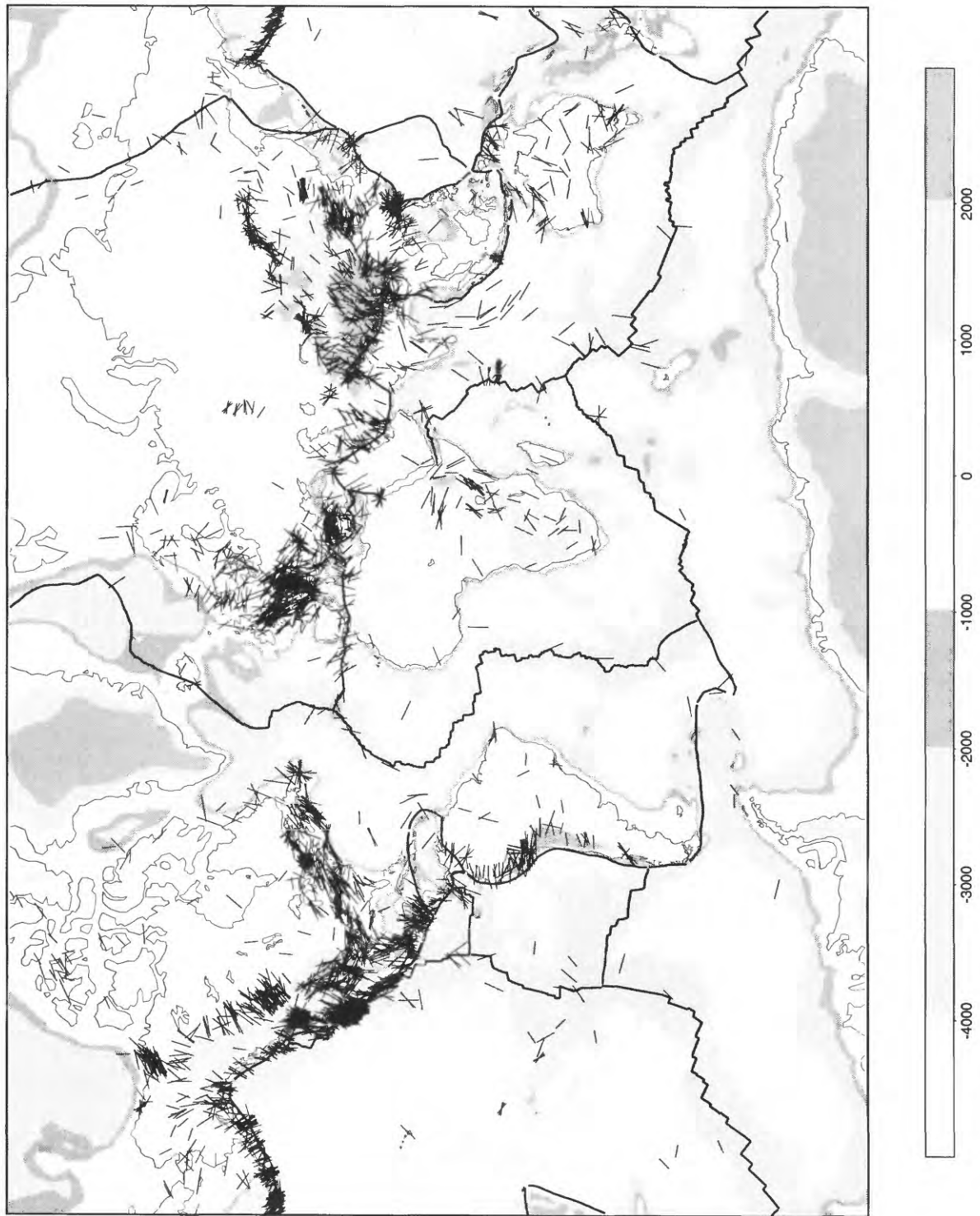


Figure 1. Maximum horizontal stress orientations on a base of average topography.

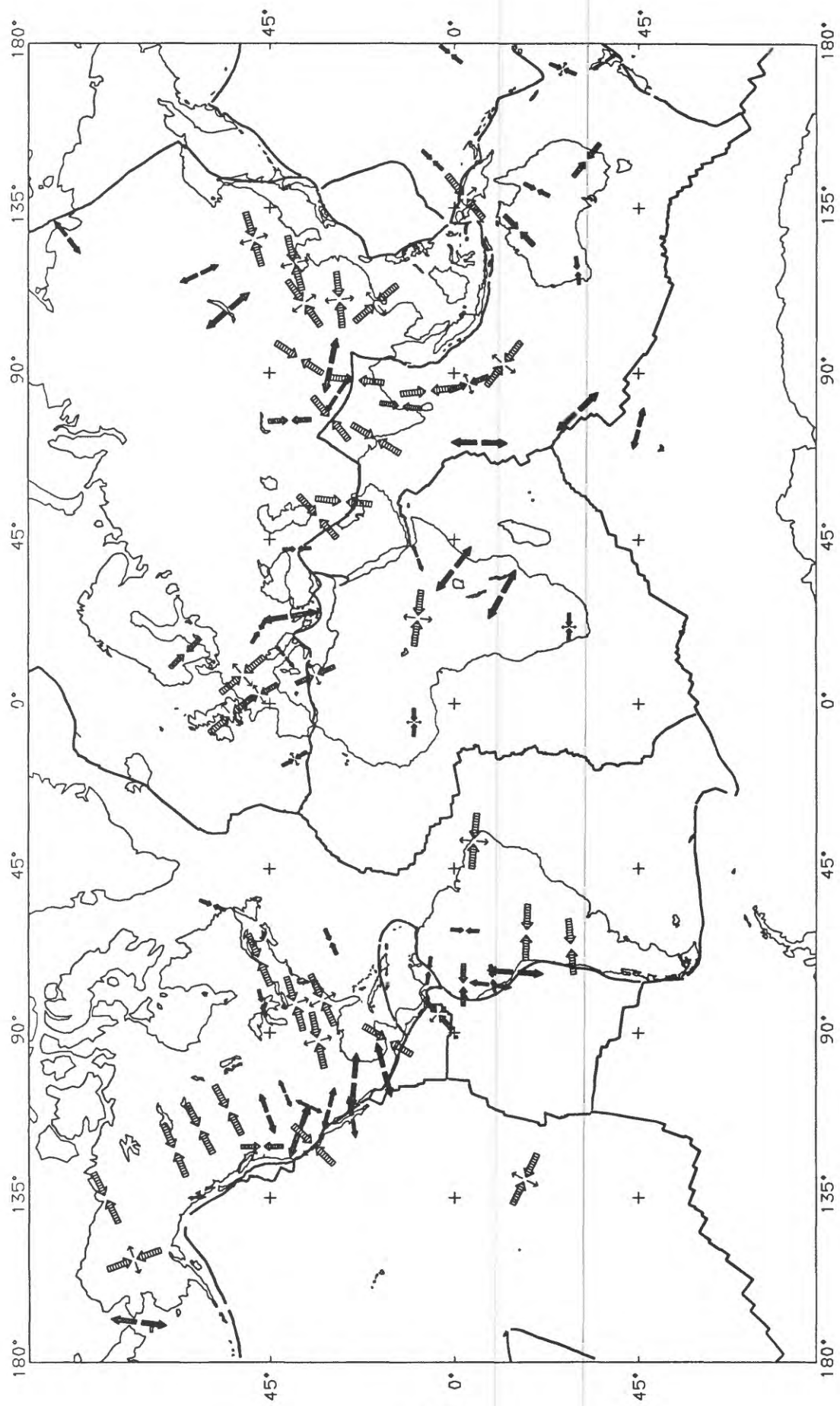


Figure 2. Generalized stress map of the world. Large arrows indicate mean stress directions for dense clusters of data. Inward-pointing arrows indicate $S_{H\max}$ orientation for compressive stress regimes (one or both of the horizontal stresses exceed the vertical stress). Outward-pointing arrows show Shmin orientations. Thick outward-pointing arrows indicate regions of extensional stress regime (both horizontal stresses less than vertical stress). Thin outward arrows plotted together with inward arrows indicate a strike-slip faulting regime. Coverage is non-uniform due to the non-uniform coverage in Figure 1.

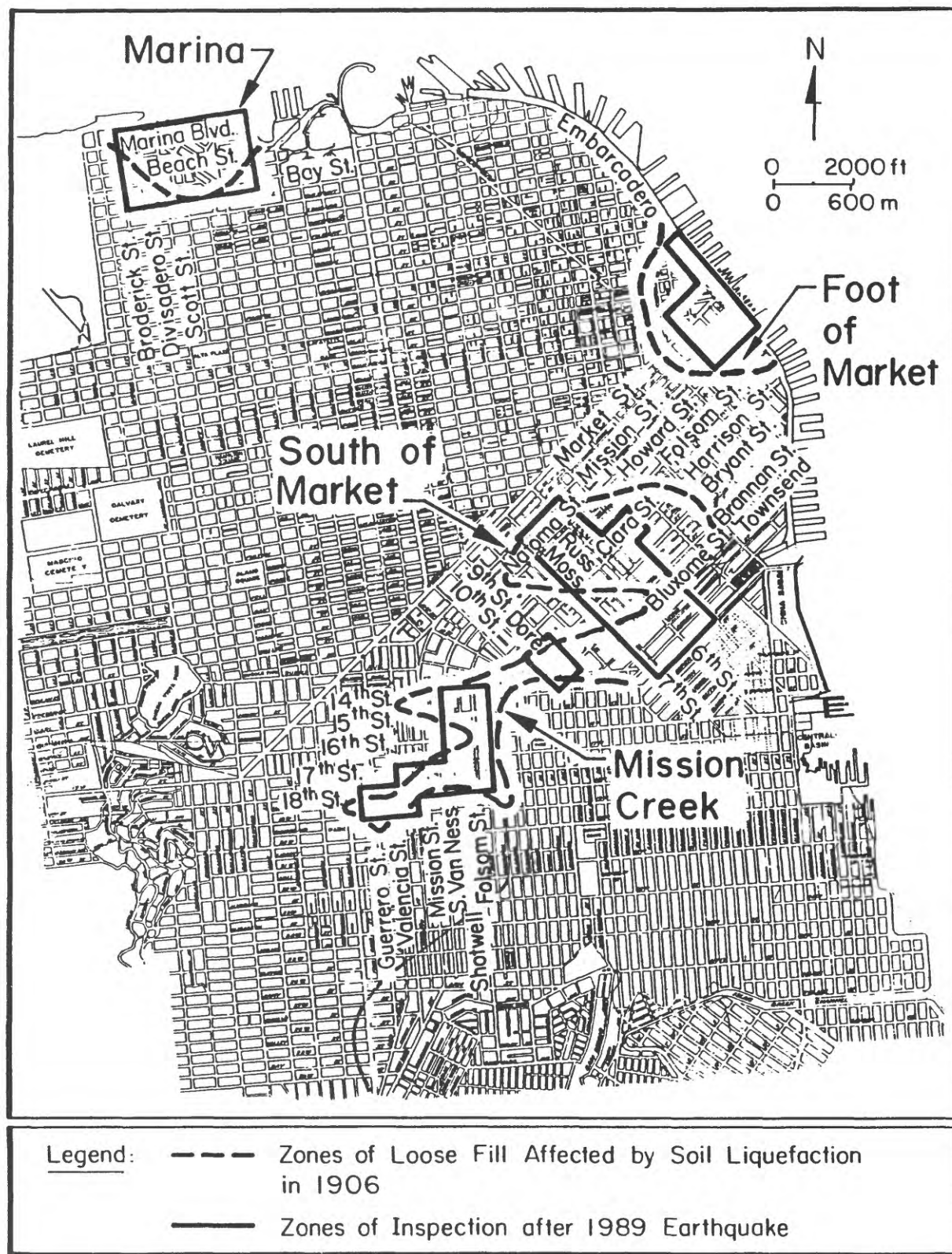


Figure 1. Principal Areas of Soil Liquefaction in San Francisco in 1906 and 1989.

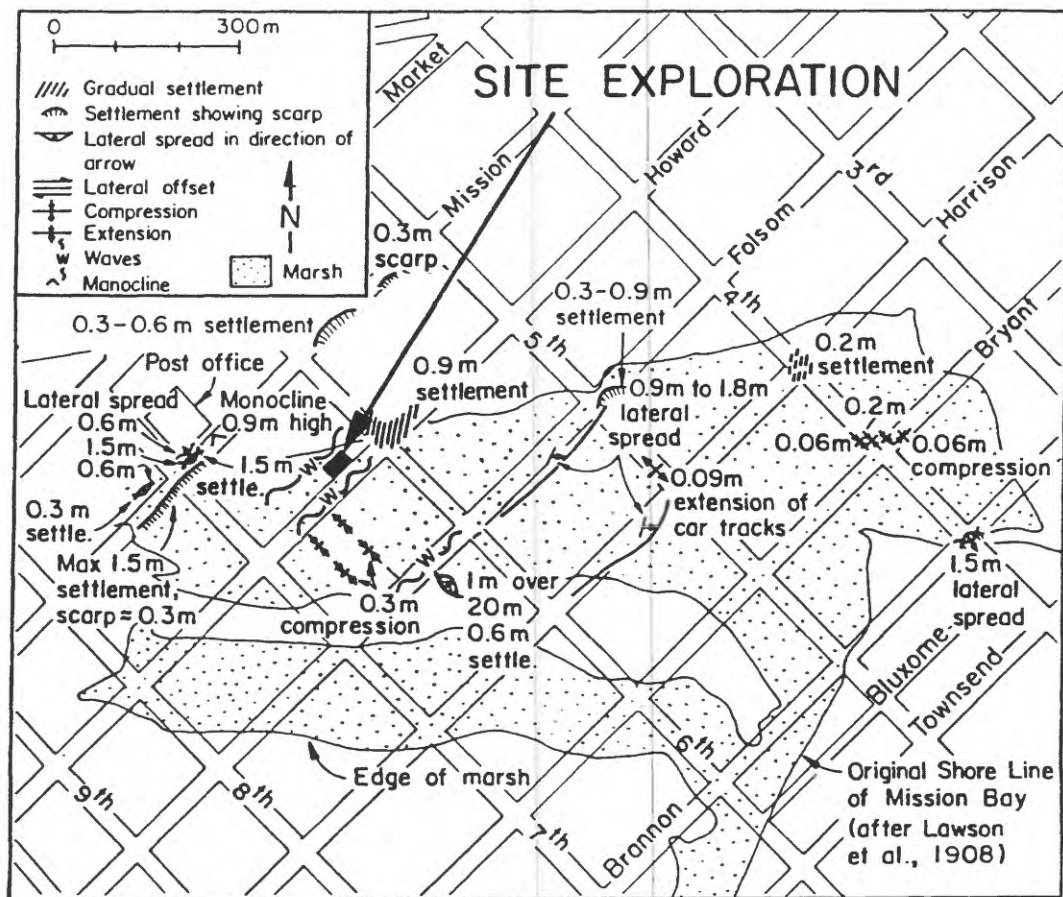


Figure 2. Plan View of the South of Market Area with 1906 Liquefaction-Induced Ground Deformation

former salt marsh. The area was filled during the years between 1850 and 1860, predominantly with material excavated from the nearby sand dunes.

After the 1989 Loma Prieta earthquake, there was much evidence of soil liquefaction and ground movements. South of Mission St., sand boils were observed along curb and building lines at various locations on 7th, 6th, Natoma, Russ, Moss, Clara, Bluxome, and Townsend Sts. From Mission to Folsom St., 10 to 30-mm-wide cracks were observed down the centerline of 7th St., with differential settlement to the east and west of the cracks. The most serious damage to the water supply of San Francisco was a break of a 300-mm-diameter cast iron main on 7th St. between Mission and Howard Sts. Water flow through this break, supplemented by losses at broken hydrants, emptied the Jones St. Tank of its entire storage of 2.8 million liters in approximately 30 minutes. Loss of this reservoir supply led to the loss of water and pressure throughout the lower zone of the Auxiliary Water Supply System (AWSS). The AWSS provides water for fire protection in San Francisco.

Investigations at this site were performed as an integrated program of CPT soundings and boreholes with SPT measurements to provide complimentary, yet independent,

assessments of subsurface conditions. The CPT soundings allowed for continuous and detailed assessment of soil lenses and variations of in-situ sand density. The conventional boreholes provided SPT measurements, piston tube sampling of Recent Bay Mud, and split spoon samples of sands and clays for classification testing. The SPT measurements were performed in the fills on a 1.2-m interval. In addition, down-hole shear wave velocity measurements were made to establish a vertical profile of in-situ shear wave modulus for dynamic evaluation of the sites. The depth to the water table was established in the fill.

Mission Creek

Figure 3 is a map of ground movements developed by O'Rourke and Lane (1989) which occurred during the 1906 earthquake superimposed on the original topography in the Mission Creek area. There is a close relationship between the original topography and the direction and distribution of soil displacements. Even relatively small topographical features, such as the ravine underlying 19th St. between Guerrero and Valencia Sts., influenced ground deformation. At this location, soil movements were canalized by the course of the buried creek. The direction of lateral spreading changed through 90 degrees, from a northerly direction on 19th St. to an easterly direction near Valencia St.

The most severe distortions occurred in areas where the former ravines narrowed, thereby restricting movements to a limited zone. In the region formerly known as "The Willows" along Valencia St. between 18th and 19th Sts., some of the most extreme disturbances occurred. The ground spread eastward down the center of the former channel of the stream, with maximum displacements of 1.8 to 2.4 m over a distance of 45 to 60 m. The displacements were largest directly in front of the former Valencia St. Hotel, which collapsed in response to the movements.

Three sites were investigated in the Mission Creek area, as shown in the figure. The sites were located at: a) Mission Playground at 19th St. and Linda St., which is the site of lateral spreading on 19th St., b) Valencia St. between 18th and 19th Sts. in the vicinity of the old Valencia St. Hotel, and c) Shotwell St. between 17th and 18th Sts. Some of the most severe liquefaction-induced damage from the 1989 Loma Prieta earthquake were observed on the middle west side of Shotwell St., where maximum building settlements on the order of 0.2 to 0.4 m occurred.

Similar to those in the South of Market area, the investigations were conducted as an integrated program of CPT soundings and conventional borings with SPT measurements and sampling. Downhole seismic shear wave velocity profiles were acquired at the Shotwell St. and Mission Playground sites.

RESULTS OBTAINED

The four sites investigated are described briefly with respect to data obtained and preliminary findings:

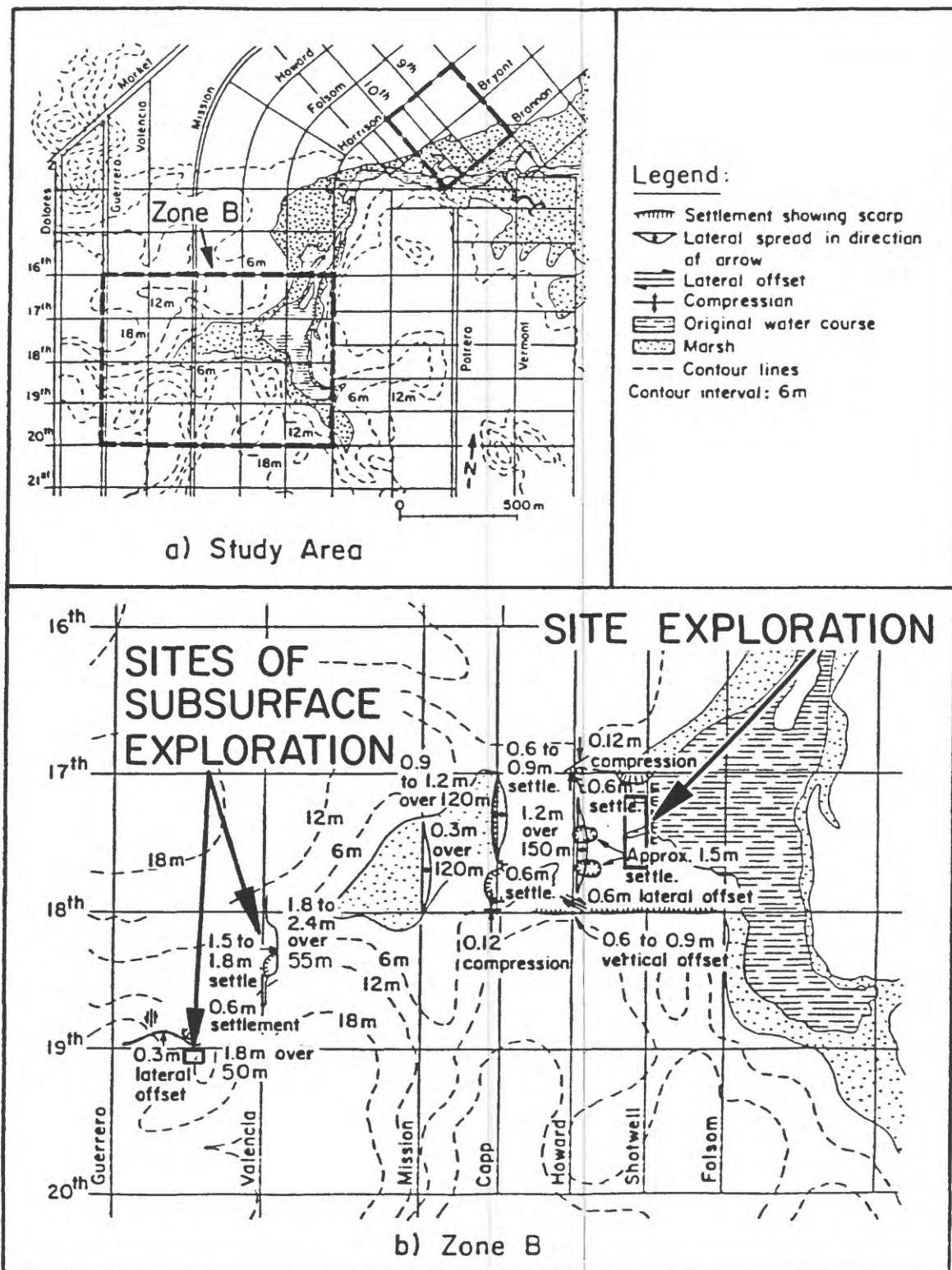


Figure 3. Plan View of 1906 Liquefaction-Induced Ground Movements and Subsurface Topography in the Mission Creek Area.

FIGURE 1. CONDITIONAL PROBABILITY OF AN EARTHQUAKE-INDUCED LANDSLIDE

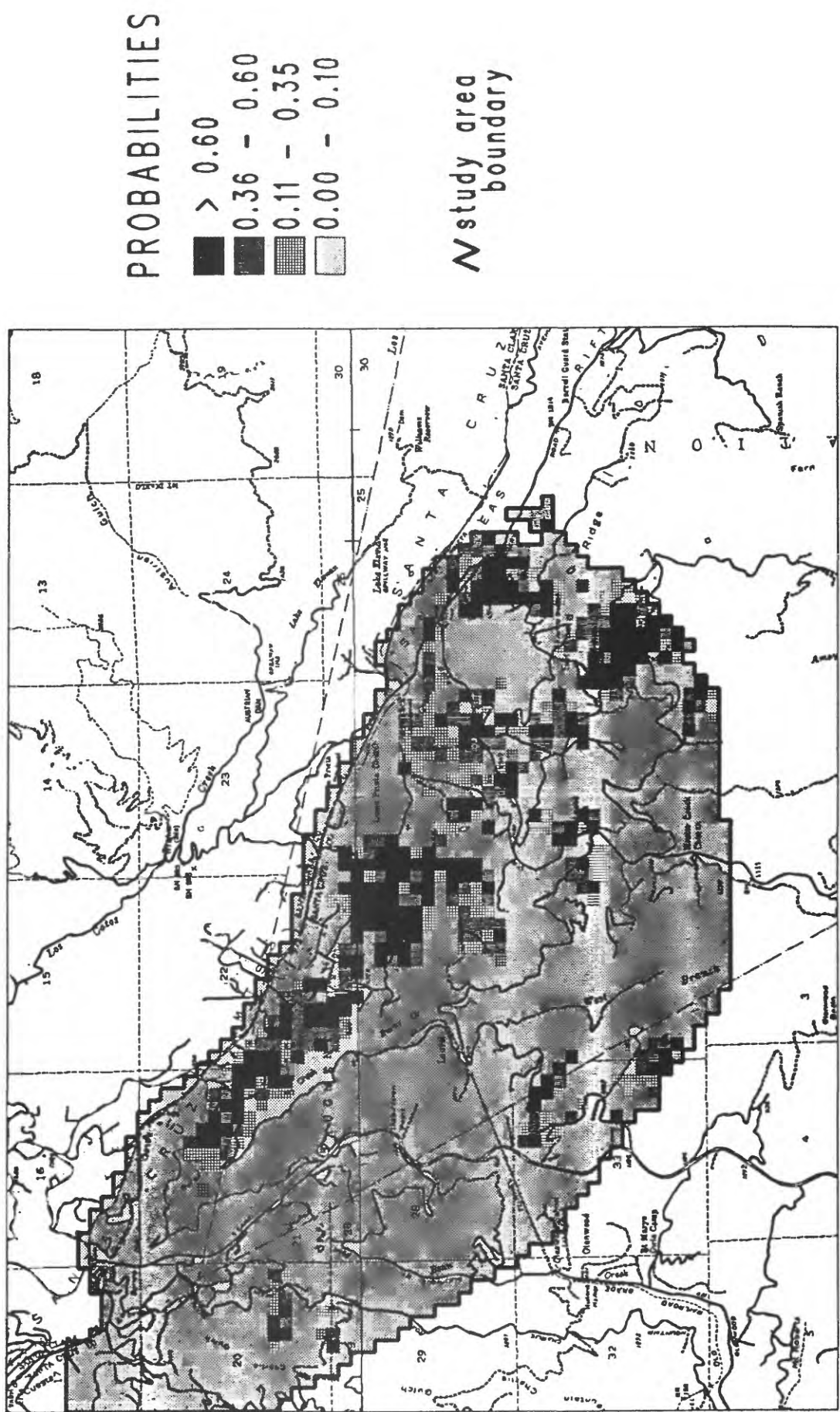
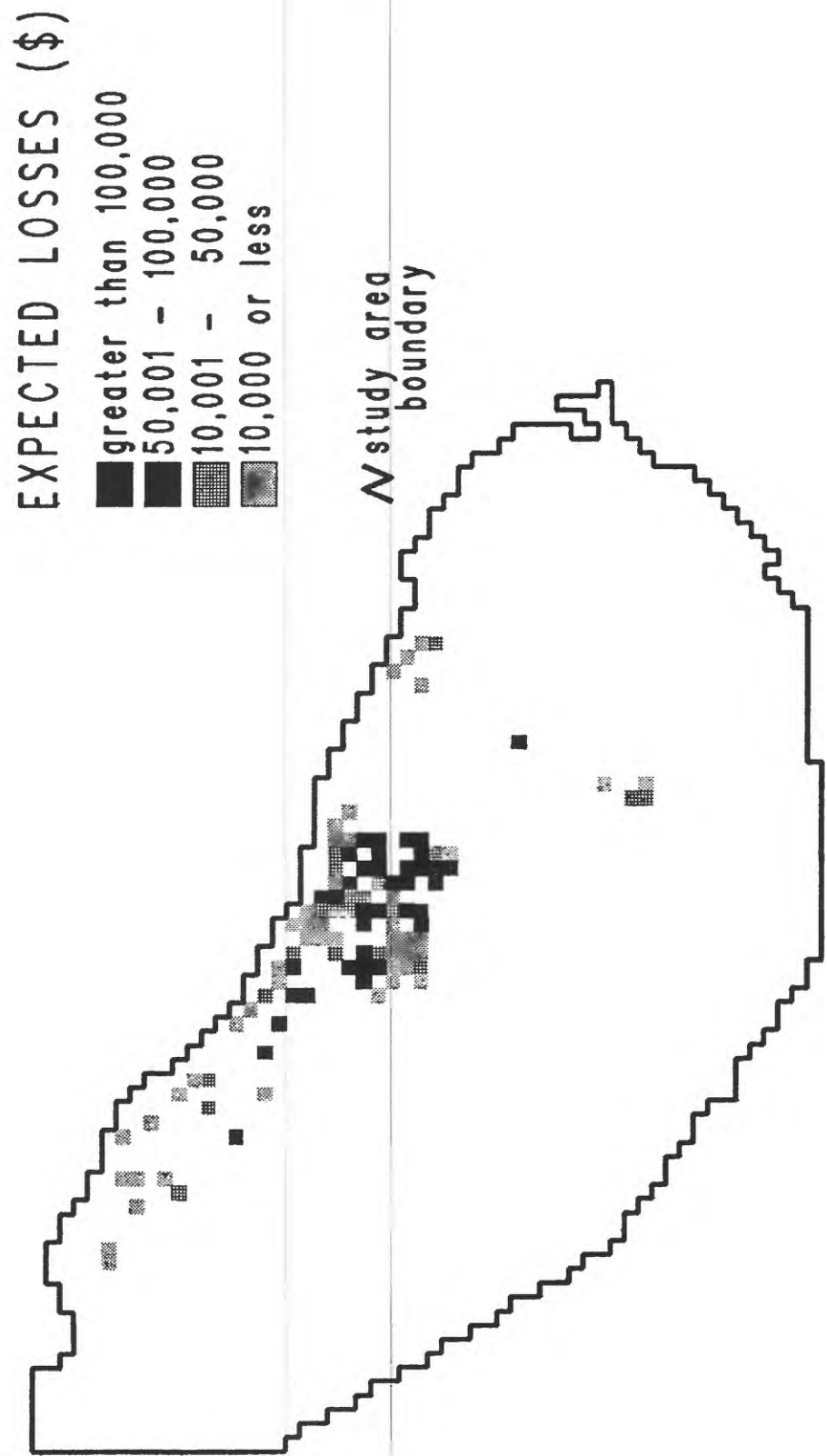


FIGURE 2. EXPECTED LOSSES FROM EARTHQUAKE-INDUCED LANDSLIDES



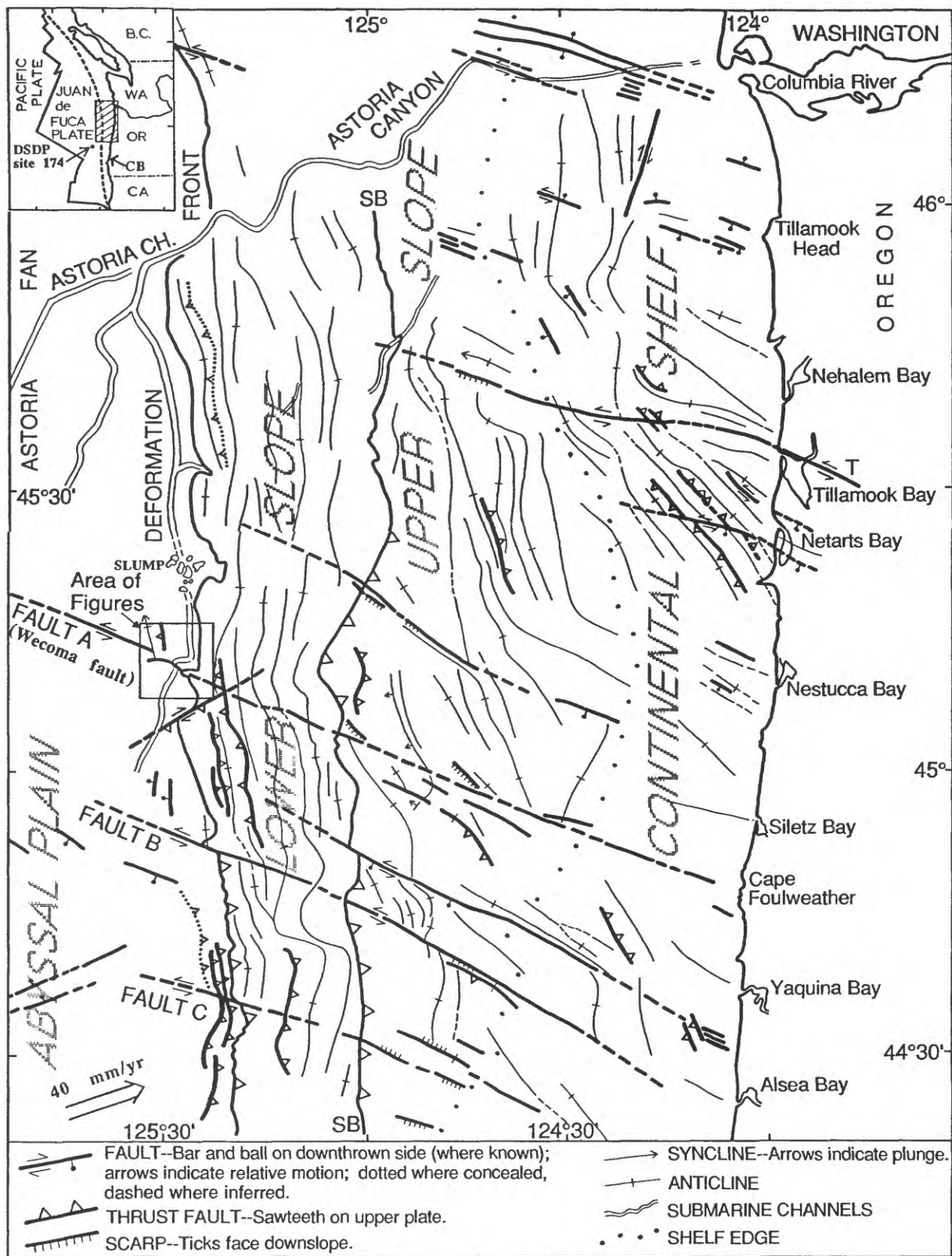


Figure 1. Structure map of the northern and central Oregon margin. Map emphasizes active features; most structures shown cut or deform the sea floor. Deformation front is a thrust fault south of Fault B, and the base of a seaward dipping ramp north of Fault B. SB = slope break; T = Tillamook Bay fault. Inset shows Juan de Fuca plate and DSDP Site 174.

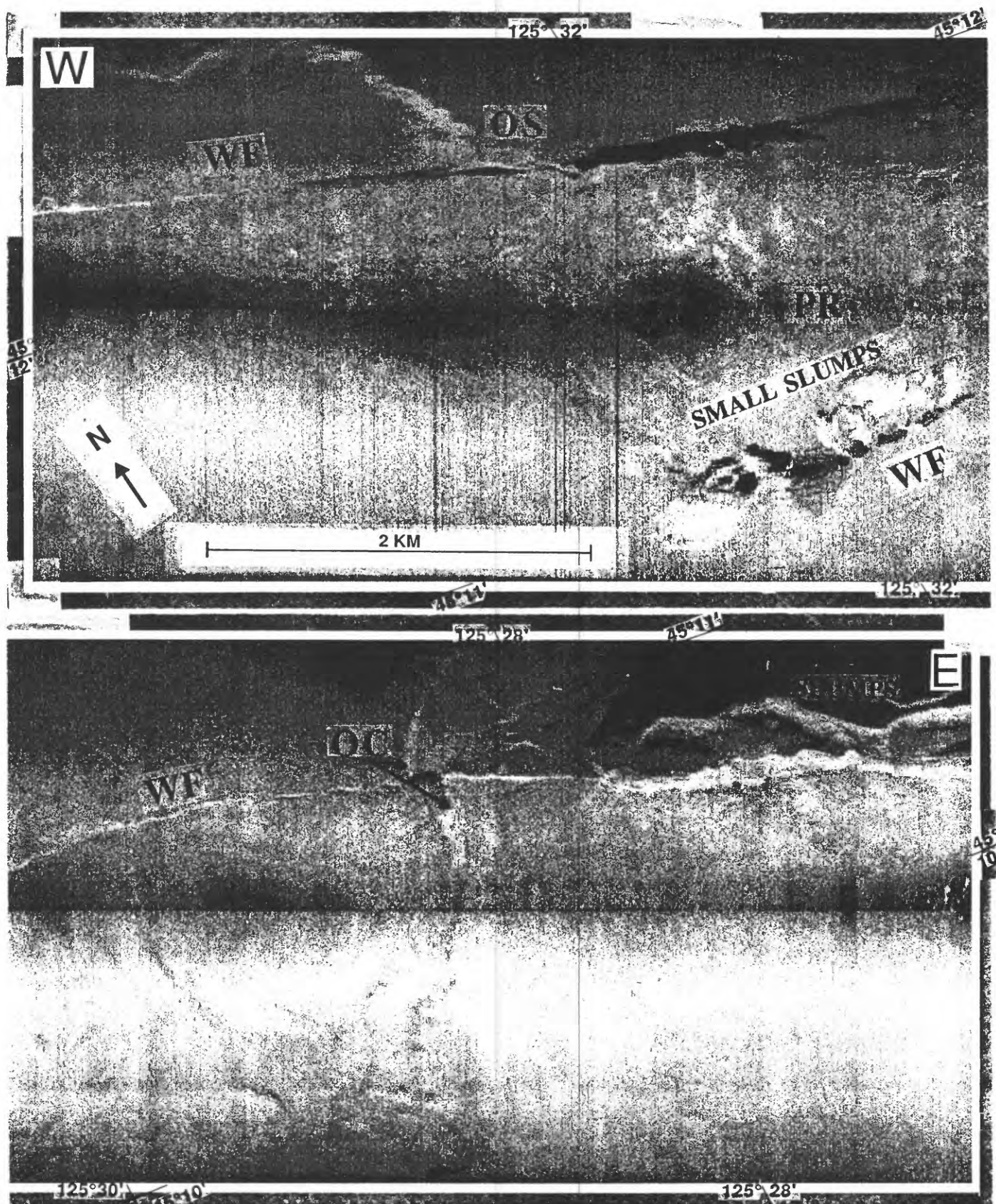


Figure 2. High resolution 2 km swath along the Wecoma fault (fault A on the abyssal plain). Note right step in trace of the Wecoma fault. PR = Pressure ridge; OC = offset channel shown by arrows; OS = offset slump scar. Note large scarp at eastern end of northern fault strand is a surficial normal fault.

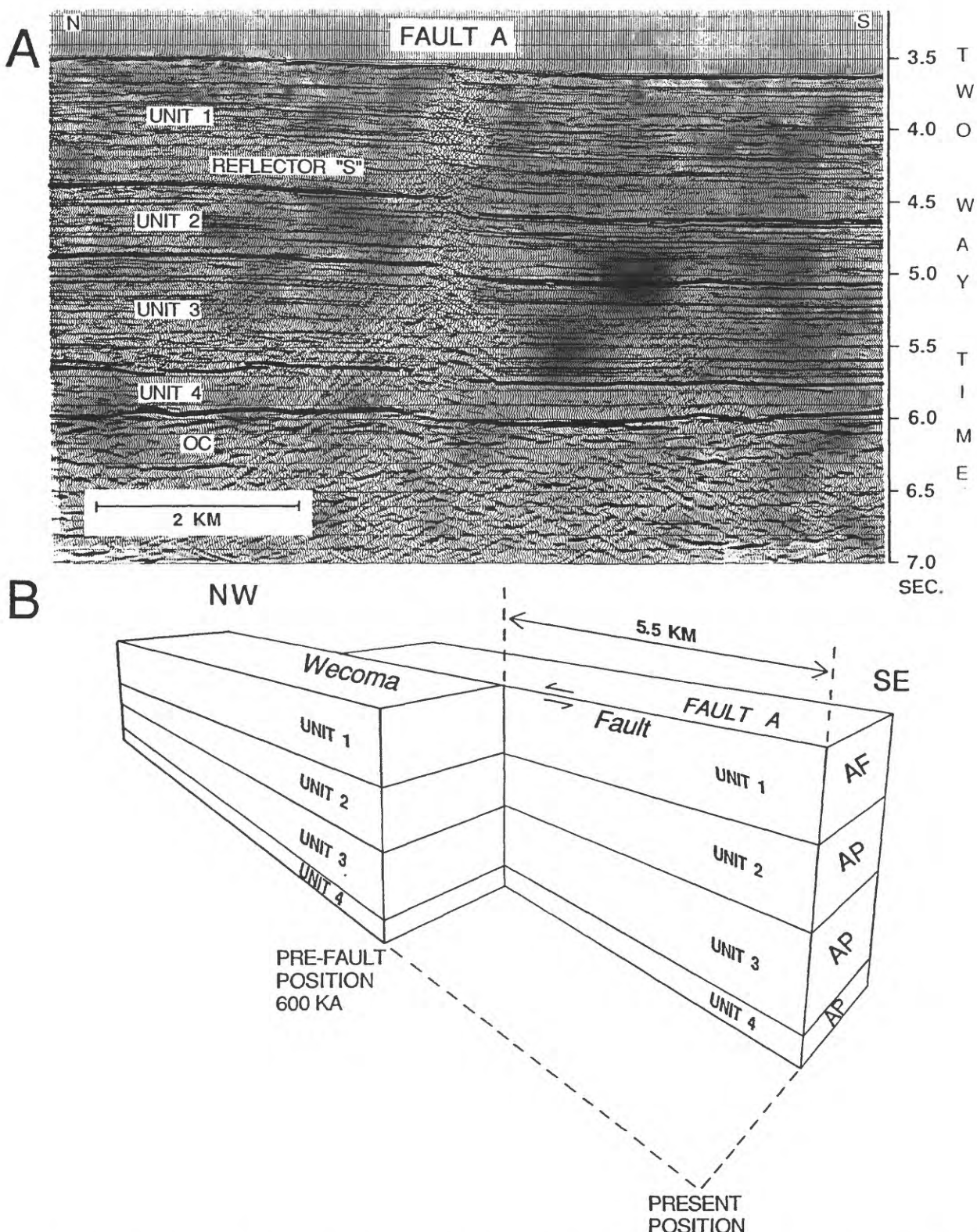


Figure 3. A) Multichannel seismic line crossing Wecoma fault (fault A) between pressure ridge and deformation front. V.E. 2:1. B) Cartoon illustrating the method used in fault A reconstruction. Fault motion was reversed until eastward thickening sediment wedges of units 2 and 3 matched, resulting in a separation of 5.5 ± 0.8 km. AF = Astoria Fan and AP = Abyssal Plain sedimentary deposits.

INITIAL THRUST RIDGE

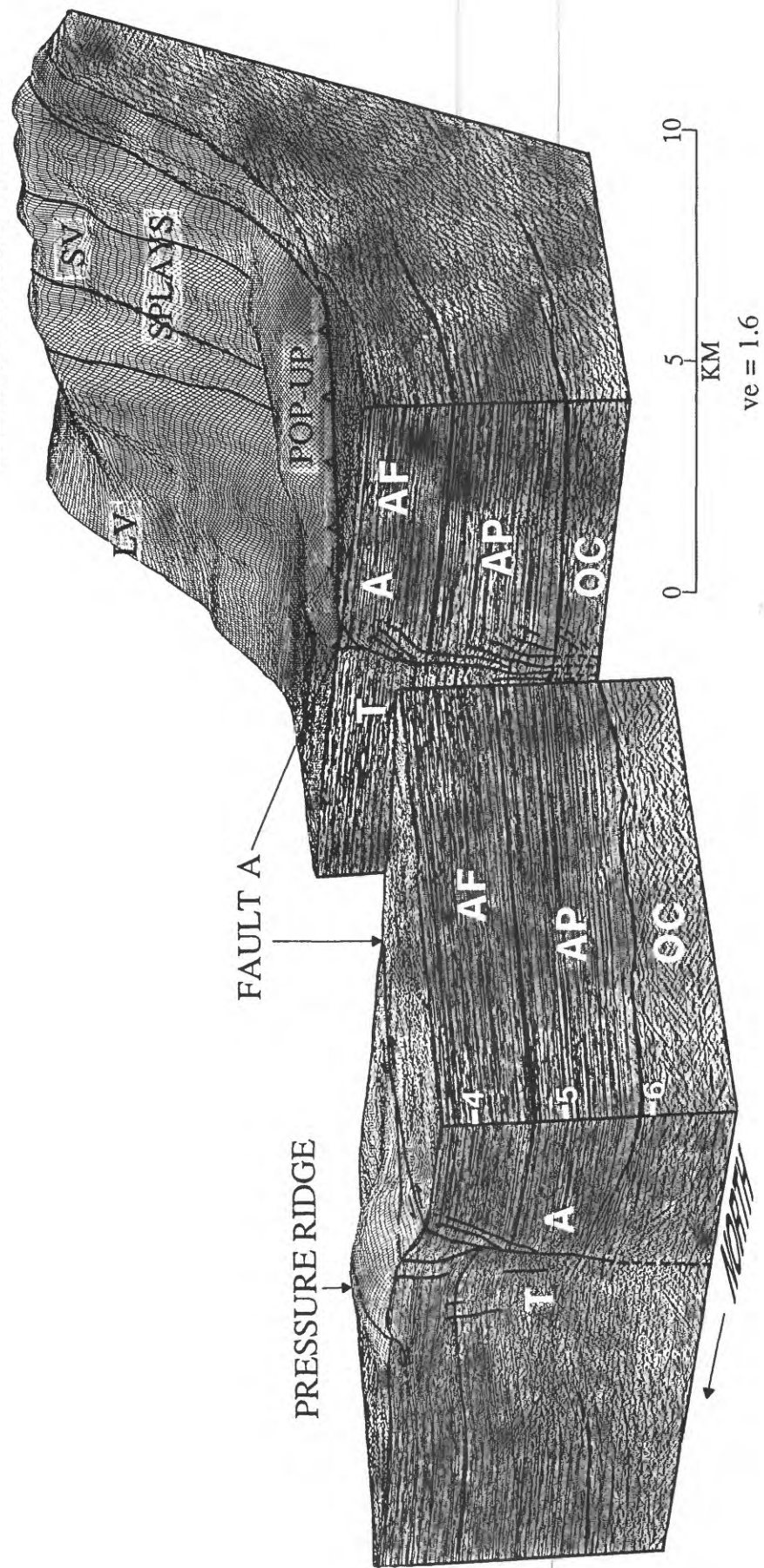


Figure 4. Composite block diagram of pressure ridge area and intersection between Fault A and the deformation front, viewed from southwest. Seismic sections (two way time) shown with selected reflectors enhanced. AP = abyssal plain section; AF = Astoria fan (note thickening across the fault and thinning over the pressure ridge); A = away; T = toward; SV = toward vergence; LV = landward vergence; OC = oceanic crust.

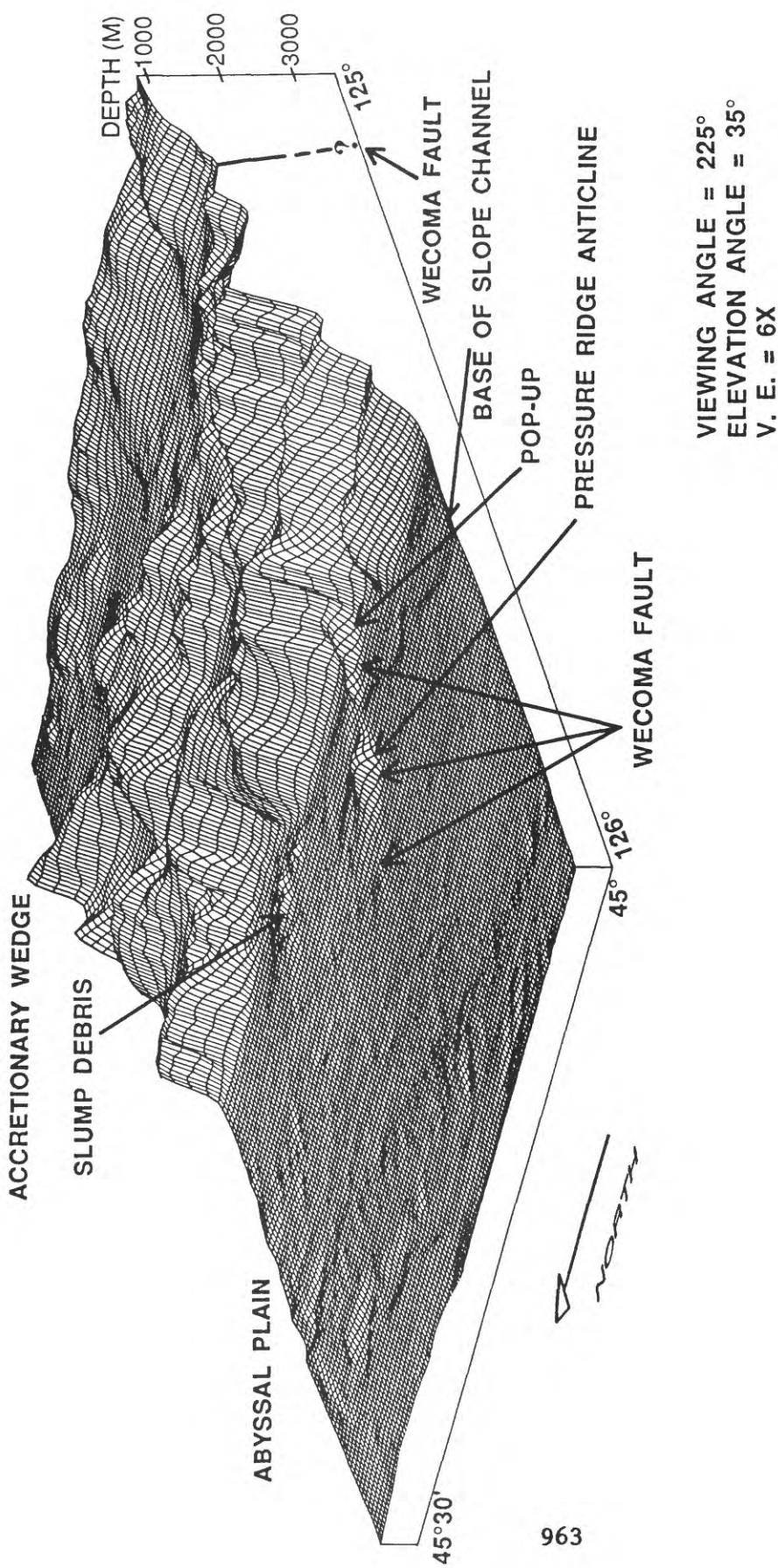


Figure 5. 3-D Perspective view of SeaBeam bathymetry from the southwest showing the physiography of the abyssal plain, and accretionary wedge in the vicinity of the Wecoma fault. Note slump debris blocking base of slope channel at foot of large slump scarp on deformation front.

Seismic Hazard Reduction Planning Process
to Develop Policies and Programs for the City of Seattle

Agreement No. 14-08-0001-G1958

City of Seattle Office for Long-range Planning
Room 200 Municipal Building
Seattle, WA 98104

Principal Investigator: Clifford Marks
(206) 684-8372

The objective of this project is to begin the process of developing a Seismic Hazard Reduction Plan. This planning effort could serve as a model for other communities in the Puget Sound region, but is mainly intended to develop and adopt policies and programs to reduce earthquake damage and loss of life within the City of Seattle.

This project will incorporate the research work currently being funded by USGS's National Earthquake Hazard Reduction Program into the City's planning process and translate seismic hazard technical information into terms that are understandable to both the general public and decision makers.

A policy framework for defining acceptable risk will be established and preliminary seismic hazard reduction policies will be prepared. Building code and other land use regulatory changes may be recommended, and input into emergency response planning will be provided. The project is also intended to coordinate the activities of various City departments regarding seismic hazard reduction issues and to establish a uniform seismic information data base.

The work program consists of the following tasks:

Task 1 Establish City Seismic Hazard Reduction Committee and Consolidate Seismic Hazard Data Used by City Departments

This first task, which has been completed in 1991, consists of the formation of a Seismic Hazard Reduction Committee to work with the Principal Investigator to ensure communication between departments on this project. This committee will give direction to the seismic hazard reduction planning activities carried out under this grant. Each department has submitted their priority issues to ensure that these are dealt with during the program. It will be an objective of this seismic hazard reduction work program to establish a uniform data base concerning seismic information to be used by all City departments.

